Politecnico di Milano
Department of Aerospace Science and Technology
Doctoral Programme In Aerospace Engineering

Mission Analysis and GNC Missionisation for Re-entry Vehicles

Doctoral Dissertation of:
Jacopo Guadagnini

Supervisor:
Gabriele De Zaiacomo

Academic Supervisor:
Prof. Michèle Lavagna

Tutor:
Prof. Maurizio Quadrio

The Chair of the Doctoral Program:
Prof. Pierangelo Masarati

2023 – Cycle XXXVI

This research was carried out at Deimos Space SLU, Madrid. Two visiting periods have been done at German Aerospace Center (DLR) in Bremen, and at Politecnico di Milano. The work is part of the H2020 ITN Program ASCenSIon. The project leading to this application has received funding from the European Union's Horizon 2020 research and innovation program under the Marie Skłodowska-Curie grant agreement No 860956.

Copyright ©2020-2023, Jacopo Guadagnini
All Rights Reserved

A Mamma e Papá.

Abstract

The reusability of spacecraft and launchers marks a revolutionary stride in space exploration and transportation, introducing an era characterised by enhanced efficiency, sustainability, and cost-effectiveness. In contrast to conventional expendable space vehicles that dispose of components after a single use, reusability entails the strategic design and engineering of spacecraft and launchers to withstand multiple missions. This shift in approach is motivated by the acknowledgment that promoting sustainability in space travel is not only environmentally conscientious but also economically advantageous. The drive towards spacecraft and launcher reusability has sparked significant investments from both private companies and governmental space agencies. Recognising the potential game-changing impact of reusable technology, numerous entities are actively channeling resources into the development and enhancement of reusable spacecraft and launchers. In this context, the new ability of a reusable system to undergo re-flight necessitates the implementation of a Mission Analysis (MA) and Guidance, Navigation, and Control (GNC) missionisation process and tool for autonomous re-entry vehicles. This reduces the customisation efforts needed for each mission.

The research work focuses on the definition and implementation of a multidisciplinary, parametric and modular Mission Analysis and GNC missionisation tool for re-entry vehicles. In this thesis a novel approach to perform the design of re-entry mission and the setting of the GNC parameters is proposed: the required analyses are inte-

grated into a multidisciplinary and parameterised framework to effectively handle design variables and the interconnections between different analyses within a unified analytical environment. The tool exploits Multidisciplinary Design Optimisation techniques to manage the Multidisciplinary Analysis framework to perform parametric optimisation and to handle the coupling between the disciplines. This operation is implemented within the Missionisation Layer, which embeds both a Multi-Objective Particle Swarm Optimisation algorithm and a metamodel technique based on Gaussian Radial Basis Functions. The aims of the missionisation tool within this research is dual: the first objective aims at obtaining an optimised end-to-end mission solution and GNC parameters tuning while satisfying specific mission and system requirements. This relates the concept of missionisation to the latest phases of the design process. The second goal uses the concept of missionisation during the early phase of the design: the tool aims at assessing the mission performance of a vehicle or a family of re-entry vehicles with respect a set of mission and system parameters to identify promising solutions within the search space.

The thesis reports the definition of the MA an GNC missionisation tool, the engineering modeling of the disciplines, the validation of the tool and the application in representative test case scenarios. The outcome of the thesis is a complete framework that can be used to perform preliminary and mid-fidelity analysis for a wide range of re-entry scenarios. However, the modular nature of the tool allows to increase the level of fidelity and accuracy quite easily.

Acknowledgements

THESE three years have been crazy roller coaster, and I will need another dissertation to thank all the incredible people who have been part of this journey. I will try to do my best, but I will definitely forget someone.

The first special thanks goes to my supervisor (and now my boss), Gabriele De Zaiacomo. Since the first day, he has given an incredible and continuous support. His expertise and suggestions helped me to grow both as an engineer and as a person. I consider myself very lucky to have met Gabriele. Then, I would like to thank Prof. Michèle Lavagna. I still remember back in March 2020 when she told me about ASCenSIon. Thank to have given me this opportunity and pushed me towards this adventure.

As I said ASCenSIon was an incredible journey, in which I met and got to know so many people. The first people I want to thank are the brilliant and somewhat crazy ASCenSIon ESRs: we went through super long meetings, discussions, trips, dinners, and, most important, parties that created a unique bond between us. So thanks Andre, Giò, Guille, Mateusz, Lily, Felix, Melissa, Chris, Richi, Livia, Albe, Lucia, Iñigo and Alice. Thank also to our coordinators Christian Bach, Alessia, Adheena, Theo and Jannis for the huge work you have done for us.

The second group of people I want to thank is the one of Madrid (but not only). I will start from the AFCC colleagues: Raquel, Jaime, Alejandro, Ale (I will do a special mention later), Gio, Fede and Peppe.

I will never stop being grateful to you for making me feel part of the group, for the technical support, for sharing with me your expertise and for the "out-of-office" experiences. But this will not finish now. Thank also to Dani, Pelayo, Pietro, Emilio, and all the amazing Deimos people I met. Gracias por todo chicos. Madrid siempre será mi segunda casa.

A special thank is for Alessandra, maybe one of the craziest and best person I have ever met. Thank for all the cervezas, for the huge parties, for the advice and thank you for your always being there for others.

I cannot skip a particular mention to the Beehive. Biagio, we have known each other for 8 years, finally we managed to do our abroad experience together. Ale, what to say, you are the Queen, I am very happy to have met you. Thank guys for your support and for your authenticity, I know that I can count on you.

A great thank to the group of italians in Madrid: Gennaro, Gabri, Fede, Fede Trova, Giorgia and Fede. Dottor Belnome, it was a pleasure to share the flat with you (also with you Giorgi), but please do not ask me again to check your Excel equations on the profit of an incremental investment at 3 a.m.

I would like also to thank Stefano during the freezing period in Bremen, and the ASTRA team during the secondment at Polimi for welcoming me into the group as if I had always been there. A particular mention is for Andre (Brando) and Michi (Beco), it was funny to share and live again the Polimi with you. And Andre the next time we will share the bed on the West Coast, but under one condition, we will bring with us the engineer Pietro (Baiedro).

I cannot forget Gabri, Vale, Pri and Ale, and the lifelong friends Mazzu and Sbalchi, I'm very grateful to say that the distance did not affect our friendship.

The second-to-last paragraph is for my family. Marc and Patty, you always give me your support and kind words when needed. None of this would have been possible without you. We shared a lot during these years despite the distance, making our family stronger than before. You will always be my model for facing life. A special mention also to Mali (my sister) and Ale (my brother) always ready to share a laugh. It has been wonderful to see your growth and success as well. The way is long, but you can always count on me.

The last paragraph is dedicated to the most important person of my life, my girlfriend Sonia. You always believed in me, even when I did not. For sure, you more than everyone else know what these

three years have been, for you and for me. How amazing, difficult, crazy, and complete they were. We decided to start a completely new chapter of our life. We lived together, we grew up, we cried, we laugh, we travelled, we lived, and we are still doing all these things, because this experience was just the beginning. I know that surely this journey was even more total for you, and I am happy for this. You have been and you are the perfect "travel" partner. Simply, I love you.

As always, *"Step by step"*.

Contents

1 Introduction **1**
1.1 Context & Motivation 2
1.2 The Research Problem 5
1.2.1 Objectives 5
1.2.2 Research Questions 6
1.3 Dissertation Overview 6
1.4 Bibliography Disclaimer 8

2 Background **11**
2.1 Space Mission Life-Cycle 12
2.2 Atmospheric Re-Entry 13
2.2.1 Classification of the Re-entry Vehicles 16
2.3 Recovery Strategies 17
2.3.1 Horizontal Landing 18
2.3.2 Vertical Landing 19
2.4 Trajectory Optimisation 22
2.5 Multidisciplinary Design Optimisation 27
2.5.1 Metamodeling Techniques 30

3 MA and GNC Missionisation Tool **33**
3.1 High-Level Architecture of the Tool 34
3.1.1 User Interface 34
3.1.2 MDA core 37
3.1.3 Missionisation Layer 38

3.2 Design Structure Matrix 42
3.3 Modularisation of the Tool 44

4 Engineering Modelling **47**
4.1 System Models 47
4.1.1 Equations of Motion 48
4.1.2 Environmental Models 51
4.2 Modelling of the Disciplines 53
4.2.1 Geometry and Mass estimation tool 54
4.2.2 Aerodynamic Database tool 56
4.2.3 Flying Quality Analysis tool 59
4.2.4 Entry Corridor tool 61
4.2.5 Footprint Evaluation tool 66
4.2.6 Trajectory Optimisation tool 68
4.2.7 GNC tool 71

5 Validation **73**
5.1 Validation of the Disciplines 73
5.1.1 GEOM tool validation 74
5.1.2 AEDB tool validation 75
5.1.3 FQA tool validation 75
5.1.4 EC tool validation 77
5.1.5 FE tool validation 78
5.2 Sensitivity Analysis 79
5.3 RETALT Missionised Solution 81
5.3.1 Problem parameters and formulation 81
5.3.2 Results 83

6 Test Cases **87**
6.1 Lifting Body Missionised Solution: Mission Design and Verification from EIP to TAEM 87
6.1.1 Objectives 88
6.1.2 Problem Modelling 89
6.1.3 Results 94
6.1.4 Summary and Comments 99
6.2 WRV Preliminary Mission Design and Mission Capabilities Evaluation 106
6.2.1 Objectives 106
6.2.2 Problem Modelling 107
6.2.3 Results 110
6.2.4 Summary and Comments 115

6.3 Mission Analysis and GNC Missionisation of a VL-RLV 119
6.3.1 Objectives 119
6.3.2 Problem Modelling 119
6.3.3 Propellant-optimal Problem formulation 122
6.3.4 Results 124
6.3.5 Summary and Comments 129

7 Conclusions and Future Work 131

Bibliography 137

List of Figures

1.1 Re-entry vehicles and reusable launcher demonstrator concepts. 4

2.1 Space mission life-cycle phases. The MA and GNC missionisation tool can be exploited during the early design phases (Pre-A, A, and B), and during the mission preparation and utilisation (D and E). [11]. 13
2.2 SPACE SHUTTLE entry corridor [5]. 15
2.3 Category subdivision of re-entry vehicles considered within this research [21]. 18
2.4 Approach and Landing strategies: SPACE SHUTTLE runway A&L (left), X38 Parafoil A&L (right). 20
2.5 First Stage vertical landing recovery scenarios: RTLS left and DRL right. 21
2.6 Representation of a multiphase problem [31]. 23

3.1 High-Level architecture of the MA and GNC missionisation tool. 34
3.2 Information flow visualisation of the MA and GNC missionisation tool. 35
3.3 Visualisation of the PSO algorithm. 40
3.4 Design Structure Matrix of the MDA core of the MA and GNC missionisation tool with all the disciplines considered. 43

3.5 High-Level architecture of the MA and GNC missionisation tool without the GEOM and AEDB disciplines. It is relative to the first test case (Section 6.1). 46
3.6 High-Level architecture of the MA and GNC missionisation tool without the TO and GNC disciplines. It is relative to the second test case (Section 6.2). 46
3.7 High-Level architecture of the MA and GNC missionisation tool without the GEOM, AEDB and FE disciplines. It is relative to the third test case (Section 6.3). 46

4.1 Horus-2B vehicle. 54
4.2 High-Level concept for the creation of one interpolating function, P_i are the geometrical parameters. 58
4.3 Block Diagram of the AEDB Tool, p_1 and p_2 are the geometrical parameters. 58
4.4 Conventions for angles, forces and torques considered within the FQA tool. In this case, the CoG and the MRC coincide. 61
4.5 Example of FQA outputs obtained using Horus-2B as baseline. 62
4.6 Example of Entry Corridor outputs obtained using Horus-2B as baseline. 66
4.7 Example of drag profiles and scheduled bank angle profiles for Horus-2B, with initial condition reported in Table 4.1, 0° latitude, 0° longitude and 60° heading angle. . 69
4.8 Example of range capability estimation for Horus-2B, with initial condition reported in Table 4.1, 0° latitude, 0° longitude and 60° heading angle. 70
4.9 Example of fitting of the reference profiles performed by the GNC tool. 72

5.1 Aerodynamic coefficients with $\delta = 0°$ for the Horus-2B. The full lines are the literature data, while the dashed lines are the profiles computed with the AEDB tool. . . 76
5.2 Aerodynamic coefficients width $\delta = 20°$ for the X38. The full lines are the literature data, while the dashed lines are the profiles computed with the AEDB tool. 76
5.3 Comparison of FQA results obtained with the FQA tool with respect to the reference (red boxes). 77

5.4 Comparison of EC results obtained with the EC tool with respect the reference. 78
5.5 Optimal (red) and estimated (green) range capability. The initial point is defined by the start. 79
5.6 Comparison of results obtained within the RETALT project (red) and the ones obtained with the TO tool. 84

6.1 Geometry representation of the considered lifting body. . 89
6.2 Aerodynamic coefficients for $\delta = 0°$ for the considered vehicle. 90
6.3 Example of CoG locations within the CoG Box. 95
6.4 FQA with respect to CoG locations considered in Figure 6.3. 96
6.5 Maps for the EIP selection analysis. 101
6.6 De-orbit manoeuvre design results. 102
6.7 Reference and nominal trajectory profiles. The nominal has been simulated with DEIMOS high-fidelity simulator with the closed-loop guidance. 103
6.8 Trajectory design and GNC tuning results. 104
6.9 Montecarlo campaign dispersion. 104
6.10 Results of the Montecarlo campaign. The nominal profiles are highlighted in red. 105
6.11 DSM of the involved disciplines for the analysed test case. 108
6.12 Performance indices example considered for this test case. 109
6.13 ESAT prediction of the optimum solutions and validation with the MDA. In the figure on the left, the ESAT predictions (blue) are compared with the exact MDA evaluations (red), while on the right the correspondent errors are reported. 112
6.14 Comparison of the inputs distribution of the Pareto solutions computed with ESAT (a) and MOPSO (b). . . . 113
6.15 Input-Output correlation for the WRV mission capability test case. Color scale is set between -0.5 and 0.5 for visualisation purposes. 114
6.16 Performance indices maps with respect to L_{ref}, X_{cog}, and b (left). Corresponding two-dimensional maps with L_{ref}=34 m (right). 117

6.17 Geometries and mission analyses performance associated to the three selected candidates. The results of each candidate are organised in column. 118
6.18 Visualisation of the geoemtry and the CoG position during the aerodynamic phase. Credit [25, 78, 96] 121
6.19 FQA for the considered vehicle during the aerodynamic phase. 121
6.20 Expected minimum propellant mass consumed for RTLS recovery strategy. 126
6.21 RTLS trajectories dispersion. 126
6.22 Expected minimum propellant mass consumed for DRL recovery strategy. 128
6.23 DRL trajectories dispersion. 128
6.24 Feasibility region for the recovery of launch vehicle of the analysed case. The intersected area (violet) means that both strategies are feasible, and that DRL is more efficient. 130

List of Tables

3.1 Qualitative definition of the parameters for the DSM in Figure 3.4. $\mathbf{X}_j$ are kept void, since they are specified only if an MDO routine is taken into account. 45

4.1 Horus-2B parameters and boundary conditions. 54
4.2 Empirical relations for the mass estimation of the components. 56
4.3 Input and Output parameters for the Geometry and Mass estimation tool. 57
4.4 Input and Output parameters for the Aerodynamic Database tool. 58
4.5 Input and Output parameters for the Flying Qualities Analysis tool. 62
4.6 Equations of the aerothermal-mechanical loads considered within the tool. 64
4.7 Input and Output parameters for the Entry Corridor tool. 65
4.8 Input and Output parameters for the Footprint Evaluation tool. 69

5.1 Mass estimation assessment. 74
5.2 Preliminary sensitivity analysis of the error for WRV with Horus-2B. The nominal value of D_{min} is 910 km, while for Δ_δ it is 6.4°. 81
5.3 Problem parameters and boundary conditions. 82

5.4 RETALT trajectory comparison for TO tool validation. . 85

6.1 Operational orbit and TAEM interface point parameters. 91
6.2 Minimum-propellant de-orbit manoeuvre formulation. . . 92
6.3 Atmospheric re-entry trajectory problem formulation. . . 93
6.4 FQA performance with respect to the CoG locations in Figure 6.3. 96
6.5 Applied dispersion for the Montecarlo campaign. 99
6.6 Qualitative definition of the parameters for the DSM in Figure 6.11 108
6.7 Problem paramters: boundary conditions, aerothermal-mechanical loads, flaps deflection constraints. 111
6.8 Design variables upper and lower bounds. 111
6.9 Three example of optimal solutions. Both the real and predicted performance indices are reported. 116
6.10 Propellant-optimal problem formulation for RTLS and DRL. 123
6.11 Problem parameters and path constraints values. 124
6.12 Domain of interest for MECO conditions. Ranges defined from [25, 94] 124

List of Acronyms

3DoF : 3 Degree of Freedom

AAO : All At Once

AEDB : Aerodynamic Database

ALI : Approach and Landing Interface

AoA : Angle of Attack

AR : Acceptance Review

AOM : AVUM Orbital Module

ATD : Aerothermal Database

AVUM : Attitude Vernier Upper Module

BC : Boundary Conditions

CAC : Calculation of Aerodynamic Coefficients

CDR : Critical Design Review

CFD : Computational Fluid Dynamics

CNES : Centre national d'études spatiales

CO : Collaborative Optimisation

CoG : Center of Gravity

CON : Control

ConOps : Concept of Operations

CONS : Constraint

DLR : Deutsches Zentrum für Luft- und Raumfahrt

DRL : Downrange Landing

DSM : Design Structure Matrix

EAGLE : Evolved Acceleration Guidance Logic for Entry

EC : Entry Corridor

ECEF : Earth Centered Earth Fixed

EDL : Entry Descent and Landing

EIP : Entry Interface Point

ENDOSIM : ENDOatmospheric SIMulator

ENV : Environment

ESA : European Space Agency

ESAT : EDLS/GNC Sizing and Analysis Tool

FE : Footprint Estimation

FFNN : Feed Forward Neural Network

FPA : Flight Path Angle

FQA : Flying Quality Analyses

FS : Flight Scenario

GA : Genetic Algorithm

gbest : global best position

GEOM : Geometry tool

GNC : Guidance Navigation and Control

GUI : Graphical User Interface

HASA : Hypersonic Aerospace Sizing Analysis

HOTSOSE : Hot Second Order Expansion method

I/O : Input/Output

IDF : Individual Discipline Feasible

INER : Inertia

IPM : Interior Point Method

IXV : Intermediate eXperimental Vehicle

JAXA : Japan Aerospace Exploration Agency

L/D : Lift to Drag ratio

LB : Lifting Body

LEO : Low Earth Orbit

MA : Mission Analysis

MARS : Multivariate Adaptive Regression Spline

MBDO : Metamodel-based multidisciplinary Design Optimisation

MCI : Mass Centering Inertia

MDA : Multidisciplinary Design Analysis

MDF : Multi Discipline Feasible

MDO : Multidisciplinary Design Optimisation

MDR : Mission Definition Review

MECO : Main Engine Cut Off

MOPSO : Multi Objective Particle Swarm Optimisation

MRC : Moment Reference Center

NLP : Nonlinear Programming

NRLMSISE-00 : United States Naval Research Laboratory Mass Spectrometer and Incoherent Scatter Radar esosphere

NWRV : Non Winged Re-entry Vehicle

pbest : personal best position

PDR : Preliminary Design Review

PP : Post Process

PRR : Preliminary Requirements Review

PSO : Particle Swarm Optimisation

QR : Qualification Review

RBF : Radial Basis Function

RBFNN : Radial Basis Function Neural Network

RCS : Reaction Control System

RETALT : RETro propulsion Assisted Landing Technologies

RLV : Reusable Launch Vehicle

RMSE : Root Mean Square Error

RTLS : Return to Launch Site

Sim : Simulator

Space Rider : Space Reusable Integrated Demonstrator for Europe Return

SQP : Sequential Quadratic Programming

SVR : Support Vector Regression

TAEM : Terminal Area Energy Management

TDB : Thermal Database

TO : Trajectory Optimisation

USSA76 : United States Standard Atmosphere

VL-RLV : Vertical Landing Reusable Launch Vehicle

VMM : Vehicle Mode Management

WGS84 : World Geodetic System

WLB : Winged Lifting Body

WRV : Winged Re-entry Vehicle

"Let's see if I remember how to do this!"
Micheal Jordan - Space Jam

CHAPTER 1

Introduction

AscenSion (Advancing Space Access Capabilities - Reusability and Multiple Satellite Injection) is born as an innovative training network with fifteen Early-Stage Researchers, ten beneficiaries, and fourteen partner organisations across Europe, to study the critical technologies for the development of the next generation of reusable space system. The network aims at identifying and advance critical technologies to prove a feasibility of launcher systems that are (partially) reusable and capable of injecting multiple payloads into multiple orbits. Fields of research and training include propulsion technologies and their reusability; Mission Engineering and Guidance, Navigation and Control (GNC); aerothermo-dynamics of re-entry and safe disposal. In this context, the objective of this research is the development of a Mission Analysis and Guidance, Navigation and Control Missionisation tool for re-entry vehicles.

Spacecraft and launcher reusability represent transformative advancements in space exploration and transportation, ushering in a new era of efficiency, sustainability, and cost-effectiveness. Unlike traditional expendable space vehicles, where components are discarded after a single use, reusability involves designing and engineering space-

craft and launchers to endure multiple missions. This paradigm shift is driven by the recognition that making space travel more sustainable is not only environmentally responsible but also economically beneficial. Reusable spacecraft and launchers are equipped to withstand the harsh conditions of space and the intense heat of re-entry, allowing them to return to Earth and be relaunched on subsequent missions.

The introduction of reusability in space technology has the potential to significantly reduce the overall cost of space exploration. By refurbishing and reusing major components, such as rocket stages and spacecraft, the expense of manufacturing new hardware for each mission is substantially diminished. This cost-effective approach opens up new opportunities for frequent and accessible space travel, fostering innovation and collaboration in both government and private space sectors. Furthermore, spacecraft and launcher reusability aligns with global efforts to minimise the environmental impact of space activities. The reduction of space debris and the efficient use of resources contribute to a more sustainable space environment, ensuring the long-term viability of space exploration and satellite deployment. In this context, the exploration of spacecraft and launcher reusability marks a pivotal moment in the evolution of space technology, promising a future where access to space is more routine, economical, and environmentally conscious.

The re-flight capability of a reusable system prompts the necessity of a Mission Analysis (MA) and GNC missionisation process and tool for autonomous re-entry vehicles which reduces the tailoring efforts required for each mission. Every scenario is, indeed, characterised by different requirements and challenges that must addressed in an efficient and reliable way, such that the mission and GNC solution is optimally tuned to fulfill the specific needs.

1.1 Context & Motivation

The word "missionisation" addresses all the operations to be performed to adapt a space system to any specific mission. It may can be considered as the customisation of a product for specific needs of a client [1]. A literature review using the keyword "missionisation" (or "missionization") yielded limited findings. This term is commonly employed in the context of certain products, such as aircraft or helicopters, to address challenges associated with adapting a vehicle to meet a customer's specific requirements. Typically, these modifications tend to

have minimal impact on the overall design and are primarily focused on avionics, which is a component that can be more readily adjusted. Nevertheless, the word "missionisation", along with the adjective "missionised", or the verb "to missionise", is currently used worldwide in several documents relative to expendable space launch vehicles by private companies and agencies. Anyway, also in this field very few information has been found, as this problem is addressed with proprietary software or internal know-how that is not accessible by the public [1]. An example is given by Reference [2], where a missionisation tool for the VEGA family [3] is presented. The concept of missionisation is approached to the launch vehicles, because this kind of vehicle requires an adaptation of the mission definition and the configuration (in some cases) depending on the customer needs. Moreover, nowadays it is taking greater significance since the cadence of launches is exponentially increasing [4].

Within this work, missionisation refers to a subset of activities dealing with the mission analysis and the tuning of the GNC parameters of a re-entry vehicle. In this context, missionisation is even less considered, since the number of re-entry vehicles and missions is relatively small. A concept of missionisation has been found in the mission analysis and GNC design of the Space Shuttle, in particular for the design of the trajectory from the entry point (EIP) to the TAEM interface. For each flight, the reference profile, the drag profile in this case, was adapted by tailoring the parameters used to design the reference profile itself [5].

However, especially due to the increasing number of reusable space vehicles for both the space access and in-orbit studies, the missionisation of the re-entry vehicles may take a key role for reducing the tailoring effort and time between each re-flight. The most famous example is the Falcon 9 by Space X, that has performed multiple landing missions, each of them characterised by specific mission challenges [6], but diverse space programs are investing on reusability and re-entry, such as Sierra Space, Space Rider, Ariane Next and CALLISTO [7, 8, 9, 10]. Figure 1.1 shows the concepts of the Dream Chaser by Sierra Space, Space Rider by ESA, and CALLISTO by CNES, DLR and JAXA.

Summarising, the mission analysis and GNC missionisation for a re-entry vehicle is the recurrent activity to tailor the mission analysis and GNC solution for the vehicle for one particular mission. Commonly, the mission design of a re-entry vehicle and the setting of the GNC are

(a) *Dream Chaser of Sierra Space (credit Sierra Space).*

(b) *Space Rider render (credit ESA).*

(c) *Callisto render (credit CNES).*

Figure 1.1: *Re-entry vehicles and reusable launcher demonstrator concepts.*

performed with a set of analysis that are carried out separately. These analyses are strictly interconnected among them, such that multiple iterations are needed to obtain a valuable solution. In this research, a novel approach is implemented in order to address this problem. The analyses are embedded in a unique multidisciplinary and parameterised framework in order to manage the design variables and the coupling between the analyses in a single analytical environment.

In this research, missionisation has a dual function. The first one pursues the optimal tuning of a set of mission and system design parameters considering specific requirements of a mission scenario. This is the direct translation of the definition reported above, and it is related to the last phases of the design process. The second function applies the concept of missionisation in the early phases of the design process: it aims at evaluating the mission performance of a vehicle or different concepts with respect to the design mission and system parameters to identify more robust and flexible solutions from the mission analysis view point. The missionisation of a re-entry vehicle is a complex and highly multidisciplinary problem, it has been addressed with

the development of a dedicated multidisciplinary tool.

1.2 The Research Problem

The research problem arises from the need of having an multidisciplinary, parameterised, standard and flexible MA and GNC missionisation tool for re-entry vehicles, that handles the mission design process in an efficient way in order to reduce the tailoring effort among each re-flight.

1.2.1 Objectives

The objective of the PhD research is the definition and implementation of a missionisation process and tool which reduces the tailoring effort for each mission. The missionisation tool aims at obtaining an optimised end-to-end mission solution and to assess the mission performance with respect to a set of mission and system parameters. These parameters affect the MA and GNC design, the solution and the performance of the mission. So, the identification of these variables are crucial for the definition of robust re-entry mission solutions and trajectories. In order to effectively tune these variables, they must be systematically categorised by defining the set of optimum invariant and variant MA and GNC parameters. The design of an end-to-end re-entry mission involves multiple disciplines and several areas of analysis, so the missionisation tool will concern a multidisciplinary framework to handle all the interactions and the couplings. In this context, the missionisation tool may be applied for different purposes depending on the phase of the mission and vehicle life-cycle. On one hand the missionisation tool can be used in the last phases of the design, like phase D and E, by providing an updated mission solution with respect to the costumer's requirements, so it will adapt a qualified MA and GNC solution for one particular mission. On the other hand, the tool will be used in early design phases, like phases 0 and A, to explore the feasible search domain space. This calculation aims to assess the mission performance with respect to the mission and system parameters and to identify the most impacting ones. The final goal, as stated previously, is the minimisation of the tailoring effort among each re-flight, since the proposed missionisation tool will manage all the set of analyses in a unique framework, and it applies a novel multidisciplinary approach with respect to the classical methods, which tend to keep disciplines and analyses separate.

The development of the of the tool answers the deliverable D4.2 of Ascension Grant Agreement. The MA and GNC missionisation tool must be validated in representative real-scenario test cases. This second point is described in the deliverable D4.10 of Ascension Grant Agreement.

1.2.2 Research Questions

To fulfill the research objectives, a set of research questions, which will guide the development of the Thesis is presented:

1. What are the aspects and challenges that must be considered when dealing with the design of robust re-entry trajectories and missions?

2. How to tackle a generic re-entry problem in a standard and parametric way?

3. How to handle all the multidisciplinary aspect required to missionise an end-to-end re-entry mission?

4. Is it possible to consider the missionisation in both the early phases and the latest phases of the design process?

1.3 Dissertation Overview

The thesis is organised in the following chapters:

Chapter 2: Background This chapters presents an introduction of the atmospheric re-entry problem and the related challenges and criticality, as well as the theoretical background of the trajectory optimisation and multidisciplinary optimisation. In particular, the first section gives an overview of the main aspects of a generic re-entry problem. The section also shows the re-entry vehicles that can be studied within the developed tool. The second section reports a snapshot of the recovery and landing strategies. The third and fourth sections introduces the problem of trajectory and multidisciplinary optimisation. The former shows the generic formulation of a multiphase optimal control problem, underlying the main elements and presenting some solving strategies and algorithms. The latter focuses more on the definition of the architectures used to formulate an MDO

problem. This last section also introduces some metamodeling techniques used in the literature.

Chapter 3: MA and GNC Missionisation Tool This chapter reports the main features of the proposed MA and GNC missionisation tool. The first section gives and overview of the high-level architecture of the tool, showing the main modules and focusing on the definition and implementation of the Missionisation Layer. The second section presents the Design Structure Matrix of the tool, while the third one underlies the flexibility of the tool, showing how it can be adapted depending on the scenario analysed.

Chapter 4: Engineering Modeling This chapter present an overview of the engineering modelling of the tool. The first section reports the main equations of motion used within the disciplines and the study cases, as well as the environmental models included within the library of the tool. In the second section, the implementation of the disciplines embedded in the tool is described, focusing on the assumptions made and the input/output parameters. For each discipline, an explanatory example of analysis is reported.

Chapter 5: Validation This chapter describes the validation process and results of each discipline. In particular, this is reported in the fist section. The second section shows a preliminary sensitivity analysis in order to assess the error propagation within the tool. In the third section, the trajectory optimisation block is validated against the results of RETALT.

Chapter 6: Test Cases This chapter presents the test cases analysed within this research. The first section shows the MA and GNC missionisation for a lifting body vehicle. The optimal tuning of the end-to-end mission analysis solution and the GNC parameters is performed; then, the obtained solution is validated and verified with DEIMOS high-fidelity simulator. This study case answers the first definition of missionisation. The second section shows how the missionisation can be considered in the early phase of the design process. This concept is applied to assess the mission capabilities of a winged re-entry vehicle with respect to a set of mission and system design variables. The third section focuses on the assessment of the per-

formance envelopes for Return-to-Launch-Site and Downrange Landing recovery strategy with respect to a broad range of Main-Engine-Cut-Off conditions.

Chapter 7: Conclusions and Future Work This chapter reports the conclusions of this research work and gives a list of recommendations for future work.

1.4 Bibliography Disclaimer

During the years of my Philosophiae Doctor (Ph.D.), I presented updates of my work in many conferences and I also had the possibility to publish part of them in peer reviewed journals. Therefore, most of the work in this dissertation has already been presented in different articles. The most significant are listed below.

- Guadagnini J., De Zaiacomo G., and Lavagna M., "Mission Performance Assessment of the Recovery and Vertical Landing of a Reusable Launch Vehicle", *MDPI Aerospace Journal*;
- Scarlatella G., Tajmar M., Bach C., Guadagnini J., De Zaiacomo G., Paniccia L., and Pastrone G. D., "Assessment of Mission Capabilities of a Reusable Heavy-lift Launch Vehicle Concept with Aerospike Engine", in AIAA SciTech (2024), Orlando, USA;
- Guadagnini J., De Zaiacomo G., and Toso F., "Multidisciplinary Design Optimisation for missionisation of re-entry vehicles: preliminary mission design and mission capabilities evaluation of winged re-entry vehicles case study", in ESA GNC-ICATT (2023), Sopot, Poland;
- Guadagnini J., and De Zaiacomo G., "Multidisciplinary Modelling for Missionisation od Re-entry Vehicles", in AIAA SciTech (2023), National Harbor, USA;
- Guadagnini J., De Zaiacomo G., and Bussler L., "Aerodynamic coefficients estimation tool for re-entry vehicle missionisation", in 2nd International Conference on Flight Vehicles, Aerothermodynamics and Re-entry Missions Engineering (FAR) by ESA (2022), Heilbronn, Germany;
- Guadagnini J., Bonetti D., and De Zaiacomo G., "Entry Corridor Analysis for vertical landing Reusable Launch Vehicles", in XXVI AIDAA Internation Congress (2021), online;

- Alforja Ruiz I., Ayala Fernández L., De Oliveira A., Dominguez Calabuig G. J., Guadagnini J., Lantelme M., "Mission Analysis, GNC and ATD for Reusable Launch Vehicles within ASCenSIon: multi-orbit multi-payload injection, re-entry and safe disposal", in 72nd International Astronautical Congress IAC (2021), Dubai, United Arab Emirates;

"Well, this little maneuver's gonna cost us 51 years!"
Joseph Cooper - Interstellar

CHAPTER 2

Background

This chapter outlines the problem of missionisation for re-entry vehicles. Firstly an overview of the phases of the space mission design life-cycle is given in Section 2.1, underlying how and where the missionisation takes part. Then, the discussion introduces the different aspects of the re-entry problem and the methodologies applied for the development of the dedicated tool.

Since the missionisation is applied to re-entry vehicle, Section 2.2 introduces the atmospheric re-entry problem, underlying the main challenges and criticality. It also present the categories of re-entry vehicles considered within this research. Moreover, Section 2.3 provides an overview of the main recovery strategies concerning the entry, descent and landing in Earth's atmosphere. This problem is highly complex and involves multiple engineering disciplines, as it will be explained in Chapter 3.1 and Chapter 4. For these reasons, the tool makes use of trajectory optimisation to obtain reference mission profiles, and MDO techniques to handle the coupling between the disciplines. Thus, Section 2.4 and Section 2.5 report an overview of the theoretical background of such methodologies.

2.1 Space Mission Life-Cycle

The space mission life-cycle consists of several distinct phases, each crucial for the successful planning, development, and execution of a space mission. Figure 2.1 reports the typical phases that are considered with the design process [11]:

- Pre-Phase A: it is a preliminary phase that involves conceptualising and planning the mission before formal initiation. This stage is crucial for setting the foundation and identifying the feasibility of the mission. It includes several activities, such as mission conceptualisation, feasibility studies, and preliminary mission planning. The results of the pre-phase A are subjected to the Mission Definition Review (MDR).
- Phase A: in this phase the detailed planning and initial concept development occur. This phase is crucial for defining the mission architecture. Some foreseen activities are the definition of the mission requirements, the design of the system architecture, and the preliminary design. This phase ends with the Preliminary Requirements Review (PRR).
- Phase B: it is a critical stage focused on further developing the mission concept established in Phase A. During Phase B, the design is consolidated. The results of this phase culminate in the Preliminary Design Review (PDR).
- Phase C: it is a pivotal stage where the detailed design is finalised, and the construction of the spacecraft begins. This phase involves the transition from design and planning to actual implementation. Some of the activities includes the finalisation of the detailed design. The phase ends with the Critical Design Review (CDR).
- Phase D: this phase follows the detailed design, construction, and testing of the spacecraft. Key activities during Phase D include: the final system integration, functional testing, validation and verification. During this phase several reviews are foreseen, such as the Qualification Review (QR) and the Acceptance Review (AR).
- Phase E: It considers all the operations and management for the launch and the operational life of the spacecraft.
- Phase F: It deals with the closeout of the mission. In the context of re-entry mission it also includes post-flight analysis.

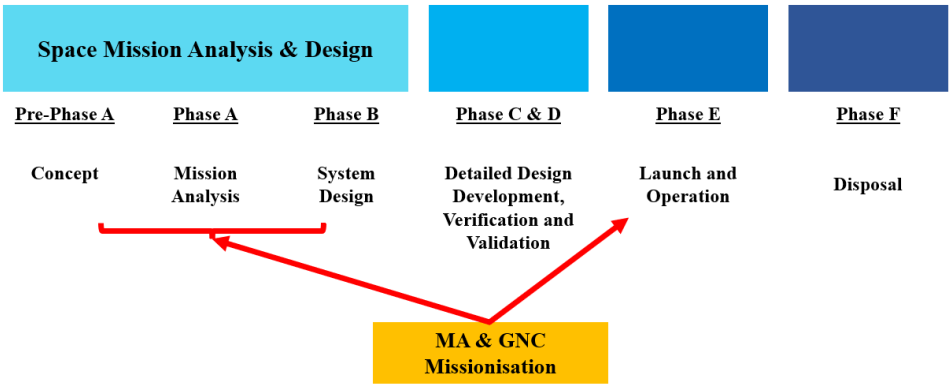

Figure 2.1: *Space mission life-cycle phases. The MA and GNC missionisation tool can be exploited during the early design phases (Pre-A, A, and B), and during the mission preparation and utilisation (D and E). [11].*

Figure 2.1 also reports where the missionisation tool developed within this research can be used. The tool, indeed, has been developed in order to answer two objectives. The first one pursues the optimal adaptation of the MA and GNC solution for one particular mission by considering precise mission and system requirements. In this case, the missionisation takes part of the activities of the phases D and E. The fist test case, in Section 6.1, shows an example of this capability of the tool.

The second objective aims at assessing the mission performance with respect to the mission and system parameters in order to evaluate different design solutions and and determine which are the more promising ones in term of user-defined performance indices. Within this research, the mission variables refers to those parameters used to delineate the mission scenario and the environment, while the system variables are the parameters that characterise the vehicle (Section 3.1). In this case, the missionisation takes part of the activities of the phase A. The second study case, in Section 6.2, addresses this point.

The other two test cases, in Section 5.3 and 6.3, can be considered in the middle between the scenarios reported above, where the missionisation is within the activities of the phase B.

2.2 Atmospheric Re-Entry

This research focuses on the analysis of re-entry trajectories into Earth's atmosphere. The principles and theories derived from this study can

also be applied to descent trajectories into the atmospheres of other celestial bodies, such as Mars, albeit with adjustments to account for diverse atmospheric conditions. When a spacecraft is in orbit around Earth, it possesses a significant amount of potential and kinetic energy. In a low Earth orbit, the total energy per kilogram is approximately 30 MJ [12]. This energy content becomes even higher for spacecraft entering Earth's sphere of influence at hyperbolic velocities, typically associated with return missions from the Moon or interplanetary journeys from Mars.

When a spacecraft needs to return to Earth, it must reduce this substantial energy to the level of potential energy that the vehicle has upon landing on Earth's surface, with zero relative velocity. The primary method to dissipate this energy is through aerodynamic friction with the spacecraft's surface as it passes through the Earth's atmosphere. However, novel applications exploit propulsive breaking manoeuvres, such as in the case of vertical landing (even if in this case the velocity is much lower). Traditionally, the Earth's atmosphere is considered to begin at an altitude of 120 km, although the official definition for the beginning of space (or the boundary of Earth's atmosphere) is at 100 km. However, for high-velocity re-entries, the noticeable influence of the atmosphere can extend to altitudes ranging from 200 to 300 km. As satellites and other spacecraft travel through these denser atmospheric layers at high velocities (hypersonic regime), they experience significant aerodynamic forces and encounter elevated temperatures due to aerodynamic heating. Managing the dissipation of the initial total energy involves adhering to specific system constraints, with dynamic pressure, thermal surface loads, and aerodynamic load factor being among the most critical factors. The outcome of this process is a typically narrow re-entry flight corridor [12, 13]. Figure 2.2 shows an example for re-entry corridor for the SPACE SHUTTLE.

The fundamental problem is to find a flight trajectory that allows the vehicle to achieve its mission with minimum demands on the vehicle system. However, unlike traditional aircraft design, the physical properties and the functions of a hypersonic vehicle and its components must be tuned to the flight trajectory and vice versa. To design and to optimize a vehicle's flight trajectory essentially involves addressing a guidance problem. Additionally, it is crucial to define the trajectory control variables, which command the vehicle to fly the trajectory. Then, physical loads and vehicle properties are introduced as systems and operational constraints in the trajectory design and optimisation

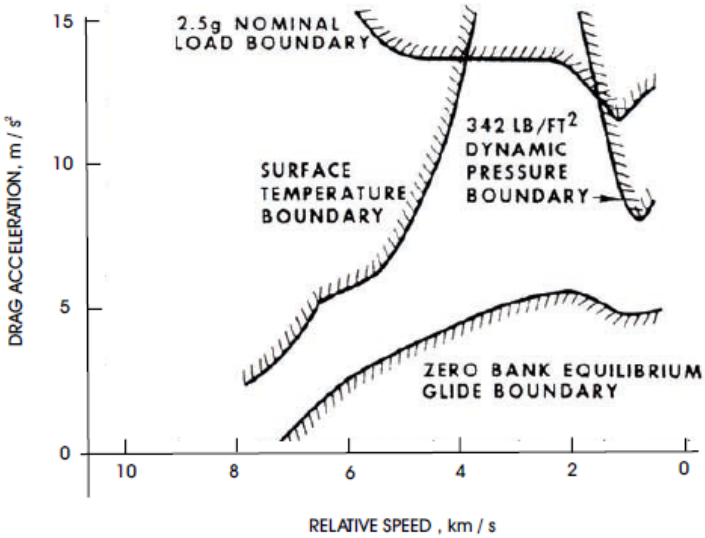

Figure 2.2: *SPACE SHUTTLE entry corridor [5].*

process. The final result are guidance laws, typically characterised by a limited number of free parameters, that are tailored to meet the mission objectives within the specified conditions.

Prerequisites for trajectory design and optimisation are flyability and controllability of the considered vehicle along the trajectory. Flyability includes longitudinal trimmability, and static and dynamic stability. Controllability is the ability to steer the vehicle along all relevant axes associated with the vehicle and its flight path throughout control devices. Usually, only a trimmed trajectory is a viable trajectory. Moreover, the shape and geometry of re-entry vehicles are of paramount significance in their overall design and functionality. These aspects directly impact the vehicle's aerodynamics, thermal protection, and mission objectives. Two critical parameters play a pivotal role in ensuring the success of a re-entry mission: the Ballistic Coefficient and the Lift-to-Drag Ratio (L/D). The ballistic coefficient is a fundamental measure of an object's aerodynamic performance during re-entry. It is defined as the ratio of an object's mass to its drag coefficient. Achieving an optimal ballistic coefficient is crucial for controlling the trajectory and ensuring a controlled descent during re-entry. On the other hand, the L/D represents the aerodynamic efficiency of a re-entry vehicle. It quantifies the ability of the vehicle to generate lift (perpendicular to the direction of motion) relative to the drag (oppos-

ing the direction of motion). A high L/D ratio is desirable for re-entry vehicles, as it enables them to glide and maneuver effectively through the atmosphere, increasing the crossrange capability. This capability is especially important for precision landing, as it allows for controlled adjustments in the trajectory to reach a specific target or landing zone [13, 14]. Section 2.2.1 gives an overview of different re-entry vehicles considered within this research.

The re-entry problem is inherently multidisciplinary, encompassing various scientific and engineering fields that must collaborate to solve its complex challenges. This multidisciplinary nature reflects the intricacies of re-entry, where every aspect, from the vehicle's shape to its guidance and control systems, must harmoniously work together to achieve a successful outcome.

2.2.1 Classification of the Re-entry Vehicles

Re-entry space vehicles are characterised by a broad variety of geometries, external shapes and dimensions. The design choices depend on the mission requirements and the aerothermal-mechanical loads that must be withstood during the mission. However, among this wide range of re-entry space vehicles, some similarities can be identified, both for what concerns the geometry and the longitudinal aerodynamic performance, at least for preliminary studies. In this research, the re-entry vehicles are subdivided into four categories, as similarly done in [13, 15]:

- **Winged Re-entry Vehicles (WRV):** this category includes the re-entry vehicles characterized by a winged configuration, high longitudinal aerodynamic efficiency (max L/D around 2 or higher in hypersonic regime), large range capabilities and the capacity of landing on a runway. This category also includes the concepts of the first stage of rockets that has the capability to land horizontally. The most famous vehicle belonging to this category is the SPACE SHUTTLE Orbiter.

- **Winged Lifting Bodies (WLB):** this group considers re-entry vehicles characterized by a winged configuration featured by large dihedral angle, medium longitudinal aerodynamic efficiency (max L/D around 1.2 in hypersonic regime), and sufficient range capabilities. In some cases, this kind of vehicles may need additional devices for the descent and landing due to low controllability in

subsonic regime. This category includes the NASA X-38, the HL-20 and the Dream Chaser [7, 16, 17].

- **Lifting Bodies (LB):** this category includes re-entry vehicle without wings, and characterized by a low longitudinal aerodynamic efficiency (max L/D around 0.7 in hypersonic regime). These vehicles need additional devices for a safe landing (parafoil or parachute). Examples of this kind of vehicles are Space Rider and IXV [8, 18].

- **Vertical Landing - Reusable Launch Vehicle (VL-RLV):** this class takes into account unconventional re-entry vehicles, especially the first stage of space launchers, that exploit the thrust for decelerating and performing a vertical landing. The iconic example is the Falcon 9 [19]. It worth mentioning that this category is further split into two sub-categories: the former considers space vehicles equipped with planar fins for the aerodynamic control. The latter comprises VL-RLV provided with petals. An example of such application is RRTB (Recovery and Return to Base) concept by Pangea Aerospace [20]. This distinction has been exploited for the definition of the Aerodynamic Database block (Section 4.2.2).

Figure 2.3 shows the categories explained above. Further classes and a more accurate subdivision may be considered. This classification has been done because the research focuses on reusable system and for the definition of two engineering disciplines embedded within the missionisation tool: the Geometry and Mass estimation (GEOM), and the Aerodynamic Database (AEDB) blocks, that can handle only these four disciplines. Said that, the missionisation tool without the GEOM and AEDB disciplines can manage other kind of re-entry or entry vehicles, such as capsules or more in general Non-Winged Re-entry Vehicles (NWRV) [15].

2.3 Recovery Strategies

In this section, an overview of the different re-entry mission profiles depending on the vehicle is given. Two main recovery strategies intended for the reusability of the system are considered: horizontal landing of re-entry vehicles and vertical landing of the first stage of launchers. This section aims at introducing the challenges and the requirements

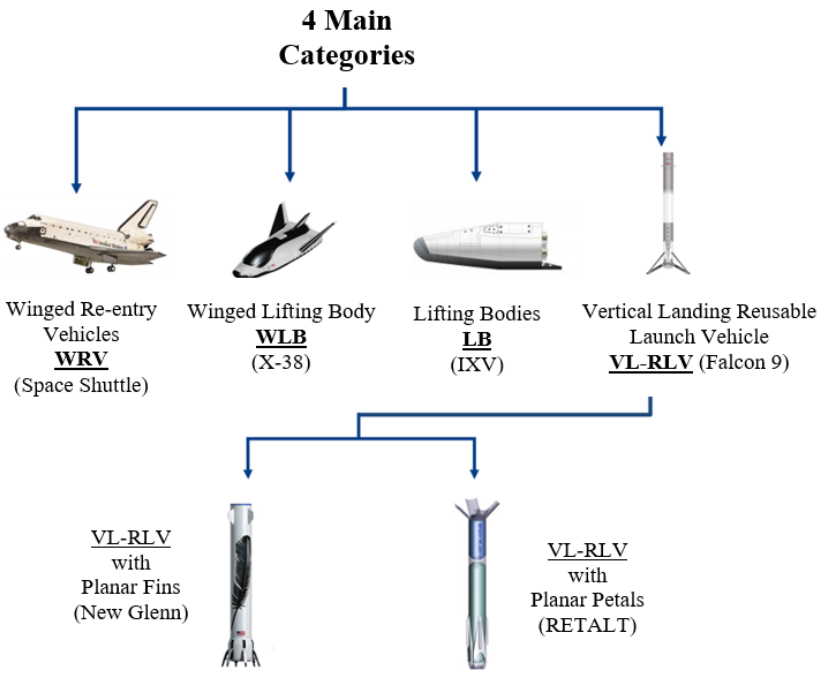

Figure 2.3: *Category subdivision of re-entry vehicles considered within this research [21].*

of the mission. For each solutions, the main characteristics and phases are highlighted.

2.3.1 Horizontal Landing

Commonly, the re-entry systems that follows this strategy, adopt aerodynamic solution to dissipate the kinetic and the potential energy up to the desired level and the re-entry is featured by shallow path. Typically, the re-entry starts at orbital velocity at the EIP, even if it can also be used for sub-orbital applications, in the context of the recovery of first stage of reusable launch vehicles [22]. This recovery strategy has the following phases:

- **Hypersonic atmospheric entry:** This phase starts at 120 km with an initial velocity of about Mach 24 (less for sub-orbital cases). The vehicle flies at hypersonic velocity and dissipates the energy by means of the aerodynamic forces at high altitude. In this phase, the critical aspect are given by the handling of the

aerothermal-mechanical loads, which define the re-entry corridor, and the definition of the trimmability and stability of the vehicle.

- **Terminal Area Energy Management (TAEM):** this phase typically starts at 25 km of altitude at about Mach 2.5 and of a distance of approximately 50 km from the landing site. In this phase the vehicle dissipates the energy in excess and makes the alignment with the Approach and Landing Interface (ALI). The final conditions depend on the ALI strategy adopted. In this phase important parameters are the maximum load factor, the angle of attack corridor for a stable flight (FQA), and stall velocity (flight envelope) [12].
- **Approach and Landing phase:** This last phase includes the final part of the runway approach and the actual landing. The characteristics of this phase depends on the adopted strategy: parafoil, or runway landing. Figure 2.4 reports two examples of approach and landing for the SPACE SHUTTLE (Figure 2.4a), and for X38 (Figure 2.4b).

The guidance strategies for this kind of vehicles usually adopt a modulation of the angle-of-attack and the bank angle in order to manipulate the drag and lift forces and control the downrange and cross range during the flight. For the first two phases, the guidance approaches can be divided into two categories [23, 24]:

- Predicting guidance: the vehicle is able to compute on-board the reference profiles of the commands by predicting the evolution of the flight by means of analytical methods, simplified methods or more complex methods. Some approaches are the predictor-corrector, fast-time prediction and closed-form guidance.
- Tracking guidance: the vehicle tracks reference profiles computed offline. Some of these methods are the path control or terminal control.

For the Approach and Landing phase the guidance method depends a lot on the adopted strategy [12].

2.3.2 Vertical Landing

The re-entry for this kind of mission starts at suborbital velocity, after the Main-Engine-Cut-Off (MECO) and the separation from the second

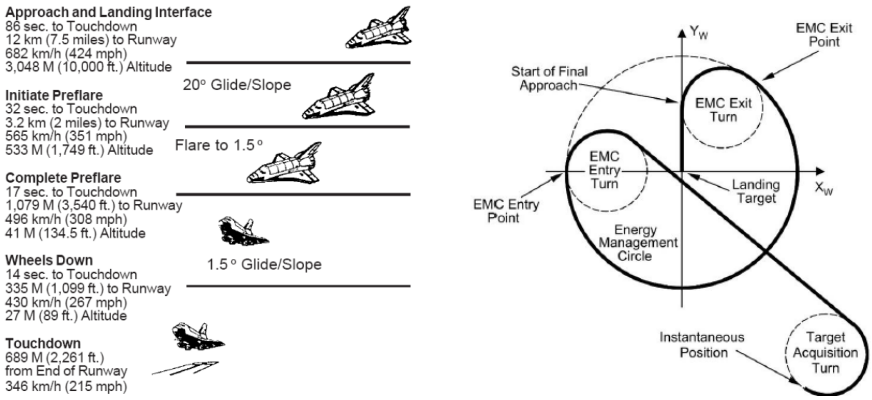

(a) *SPACE SHUTTLE runway A&L (Credits NASA)* **(b)** *X38 Parafoil A&L (Credits NASA)*

Figure 2.4: *Approach and Landing strategies: SPACE SHUTTLE runway A&L (left), X38 Parafoil A&L (right).*

stage occurred. The vehicle performs several maneuvers in order to achieve a pinpoint landing. In most of the case, a powered phase is needed, so a flip-over maneuver is performed to orient the main engine toward the flight direction. Due to the high-ballistic coefficient of the vehicle, a pure aerodynamic solution, by using drag and lift, is not enough to slow down the vehicle and dissipate the energy. Thus, a retro-propulsive maneuver is carried out to reduce the velocity before the aerodynamic phase to decrease the aerothermal-mechanical loads during the flight. Then, in order to have a precise soft landing the engine is switch on again to perform the so-called landing burn.

For the recovery of a first stage of a reusable space launcher two mission profiles are considered. The first one is the Return-to-Launch-Site (RTLS). In this case, the first stage of the space launcher returns towards the launch site or in its proximity, where it performs a precise landing. It includes five mission phases:

1. **Boost-back**: phase to achieve the inversion of the velocity and the targeting landing site;

2. **Ballistic**: phase in high-atmosphere in which the vehicle performs a ballistic flight. Here, the vehicle performs a flip-over manoeuvre to orient the engine toward the flight direction;

3. **Entry Burn**: phase where the vehicle performs the entry burn to reduce the velocity while entering the denser atmosphere. This

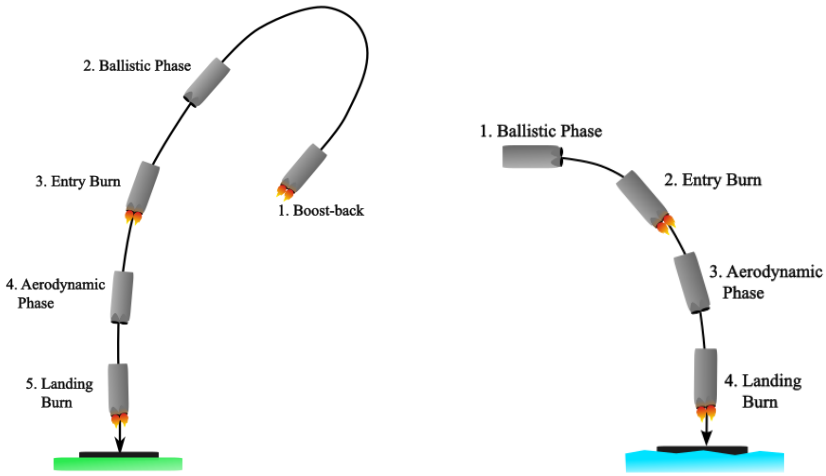

(a) *RTLS* **(b)** *DRL*

Figure 2.5: *First Stage vertical landing recovery scenarios: RTLS left and DRL right.*

phase might not be necessary;

4. **Aerodynamic phase:** phase where the vehicle is controlled with aerodynamic control;

5. **Landing Burn**: phase in which the landing burn is performed to reduce the velocity till the pinpoint touchdown;

The second option is called DownRange Landing (DRL), and it foresees the landing of the rocket first stage on a floating barge in the sea. It consists of four mission phases equal to the RTLS ones except for the boost-back [25, 26]. Figure 2.5 shows the mission profiles for RTLS and DRL.

The atmospheric re-entry, descent and precision soft-landing on Earth is very challenging mainly due to the atmosphere presence which entails uncertainties and nonlinearities, and the fast dynamics involved. This is made possible thank to advanced and adaptive guidance and control methods which, part of a global GNC system, steer the vehicle towards the desired landing site. In particular, these vehicles use a real-time guidance strategy which solves the optimisation problem during the flight taking information from the navigation system. This solution has been demonstrated by Space X, and it is possible by ex-

ploiting a convex representation of the landing problem both during the atmospheric and the powered phases. These methods include for instance the successive convexification and lossless convexification algorithms [27] [28] [29].

2.4 Trajectory Optimisation

In the context of mission analysis and design, a trajectory optimisation routine is a crucial analysis that must be performed. Trajectory optimisation is the technique of designing a trajectory that minimises or maximises a prescribed performance quantity, while satisfying a set of constraints [30, 31]. The generation of an entry trajectory is, in fact, a constrained optimisation problem. These constraints include particular path constraints, some limitation on the control action that can be applied, and boundary conditions. In general, the entry and landing problem is a multiphase optimisation problem and each phase can be characterised by different constraints and objectives. This discipline have been included in the MA and GNC missionisation tool, for the adaptation of the mission analysis and GNC to a particular mission. Depending on the particular requirements and features of a specific mission, the tool is capable to adapt the solution by computing the optimum trajectory and mission profile.

Theoretical background overview

Trajectory optimisation is a particular case of an optimal control problem. A multiphase optimal control problem can be formulated as a collection of P phases as show in Figure 2.6. Commonly, the independent variable t is defined in the region $t_0^{(p)} \leq t \leq t_f^{(p)}$. For many application cases the independent variable t is time and the phases are sequential, such that $t_f^{(p)} = t_0^{(p+1)}$. Generally, neither of these assumptions is required.

The objective of the optimal control problem is to find the control $\boldsymbol{u}(t)^{(p)}$ and a set of parameters, such as the final time of each phase $t_f^{(p)}$, while minimising (or maximising) a cost function J and satisfying a set of constraints. Typically, the constraints of an optimal control problem are:

- **Dynamics constraints:** A system of ordinary differential equations that describes the dynamics of the problem. Typically, this

system constitutes a set of equality constraints:

$$\dot{\boldsymbol{x}}^{(p)}(t) = \mathbf{f}^{(p)}(\boldsymbol{x}^{(p)}(t), \boldsymbol{u}^{(p)}(t), \boldsymbol{p}, t) \tag{2.1}$$

where $\boldsymbol{x}^{(p)}(t)$ is the vector of the state variables, $\boldsymbol{u}^{(p)}(t)$ is the vector of control variables, and , $\boldsymbol{p}$ is the vector of parameters.

- **Path Constraints:** A set of algebraic equality and inequality constraints:

$$\boldsymbol{g}_L^{(p)} \leq \boldsymbol{g}^{(p)}(\boldsymbol{x}^{(p)}(t), \boldsymbol{u}^{(p)}(t), \boldsymbol{p}, t) \leq \boldsymbol{g}_U^{(p)} \tag{2.2}$$

- **Boundary Conditions:** A set of constraints that specifies the conditions at the initial and the final points:

$$\begin{aligned} \boldsymbol{\Psi}_0 &= \boldsymbol{\Psi}^{(1)}(\boldsymbol{x}^{(1)}(t_0^{(1)}), \boldsymbol{u}^{(1)}(t_0^{(1)}), \boldsymbol{p}, t_0^{(1)}) \\ \boldsymbol{\Psi}_f &= \boldsymbol{\Psi}^{(P)}(\boldsymbol{x}^{(P)}(t_f^{(P)}), \boldsymbol{u}^{(P)}(t_f^{(P)}), \boldsymbol{p}, t_f^{(P)}) \end{aligned} \tag{2.3}$$

  where P is the last phase.

- **Simple bounds:** Upper and lower bounds that limits the state and control variables.:

$$\begin{aligned} \boldsymbol{X}_L^{(p)} &\leq \boldsymbol{x}^{(p)}(t) \leq \boldsymbol{X}_U^{(p)} \\ \boldsymbol{U}_L^{(p)} &\leq \boldsymbol{u}^{(p)}(t) \leq \boldsymbol{U}_U^{(p)} \end{aligned} \tag{2.4}$$

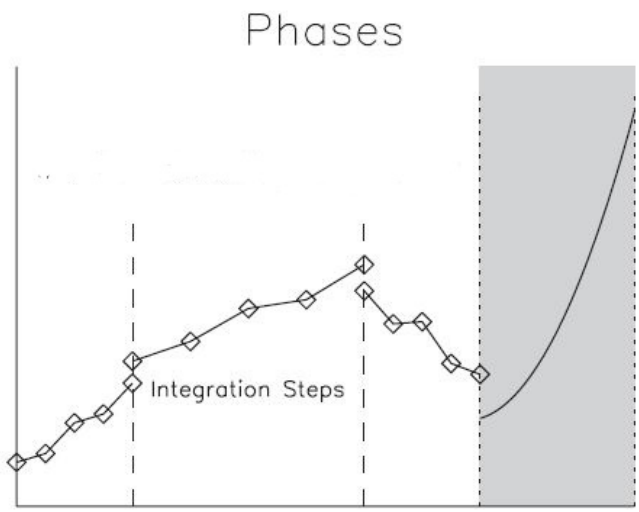

Figure 2.6: *Representation of a multiphase problem [31].*

- **Linkage Conditions:** A set of conditions that guarantee the continuity of the solution among the phases.

$$\begin{aligned}&\boldsymbol{\Gamma}^{(s)}(\boldsymbol{x}^{(s)}(t_f^{(s)}), \boldsymbol{u}^{(s)}(t_f^{(s)}), \boldsymbol{p}, t_f^{(s)}) = \\ &= \boldsymbol{\Gamma}^{(s+1)}(\boldsymbol{x}^{(s+1)}(t_0^{(s+1)}), \boldsymbol{u}^{(s+1)}(t_0^{(s+1)}), \boldsymbol{p}, t_0^{(s+1)})\end{aligned} \tag{2.5}$$

  with $s = 1, ..., P-1$.

The general form of the cost function for a multi-phase optimal control problem is:

$$J = \phi(\boldsymbol{x}^{(p)}(t), \boldsymbol{u}^{(p)}(t), \boldsymbol{p}, t) + \sum_{j=1}^{P} \int_{t_0^{(j)}}^{t_f^{(j)}} w^{(j)}(\boldsymbol{x}^{(p)}(t), \boldsymbol{u}^{(p)}(t), \boldsymbol{p}, t)dt \tag{2.6}$$

So a generic optimal control problem can be described as:

$$\begin{aligned}
\text{minimise} \quad & J = \phi(\boldsymbol{x}^{(p)}(t), \boldsymbol{u}^{(p)}(t), \boldsymbol{p}, t) + \\
& \quad + \sum_{j=1}^{P} \int_{t_0^{(j)}}^{t_f^{(j)}} w^{(j)}(\boldsymbol{x}^{(p)}(t), \boldsymbol{u}^{(p)}(t), \boldsymbol{p}, t)dt \\
\text{subject to} \quad & \\
& \dot{\boldsymbol{x}}^{(p)}(t) = \mathbf{f}^{(p)}(\boldsymbol{x}^{(p)}(t), \boldsymbol{u}^{(p)}(t), \boldsymbol{p}, t) \\
& \boldsymbol{g}_L^{(p)} \leq \boldsymbol{g}^{(p)}(\boldsymbol{x}^{(p)}(t), \boldsymbol{u}^{(p)}(t), \boldsymbol{p}, t) \leq \boldsymbol{g}_U^{(p)} \\
& \boldsymbol{\Psi}_0 = \boldsymbol{\Psi}^{(1)}(\boldsymbol{x}^{(1)}(t_0^{(1)}), \boldsymbol{u}^{(1)}(t_0^{(1)}), \boldsymbol{p}, t_0^{(1)}) \\
& \boldsymbol{\Psi}_f = \boldsymbol{\Psi}^{(P)}(\boldsymbol{x}^{(P)}(t_f^{(P)}), \boldsymbol{u}^{(P)}(t_f^{(P)}), \boldsymbol{p}, t_f^{(P)}) \\
& \boldsymbol{\Gamma}^{(s)}(\boldsymbol{x}^{(s)}(t_f^{(s)}), \boldsymbol{u}^{(s)}(t_f^{(s)}), \boldsymbol{p}, t_f^{(s)}) = \\
& = \boldsymbol{\Gamma}^{(s+1)}(\boldsymbol{x}^{(s+1)}(t_0^{(s+1)}), \boldsymbol{u}^{(s+1)}(t_0^{(s+1)}), \boldsymbol{p}, t_0^{(s+1)}) \\
& \boldsymbol{X}_L^{(p)} \leq \boldsymbol{x}^{(p)}(t) \leq \boldsymbol{X}_U^{(p)} \\
& \boldsymbol{U}_L^{(p)} \leq \boldsymbol{u}^{(p)}(t) \leq \boldsymbol{U}_U^{(p)} \\
& \qquad\qquad\qquad\qquad \text{with} \quad p = 1, ..., P \\
& \qquad\qquad\qquad\qquad \text{and} \quad s = 1, ..., P-1
\end{aligned} \tag{2.7}$$

Solving methodologies

The methods to solve an optimisation problem can be categorised in indirect and direct methods. The indirect methods attempt to find

a minimum by solving the necessary conditions of optimality. They include Pontryagin's Maximum Principle based methods [32]. On one hand, indirect methods can achieve very accurate solutions. On the other hand, they present several drawbacks which make challenging to find an optimal solution for complex problem, for instance they require a priori knowledge of the structure of the optimal solution [30, 31]. Numerical methods that avoid the drawbacks of indirect methods can be found in the direct optimisation methods, which have been studied extensively over the last 30 years, and have proved to be powerful tools for solving practical optimal control problems. The basic idea of direct optimisation methods is to discretise the control problem, and then apply Nonlinear Programming (NLP) techniques to the resulting finite-dimensional optimisation problem.The process of discretising an optimal control problem is called transcription [32]. Several transcription methods exist and the most used ones are [31]:

- **Shooting method:** this technique is based on simulation. It flaws of accuracy when the problem is complex and an extremely good guess solution is not provided. This method can be extended with a multiple shooting technique, which breaks the problem in pieces, which tends to be easier to solve than a single shooting one.

- **Direct collocation:** It works by approximating the state and control variables using polynomial functions. Commonly used collocation schemes are the trapezoidal collocation and Hermite-Simpson collocation. The direct collocation technique is less sensitive to the initial guess with respect to the shooting method, but it has to managed a larger number of decision variables.

- **Orthogonal collocation:** It is a subset of direct collocation, that exploits orthogonal polynomials to approximate the state and control variables.

- **Pseudospectral discretisation:** In pseudospectral discretisation the entire trajectory is represented by a collection of basis functions in the time domain. The basis functions need not be polynomials. Pseudospectral discretisation is also known as spectral collocation. When used to solve a trajectory optimisation problem whose solution is smooth, a pseudospectral method will achieve spectral (exponential) convergence. If the trajectory is

not smooth, the convergence is still very fast, faster than Runge-Kutta methods.

After having applied the transcription to the starting optimal control problem, the resulting NLP has to be solved. The selection of an algorithm is strictly related to nature of the problem, i.e. if it is nonconvex or convex. In one hand, convex problem are relatively easy to solve because a unique global minimum exists. On the other hand, nonconvex ones are typically featured by multiple local minimum that make the problem difficult to be solved. To be clear, a local minimum is defined as a solution x^* for which a function f is smaller than at all other feasible nearby points. A global minimum is instead a point with the lowest function value among all feasible points in the design space. For convex problems, local solutions are also global solutions. Unfortunately, most practical problems are noncovex with numerous local minima, complicating the search for the global optimum. The classical algorithms used to solve an optimal control problem, or more in general an optimisation problem, can be divided in gradient-based algorithms and global optimisation algorithms.

Local, or gradient-based, optimisation algorithms include a broad class of techniques with the common feature of exploiting the information from the gradient of constraints and objective to compute a search direction towards feasibility and optimality. This group includes Sequential Quadratic Programming (SQP) [33] algorithms and Interior-Point methods (IPMs) [34].

Global algorithms are based on heuristic and metaheuristic methods that emulate some natural processes to convergence to the global optimum. Examples of these algorithms are Genetic Algorithm (GA) [35] and Particle Swarm Optimisation (PSO) [36].

Both methodologies have advantages and drawbacks. For gradient-based algorithms, the convergence is affected by the selection of the initial starting guess and the optimiser may convergence to a local optimum. However, if the gradient can be computed efficiently, the computational cost of these methods may be far less with respect to the global optimisation. For what concerns global optimisation algorithms, the information of the gradient and the initial guess are not necessary, in fact, they rank the solution depending on the constraints violation and the objective function, and update the solution exploiting a random search and by imitating nature-based heuristic methods, starting from a randomly-defined initial guess. On the other side, global algo-

rithms requires larger number of function evaluations, resulting on a slow convergence, and they are very sensitive to the setting parameters. For these reasons, global and local algorithms are used in synergy by exploring the domain first and then refining the solution.

2.5 Multidisciplinary Design Optimisation

Multidisciplinary Optimisation (MDO) is a vast and diverse research domain that spans various facets, including strategies for problem decomposition and formulation, MDO frameworks, and related areas such as engineering modeling, global and local optimisation, sensitivity analyses, and metamodeling techniques. Due to the extensive scope of this field, it is not feasible to provide a comprehensive overview within the constraints of length limitations, nor is it the primary focus of this dissertation. Nevertheless, this section aims at offering an overview, with a particular emphasis on topics closely connected to this research.

The general mathematical formulation of an MDO problem can be written in this way [37, 38]:

$$\begin{aligned}
&\text{minimise} \quad \boldsymbol{f}(\boldsymbol{X}) \\
&\text{with} \quad \boldsymbol{X} = [\boldsymbol{X}_1, \boldsymbol{X}_2, ..., \boldsymbol{X}_{N_d}]^T \\
&\text{such that} \\
&D_i(\boldsymbol{X}_i, \boldsymbol{X}_{ij}, \boldsymbol{Y}_i) = 0, \quad i = 1, ..., N_d \\
&g_i(\boldsymbol{X}_i, \boldsymbol{X}_{ij}, \boldsymbol{Y}_i) \leq 0, \quad i = 1, ..., N_d \\
&\boldsymbol{X}_{LB} \leq \boldsymbol{X} \leq \boldsymbol{X}_{UB}
\end{aligned} \tag{2.8}$$

where $\boldsymbol{f}(\boldsymbol{X})$ are the objective functions (in general multiple objective can be considered), N_d is the number of the disciplines. $\boldsymbol{X}$ is the vector of design variables, $\boldsymbol{X}_i$ are the design variables for the discipline i, $\boldsymbol{Y}_i$ are the output of the ith discipline, while $\boldsymbol{X}_{ij}$ are the coupling variables. $D_i(\boldsymbol{X}_i, \boldsymbol{X}_{ij}, \boldsymbol{Y}_i)$ and $g_i(\boldsymbol{X}_i, \boldsymbol{X}_{ij}, \boldsymbol{Y}_i)$ are the state equations representing the analysis model of the disciplines, and the respective constraints. The design variables typically have a lower ($\boldsymbol{X}_{LB}$) and an upper ($\boldsymbol{X}_{UB}$) bound.

One crucial aspect to address when implementing MDO is the organisation of discipline analysis models, and optimisation software in harmony with the problem formulation, all with the goal of achieving an optimal design. This procedure is tackled with decomposition techniques [39]. A multidisciplinary problem can be decomposed in different ways, which imply different optimisation architecture. The

different disciplines, in fact, can be either optimised simultaneously within a unique system or individually [37, 40]. Two primary architectures can be identified: single-level MDO and multi-level MDO.

In a single-level MDO architecture, all disciplines and subsystems are considered simultaneously within a single optimisation framework. This approach is suitable for problems where interactions between disciplines are relatively simple, and it allows for a holistic optimisation of the entire system. It is often more computationally efficient than multi-level MDO, as it avoids the complexities associated with nested optimisation loops. Three single-level methods are:

- *Multi Discipline Feasible:* The Multi Discipline Feasible (MDF) method is the most used one. It is also named "Nested Analysis and Design" (NAND), "Single NAND-NAND" (SNN) and "All-in-One". The architecture of the MDF method is similar to the one of conventional optimisation problem with a single system. However, a fundamental distinction in MDF lies in the fact that the discipline of the classical optimisation problem is replaced by a complete multidisciplinary analysis. This MDA is executed at each iteration. Thus, all the subsystems are coupled in an analysis module that assesses the feasibility of the solution at each iterative step. Once the MDA is evaluated, the analysis module output vector is used by the system-level optimiser to compute the cost function and the constraints. Within this method, the the optimisation algorithm control only the design variables $\boldsymbol{X}$ [39, 37].

- *Individual Discipline Feasible:* The Individual Discipline Feasible (IDF) formulation allows to avoid to evaluate a complete MDA at each iterative step of the optimisation process. The primary distinction between MDF and IDF lies in the role of the optimiser. In IDF, the optimiser assumes the additional responsibility of coordinating the various subsystems and employs extra variables, the coupling variables ($\boldsymbol{X}_{ij}$), to facilitate this coordination. In each iteration, the individual subsystems are independently feasible, but the coupling consistency is not guaranteed. This method permits to break up the original problem into several subsystems. Thus, additional compatibility constraints are imposed that has to be satisfied once convergence is met. Consequently, the IDF process should not be stopped till convergence is reached. This decomposition method increases the number of optimisation variables

and constraints, however parallelisation among the disciplines is possible.

- *All-At-Once:* in All-At-Once (AAO) neither individual discipline feasibility nor multidisciplinary feasibility is guaranteed, instead they have to be satisfied by the optimisation algorithm. This approach uses the optimisation process to concurrently optimise the design of the system and to solve the governing equations. It maintains direct control over the values of all design, state (dependent disciplinary variables), and coupling variables. In AAO, full disciplinary analyses are bypassed, and the governing equations serve the purpose of assessing the residuals exclusively. It is the responsibility of the single-level optimiser to meet these equations with the help of additional disciplinary compatibility constraints. Consequently, the AAO method does not ensure any form of feasibility until convergence is achieved, but it offers the advantage of skipping time-consuming analyses in favor of much faster residual evaluations. The AAO is the easiest way to solve MDO problems, however, for complex subsystems, the number of variables and constraints to be managed by the optimiser may explode.

Within this research, the MDF method has been employed, especially due to use of metamodeling technique [38]. However, also the AAO approach can be used by exploting the Trajectory Optimisation block, since it can handle parametric optimisation.

On the other hand, multi-level MDO architecture involves a hierarchical approach. It divides the system into multiple levels, with each level optimising a specific aspect of the design. This approach is especially useful when dealing with highly complex systems where the interactions between disciplines are intricate and may require separate optimisation efforts. Multi-level MDO typically includes nested optimisation loops, where higher-level optimisations influence the parameters and constraints at lower levels. The simplest example of multi-level MDO is given by the *Collaborative Optmisation* (CO) [37, 40].

The choice between single-level and multi-level MDO architectures depends on the nature of the design problem and the trade-offs between computational complexity and accuracy. Single-level MDO is more straightforward and computationally efficient but may not capture all nuances of the system. Multi-level MDO, while more intricate, provides a more comprehensive understanding of the design space and can lead

to improved solutions in highly complex and interconnected systems.

Both single-level and multi-level MDO architectures play a vital role in the field of engineering and design, offering flexible tools to tackle a wide range of optimisation challenges in the quest for more efficient and innovative solutions. Joaquim R.R.A. Martins [37] provides a survey of all the architectures in the literature using an unified description.

The second crucial aspect of MDO is the optimisation method. The discussion, in this case, is very similar to the one done for the trajectory optimisation. The main point here is the selection among a gradient-based (or local) optimisation algorithm, and global ones. One of the biggest advantages on using global algorithms is given by the fact that gradient-based techniques are not well suited to multi-objective optimisation. If the problem formulation is extended to N_{OBJ} contrasting criteria, to be concurrently optimised, the typical optimality definition based on the objective function value is not applicable, and has to be replaced by the concept of Pareto-optimality. A solution is said to be non-dominated or Pareto-optimal, if a given objective cannot be improved without degradation of any of the others. Commonly, for multi-objective problems a set of non-dominated optimal solutions exists, and it is called Pareto front. The objective of optimisation is to attain a set of solutions that not only closely approximate the actual Pareto front of the problem but also exhibit a uniform distribution of solutions across its entire range. Within this thesis, a Multi-Objective Particle Swarm Optimisation (MOPSO) algorithm has been included in the Missionisation Layer of the tool.

2.5.1 Metamodeling Techniques

As previously mentioned, the computational effort involved in MDO is contingent on the chosen MDO architecture and the evaluation of disciplinary analyses. To mitigate the computational efforts associated with demanding black-box optimisation problems, techniques known as Metamodel-based Design Optimisation (MBDO) have been developed. In this context, the MDO problem is treated as a constrained nonlinear optimisation problem, with the MDA process being substituted by a surrogate model.

Within the realm of literature, one can find various Metamodel-based MDO methods, categorized into static and dynamic approaches. In the former, metamodels are generated based on a predefined set of samples, while in the latter, metamodels are adaptively refined

throughout the optimisation process. It is essential to emphasize that the predictive accuracy of these metamodels must be verified to ensure the accuracy of the results. Several techniques utilized for creating these metamodels include:

- **Polynomial response surface method**: this method exploits a multivariate linear regression function to fit the simulation model or the MDA process;
- **Radial Basis Functions (RBF)**: this approach is an interpolation method based on the function value at the sample points;
- **Kriging** this method uses optimal estimation interpolation technique by combining a global approximation model and stochastic process;
- **Artificial Neural Networks**: this method employs artificial neural networks to approximate the nonlinear functions. This group includes Feed-Forward Neural Networks (FFNN) and Radial Basis Function Neural Networks (RBFNN);
- **Multivariate Adaptive Regression Splines (MARS)**: it is a regression procedure that automatically models nonlinearities and interactions through fitting functions.
- **Support Vector Regression (SVR)**: this technique is one of the most popular supervised learning algorithms, which is used for classification and regression problems

These techniques have unique features and the most suitable one depends on the problem itself. Two criteria that may be taken into account for the selection of the metamodel method are the accuracy of the prediction [38], and the computational effort needed to build the surrogate model. Within this research, Gaussian Basis Functions have been employed due to their flexibility, and computational efficiency. Moreover, depending on the choice of RBF and its parameters, it can provide global approximation or focus on local behavior, which is valuable for different modeling scenarios.

"With great power there must also come great responsibility."
Uncle Ben - Spider Man

CHAPTER 3

MA and GNC Missionisation Tool

THIS chapter presents an overview of the MA and GNC missionisation tool architecture. The tool has been written in `MATLAB` and it has been built by following a modular and structured approach with the objective to obtain a software which is easy to set up, maintain, improve over time, and that can be exploited for a broad variety of cases. The idea behind the software is to have a multidisciplinary tool that can be used in different stages of the design process with the level of accuracy and complexity defined by the user. The development of a unique multidisciplinary tool aims at solving complex multidisciplinary analyses required by the missionisation in an efficient way. This goal is pursued through a structured organisation of disciplines and the I/O parameters of each elements of the tool. Moreover, the modular structure of the tool allows the integration of external modules, as well as the testing and validation of the single parts.

The chapter describes the High-Level architecture of the tool in Section 3.1, explaining the main modules. An overview of the so-called Missionisation Layer is given in Section 3.1.3. Section 3.2 presents the Design Structure Matrix (DMS) to synthesise the multidisciplinary design analysis core of the tool, while Section 3.3 highlights the mod-

ularity and the flexibility of the tool.

3.1 High-Level Architecture of the Tool

Figure 3.1 shows the High-Level architecture of the missionisation tool. The tool is constituted by three main modules and two submodules. The three main modules are the User Interface, the MDA core and the Missionisation Layer, while the submodules are the Post-Process unit and the auxiliary functions. Each part of the tool has specific tasks that allows the user to set up the problem, perform the analysis, display and store the results. The information flow and the functional breakdown of the tool is reported in Figure 3.2.

3.1.1 User Interface

The User Interface is constituted by the input file and has the objective to build the problem that the user wants to study. It sets up all the parameters related to the environment, the mission scenario and the vehicle. From the User Interface, it is possible to specify all the configuration and setting parameters needed by each discipline to perform the analysis, such as the domain of interest, the discretisation points and customised function handles. Moreover, the user can define the analyses to be run by setting which disciplines have to be called, and the tasks of the Missionisation Layer.

The input file is based on a standard and structured organisation of

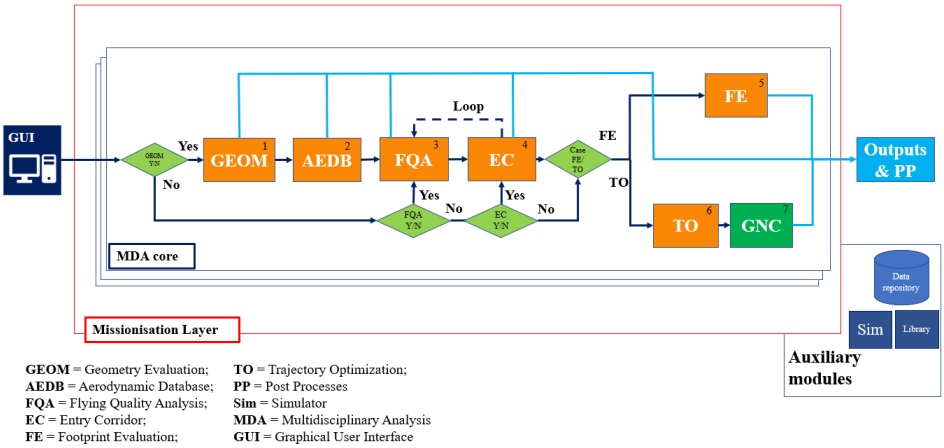

Figure 3.1: *High-Level architecture of the MA and GNC missionisation tool.*

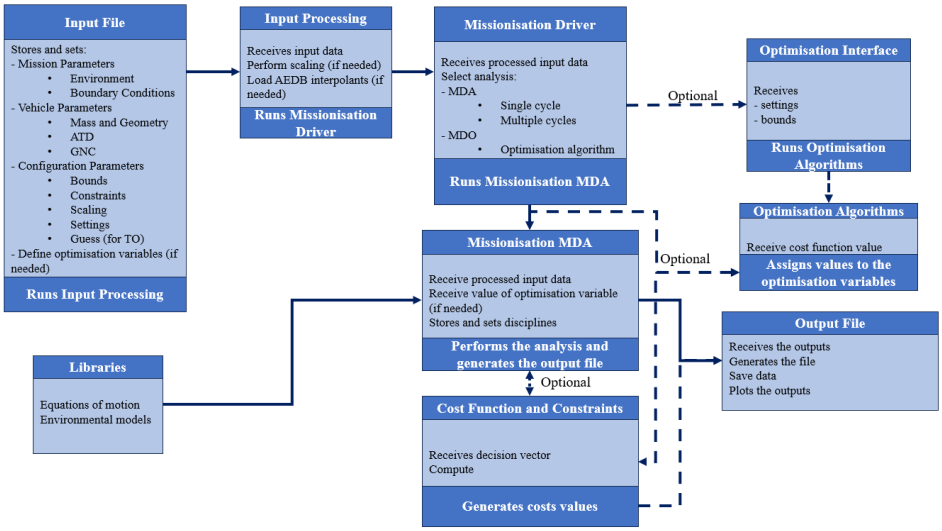

Figure 3.2: *Information flow visualisation of the MA and GNC missionisation tool.*

the parameters used to define the problem. The objective is to have a common approach to tackle a general re-entry problem. The user can define either new mission scenario or different versions of the same mission. The organisation of the parameters has been developed in three levels. The first level indicates the main category of the parameters and it can be of three types:

- **Mission:** set of parameters used to describe the mission scenario and the environment;
- **System:** set of variables to characterise the vehicle and its subsystems;
- **Configuration:** set of parameters used to specify the settings of the tool and each discipline;

Regarding the category of "Mission", the second level is defined by:

- **Flight Scenario (FS)**: it includes the variables to define the mission scenario. This second level is further subdivided into a third level, which is constituted by these fields:
  - ENV: parameters for the characterisation of the environment;
  - BC: variables for the definition of the boundary conditions, such as EIP and landing positions;

- **ConOps**: it defines the phases of the mission. So far, it has only one field:
  - VMM: parameters to describe the features of the phases of the mission.

For what concerns the "System" level, the second level is constituted by:

- **MCI**: this field handles all the parameters for the characterisation of the mass and geometry of the vehicle. This level has the following fields:
  - MASS: variables which specify the mass budget of the vehicle;
  - GEOM: parameters to define the geometry of the vehicle;
  - INER: specification of the inertia of the vehicle;
- **ATD**: it includes variable for the definition of the AEDB and the thermal model. The fields are:
  - AEDB: definition of the aerodynamic database;
  - TDB: definition of the thermal model;
- **GNC**: it considers the variables of the GNC, such as reference profiles for the guidance, parameters for the control and the constraints of the vehicle. This level has the following fields:
  - GUID: parameters related to the guidance;
  - NAV: parameters related to the navigation;
  - CON: control parameters;
  - CONS: constraints of the vehicle. It includes also the specification of the propulsive subsystem if present;

Each variable used for the description of the problem enters in one of these structures. For instance, the parameter to define the Earth angular speed is given by `mission.fs.env.omE`.

The parameters included in these two levels are characterized by an attribute, that can be used by the user to keep track of the variant parameters for different mission versions and specify if a parameter must be optimised by the Missionisation Layer. The attributes are:

- **Invariant:** data that never change from mission to mission (for a specified vehicle and environment);

- **Variant:** Data that can change from mission to mission (for a specified vehicle and environment);
- **Optimization:** Variables that must be optimised;

For what concerns the "Configuration" level, the second level embeds the following fields:

- **GEOM**: Parameters to set-up the Geometry and Mass tool;
- **AEDB**: Parameters to set-up the Aerodynamic Database tool;
- **FQA**: Parameters to set-up the Flying Qualities Analysis tool;
- **EC**: Parameters to set-up the Entry Corridor tool;
- **FE**: Parameters to set-up the Footprint Evaluation tool;
- **TO**: Parameters to set-up the Trajectory Optimisation tool;
- **GNC**: Parameters to set-up the GNC tool;
- **shared**: Parameters which are shared by more disciplines;

This scheme has been used to define all the inputs of each discipline embedded in the MDA core. For the disciplines that have customisable functions (see Section 4.2), the user has to follow the same procedure to define the input parameters. The same discussion is applied whenever a new discipline is added to the MDA core, or a specific discipline is substituted by an user-defined one.

3.1.2 MDA core

The main module of the software is the MDA core. It comprehends a minimum set of disciplines to assess the performance required during the design of a re-entry mission. Section 4.2 describes in detail the engineering modelling of the disciplines included, however a brief overview is given below. The missionisation tool includes:

- Geometry and Mass estimation tool (GEOM), which estimates the reference surface and dry mass of the vehicle from a minimum set of geometric parameters.
- Aerodynamic Database tool (AEDB), which provides a representative AEDB of the vehicle, if needed.

- Flying Qualities Analysis tool (FQA), which computes the domain where the vehicle can fly in a trimmed and stable configuration;
- Entry Corridor Analysis tool (EC), which evaluates the domain in which the vehicle can fly without violating the aerothermal -mechanical loads.
- Footprint Evaluation tool (FE), which computes the feasible range capability of the vehicle.
- Trajectory Optimization tool (TO), which solves single or multi-phase optimal control problem and computes an end-to-end mission profile.
- Guidance, Navigation and Control tool (GNC), that allows an automatic translation of the output of the TO tool in a format required by external GNC models.

As shown in Figure 3.1, these disciplines are strictly interconnected, especially in term of input/output relation. The inputs parameters of a discipline are the outputs of a previous one. The MDA core allows for carrying out the complex multidisciplinary analyses required by the MA and GNC missionisation by accounting for the coupling between the variables and the disciplines within a unique tool.

3.1.3 Missionisation Layer

The Missionisation Layer is the external layer of the tool, that can exploit the MDA core for several purposes. The analyses that can be performed range from a single MDA cycle, parametric and preliminary sensitivity analysis, to a parametric optimisation of both mission and system parameters specified by the user as reported in Section 3.1.1. The kind of analysis is specified in the input file, and the process is ruled by the Missionisation Driver as shows in Figure 3.2.

Multidisciplinary Design Analysis

The first kinds of analysis that can be performed with the Missionisation Layer are the single MDA cycle and the parametric MDA analysis. The single MDA cycle is used to analyse and design a specific mission scenario or different versions of the same mission. In this case the input parameters are scalar and are considered fixed by the Missionisation Layer. The user collects the required data, sets the input file and runs the simulation.

The parametric MDA analysis, instead, runs multiple MDA cycles in a set of prescribed values of the input parameters specified by the user. In this case, it is possible also to apply user-defined uncertainties to the parameters. The variation of the values of the inputs can be both predefined by the user or randomly generated. The output of routine are used to create performance maps of the figures of merit, and perform preliminary sensitivity and correlation analysis, in order to evaluate the mission capability and performance with respect the inputs parameters. This application can support the mission design lifcycle in different phases of the design process.

Multisciplinary Design Optimisation within Missionisation

The Missionisation Layer can also perform a parametric optimisation of both mission and system parameters. This case is similar to the parametric MDA analysis, but the values of the inputs parameters are ruled by an optimiser to maximise or minimise a set of figures of merit. The followed approach is the same of the Multidisciplinary Design Optimisation (MDO) [39, 41, 42], but within the missionisation the objective is to support the mission design process rather than the accurate definition of the optimal design of a re-entry vehicle. In particular, the MDO capability of the Missionisation Layer can be exploited to pursue the following goals:

- Optimal tuning of a set of design mission and system parameters concerning specific requirements of a mission scenario. This case typically applies to the last phases of the design process in order to adapt the MA and GNC solution to the particular scenario.

- Evaluation of the mission performance of different concepts with respect to the design mission and system parameters to help the user to identify and explore promising regions of the search space domain during the design process. This approach is followed during the early phase of the design to perform trade-offs studies and to provide robust solutions options in terms of mission analysis already at this stage.

In both cases, the MDO allows the simultaneous variation of the design variables by taking into account the connections and the dependencies between the disciplines considered and optimising the desired performance. The Missionisation Layer can manage both single

objective and multiobjective problems. The capability of the Missionisation Layer can be increased in future development, by including higher-fidelity disciplines within the MDA cycle.

The basic MDO framework implemented within the Missionisation Layer follows two approaches. The first one employs a Multi-Objective Particle Swarm Optimisation algorithm, while the second method uses a metamodelling technique to approximate the original problem and compute the optima. In both cases, the optimisation problem has been formulated with the Multidisciplinary Feasible (MDF) architecture, in which the optimiser manages only the "real" design variables and ensures the multidisciplinary feasibility at each evaluation along the optimisation process [39, 41, 42, 37].

Multi-Objective Particle Swarm Optimisation

MOPSO, is an extension of the single objective Particle Swarm Optimisation (PSO). MOPSO is a population-based stochastic algorithm that employs the coordinated movement of a swarm of particles [43]. MOPSO is very efficient and effective in solving multiobjective problems, and it has been used extensively in the literature in the fields of spacecraft and launcher design. The working principle of the MOPSO is equal to the PSO, but employs Pareto-dominance principles to select the set of non-dominated solutions and build the Pareto Front [43].

Figure 3.3 schematises the PSO algorithm. First, an initial random set of solutions of the optimisation problem is generated, and the cost function and the constraints are evaluated. In PSO, each solution $\boldsymbol{X}$ is called particle, while the set of solution is the swarm. After having evaluated the model, the particle personal best position ($pbest$, y_{ij}^{k}) and

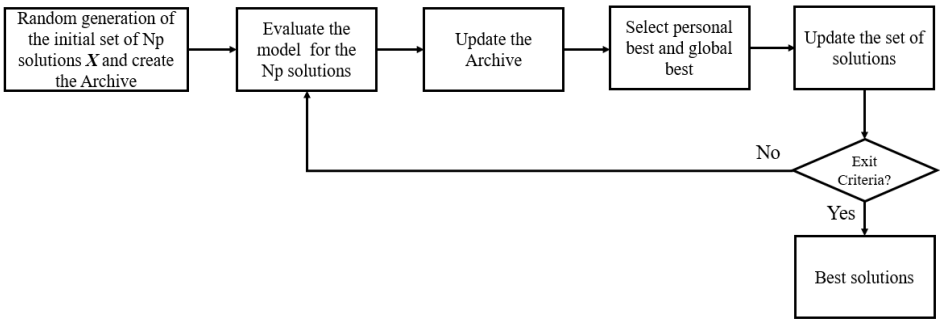

Figure 3.3: *Visualisation of the PSO algorithm.*

the global best position (*gbest*, $\hat{y}_j^k$) are selected, and the solutions are updated with the following equations:

$$\begin{aligned} v_{ij}^{k+1} &= wv_{ij}^k + c_1 r_1 (y_{ij}^k - x_{ij}^k) + c_2 r_2 (\hat{y}_j^k - x_{ij}^k) \\ x_{ij}^{k+1} &= x_{ij}^k + v_{ij}^{k+1} \end{aligned} \tag{3.1}$$

In Eq.(3.1), v_{ij}^k is the velocity of the particle i in the dimension $j = 1, ..., n_x$ at the iteration k, x_{ij}^k is the position of the particle i in the dimension j at the iteration k. w is the inertia constant, c_1 and c_2 are the cognitive and social acceleration constants, while r_1 and r_2 are random values in the range of [0, 1], with a uniform distribution. Moreover, the algorithm includes a function that corrects the positions of the particles that exceed the defined bounds.

The *pbest* is the best position that the particle i has visited since the first step. *gbest*, instead, is the best position found by any of the particle so far [39, 36]. This operation is done iteratively till the exit conditions are met.

During the optimisation process, the MDA cycle has to be evaluated multiple times, in particular $N_p \times N_{gen}$, where N_p is the number of the particles and N_{gen} is the number of the generation (or the iteration). This may require a large computational time depending on the evaluation time of a MDA cycle. For these reason, metamodelling techniques have also been explored within this work.

Metamodelling Technique

The second approach employs a DEIMOS Space proprietary tool called EDLS/GNC Sizing and Analysis (ESAT) [44], which exploits a metamodelling technique to approximate the original problem and to support trade-off process [38]. It has been successfully used by DEIMOS for the MDO of EDL systems for Mars and Titan explorations [45, 46]. ESAT is a metamodelling tool that generates performance maps by evaluating a user-defined external module seen as a black box. ESAT calls such external module in a prescribed set of sample points, and it interpolates the obtained responses with Radial Basis Functions (RBFs), in order to get predictions of the performances in any point of the search space domain. Furthermore, ESAT can exploit the metamodel to solve single or multiobjective problems.

As reported above, ESAT uses Gaussian RBFs to build the surrogate model. A general RBF metamodel can be formulated as (Eq.(3.2)):

$$f_{RBF}(\boldsymbol{z}) = \hat{\boldsymbol{y}} = \sum_{i=1}^{N} \omega_i \phi(||\boldsymbol{z} - \boldsymbol{z}_i||) \tag{3.2}$$

where N is the number of sample points; $\phi(||\boldsymbol{z} - \boldsymbol{z}_i||) = \phi(r)$ is the radial function. In this case, the radial function is given by the Gaussian shape $\phi(r) = -e^{-cr}$. ω_i are the weight coefficients, and c is the shape parameter, which affects the conditioning of the problem [38]. The coefficient vector $\boldsymbol{\omega}$ is calculated in this way (Equation 3.3):

$$\begin{aligned} \boldsymbol{\omega} &= \boldsymbol{A}^{-1}\boldsymbol{y} \\ \boldsymbol{y} &= [y_1, y_2, ..., y_N]^T \\ \boldsymbol{A} &= \begin{bmatrix} \phi(||\boldsymbol{z}_1 - \boldsymbol{z}_1||) & \dots & \phi(||\boldsymbol{z}_1 - \boldsymbol{z}_N||) \\ \vdots & \ddots & \vdots \\ \phi(||\boldsymbol{z}_N - \boldsymbol{z}_1||) & \dots & \phi(||\boldsymbol{z}_N - \boldsymbol{z}_N||) \end{bmatrix}_{N \times N} \end{aligned} \tag{3.3}$$

However, in the literature several metamodeling methodologies exist [38, 47, 48, 49]. Future development of the MA and GNC missionisation may include different metamodeling techniques.

The advantage of this approach is that the number of calls needed to create the surrogate model is commonly smaller than the one used by an heuristic methods to converge [38]. Moreover, the evaluation time of the metamodel (the performance maps) is much lower than the run time of the external module, in fact the surrogate can be probed practically in real time on consumer hardware. Nevertheless, the metamodel accuracy must be verified, especially when the problem has a high number of design variables [38, 47]. It worth highlighting that the evaluation of the MDA core for both MOPSO and ESAT can be performed in parallel to save computational time.

3.2 Design Structure Matrix

An essential step in creating a versatile multidisciplinary tool involves conducting a critical analysis to uncover the interconnections between the various disciplines comprising the tool. This examination enables to discern the specific input parameters required by each discipline to execute its functions. Additionally, it reveals the interconnectedness between these disciplines and identifies the existence of any feedback loops. To facilitate this comprehensive process, various methodologies can be employed, with one of the most prevalent being the Design

Configuration	C1	C2	C3	C4	C5	C6	C7	OUTPUTS
System and mission (variant/invariant)	P1	P2	P3	P4	P5	P6	P7	
System and Mission Optimization	X1	X2	X3	X4	X5	X6	X7	
	GEOM(1)	X12		X14	X15	X16		Y1
		AEDB(2)	X23					Y2
			FQA(3)	X34	X35	X36	X37	Y3
			X43	EC(4)	X45	X46		Y4
					FE(5)			Y5
						TO(6)	X67	Y6
							GNC(7)	Y7
								FoM, performance

MDA Core Missionisation Layer

Figure 3.4: *Design Structure Matrix of the MDA core of the MA and GNC missionisation tool with all the disciplines considered.*

Structure Matrix (DSM) approach. DSM offers a powerful means of visualizing all the disciplines and their interactions in a single, unified diagram, offering a holistic overview of the multidisciplinary endeavor. [50]. The DSM shows in a matrix form the following information:

- Diagonal: disciplines which constitute the MDA cycle;
- Columns: Input parameters requested by a discipline and Input variables from other disciplines;
- Rows: Output parameters of a discipline;

When two disciplines share both inputs and outputs, this creates an internal loop, necessitating a convergence process to ensure that both disciplines conduct their analyses in a coherent manner.[44].

Figure 3.4 shows an example of DSM for the MDA core of the missionisation tool when all the disciplines are considered. In the figure, $\mathbf{C}_j$ are the configuration parameters for discipline j, $\mathbf{P}_j$ are the system and mission parameters (both variant and invariant) for discipline j, $\mathbf{X}_j$ are the optimisation variables for discipline j, while $\mathbf{X}_{ji}$ are the coupling variables, i.e. the outputs of the discipline j that are inputs for discipline i. Lastly, $\mathbf{Y}_j$ are the outputs of the discipline j.

Since the tool can be used for different analysis, the considered disciplines, and so the parameters, modify depending on the analysed

scenario and the DSM can change. However, Figure 3.4 gives an idea for a general case.

In this case, the MDA cycle is constituted by the sequential execution of geometry and mass, aerodynamic, flying qualities, entry corridor, landing footprint, trajectory and GNC tuning analyses. The DSM easily shows the dependencies between the disciplines, for instance the outputs of the GEOM affect the EC, the FE and the TO, since the estimated mass and reference surface are used in the models of these disciplines. Furthermore, it can be noted that between FQA and EC exists a loop, because the computation of the trim line affects the existence of a feasible entry corridor (Section 4.2). Table 3.1 reports a qualitative definition of the parameters which enters in the DSM analysis reported in Figure 3.4. $\mathbf{X}_j$ must be specified only if the optimisation routine is considered within the Missionisation Layer.

3.3 Modularisation of the Tool

As introduced in the previous sections, the MA and GNC missionisation tool has been developed with a layered structure, emphasizing the separation and modularity of disciplines as much as possible. This feature simplifies future improvement, such as the embedment of more complex models and higher-fidelity disciplines, and maintenance.

The developed multidisciplinary tool exhibits remarkable flexibility, adapting seamlessly to diverse applications and scenarios. Its inherent versatility empowers users to tailor its functionality to specific needs, making it a dynamic solution capable of addressing a wide range of interdisciplinary challenges. Figures from 3.5 to 3.7 show how the High-Level architecture of tool modifies depending on the scenarios analysed within this work (Section 6), reporting, in particular, the active and inactive disciplines. The tool have been applied to different vehicle classes, such as Lifting Bodies, Winged Re-entry Vehicles, and Vertical Landing RLV, by considering different stages of the mission design process.

Table 3.1: *Qualitative definition of the parameters for the DSM in Figure 3.4. $\boldsymbol{X}_j$ are kept void, since they are specified only if an MDO routine is taken into account.*

ID	Parameters	ID	Parameters
$\boldsymbol{P}_1$	Vehicle class, Aero-mechanical loads, Payload mass, Vehicle dimensions	$\boldsymbol{X}_{12}$	Slenderness ratio, Wing aspect ratio
$\boldsymbol{P}_2$	Vehicle class	$\boldsymbol{X}_{14}$	Reference surface, Mass
$\boldsymbol{P}_3$	Max and Min flap deflection, MRC position, CoG position w.r.t. MRC	$\boldsymbol{X}_{15}$	Reference surface, Mass
$\boldsymbol{P}_4$	Aerothermal-mechanical loads, Environment parameters, Boundary conditions	$\boldsymbol{X}_{16}$	Reference surface, Mass
$\boldsymbol{P}_5$	Environment parameters, Boundary conditions	$\boldsymbol{X}_{23}$	Untrimmed AEDB
$\boldsymbol{P}_6$	Environment parameters, Vehicle parameters Boundary conditions, Number of phases	$\boldsymbol{X}_{34}$	Trimmed AEDB, AoA trim line
$\boldsymbol{P}_7$	Environment parameters, Vehicle parameters Boundary conditions	$\boldsymbol{X}_{35}$	Trimmed AEDB, AoA trim line
$\boldsymbol{C}_1$	Flags	$\boldsymbol{X}_{36}$	Trimmed AEDB, AoA trim line
$\boldsymbol{C}_2$	Flags	$\boldsymbol{X}_{37}$	AoA trim line
$\boldsymbol{C}_3$	AoA, Ma ranges, discretisation points, Flags	$\boldsymbol{X}_{43}$	AoA trim line
$\boldsymbol{C}_4$	Discretisation points, Guesses, Scaling, Flags	$\boldsymbol{X}_{45}$	Entry corridor bounds
$\boldsymbol{C}_5$	Discretisation points, Flags	$\boldsymbol{X}_{46}$	Entry corridor bounds
$\boldsymbol{C}_6$	Functions handles for cost and constraints Bounds, Nodes number, Guess	$\boldsymbol{X}_{67}$	Reference trajectory
$\boldsymbol{C}_7$	Functions handles for GNC specifications GNC parameters	$\boldsymbol{Y}_1$	
$\boldsymbol{X}_1$	-	$\boldsymbol{Y}_2$	Dry mass, Reference Surface, Slenderness and Wing aspect ratios
$\boldsymbol{X}_2$	-	$\boldsymbol{Y}_3$	Trimmed AEDB, AoA trim line
$\boldsymbol{X}_3$	-	$\boldsymbol{Y}_4$	Entry corridor bounds
$\boldsymbol{X}_4$	-	$\boldsymbol{Y}_5$	Landing footprint
$\boldsymbol{X}_5$	-	$\boldsymbol{Y}_6$	Reference trajectory Optimised parameters
$\boldsymbol{X}_6$	-	$\boldsymbol{Y}_7$	Tuned GNC parameters
$\boldsymbol{X}_7$	-		

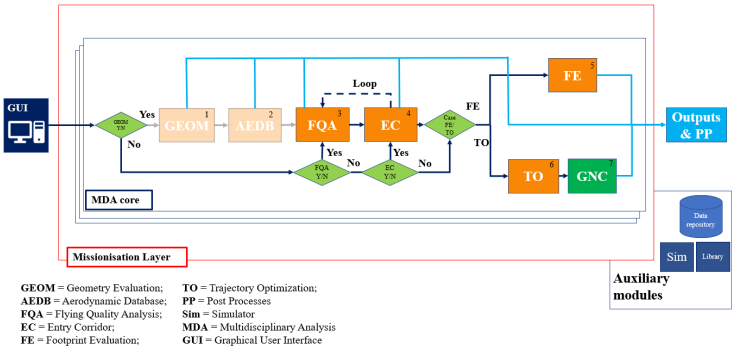

Figure 3.5: *High-Level architecture of the MA and GNC missionisation tool without the GEOM and AEDB disciplines. It is relative to the first test case (Section 6.1).*

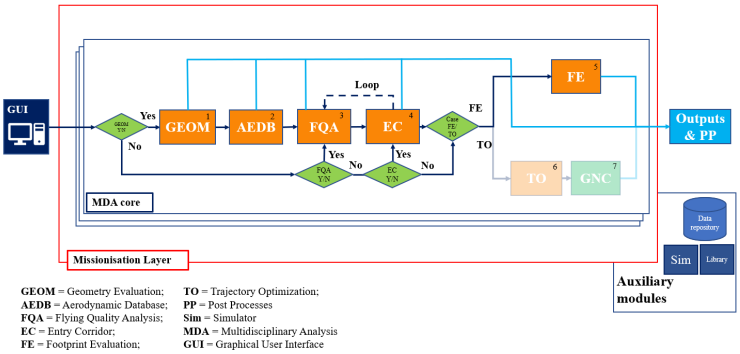

Figure 3.6: *High-Level architecture of the MA and GNC missionisation tool without the TO and GNC disciplines. It is relative to the second test case (Section 6.2).*

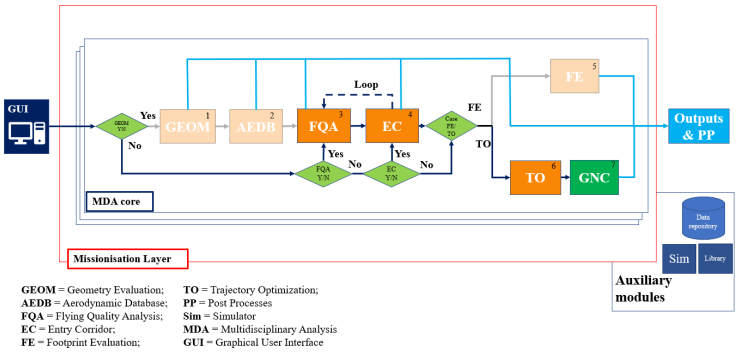

Figure 3.7: *High-Level architecture of the MA and GNC missionisation tool without the GEOM, AEDB and FE disciplines. It is relative to the third test case (Section 6.3).*

"Do or do not. There is no try"
Yoda - The Empire Strikes Back

CHAPTER 4

Engineering Modelling

This chapter describes in detail the engineering modelling of the system models and the disciplines included in the MDA. The design of an end-to-end mission and the evaluation of the performance, in the context of re-entry vehicles, fall into the atmospheric flight area. In particular, the missionisation of an autonomous re-entry vehicle is a multidisciplinary problem which requires the evaluation of several performance through multiple analyses. For these reasons, a minimum set of disciplines has been considered, dealing with aerodynamics, flying qualities, and mission analysis, such as entry corridor and range capabilities definition, and trajectory optimisation. It worth mentioning that the missionisation tool can handles a wide range of re-entry vehicles, from conventional lifting bodies to more novel vertical landing reusable launch vehicles.

4.1 System Models

This section reports a brief description of some dynamics and environmental models included in the libraries of the MA and GNC missionisation tool.

4.1.1 Equations of Motion

The equations of motion used for the development of the disciplines and the test cases considers the vehicle as a point mass on an Earth Centered Earth Fixed (ECEF) reference frame with 3 DoF. The dynamic equations reported below are expressed both in spherical coordinates and Cartesian coordinates. Moreover, the independent variable can be either time or energy. The mathematical formulation is different, but they are perfectly equivalent from a physical view point. The definition with respect to energy has been used for the development of the EC and FE tools. For a deeper explanation the reader can see [51, 12, 52]. These equations can be adapted to different planets by changing the corresponding parameters. Hereafter the following notation is used, if not differently specified: boldface italic letters denote vectors in $\mathbb{R}^n$, lightface italic letters indicate scalar parameters.

3DoF equations of motion in rotating spherical Earth with spherical coordinates

The motion of an unpowered vehicle in a planetary atmosphere with spherical coordinates is described by the following set of equations [12, 51]:

$$
\begin{aligned}
\dot{h} &= V \sin\gamma \\
\dot{\theta} &= \frac{V \cos\gamma \sin\psi}{r \cos\phi} \\
\dot{\phi} &= \frac{V \cos\gamma \cos\psi}{r} \\
\dot{V} &= -D - g \sin\gamma + \omega_E^2 r \cos\phi(\sin\gamma \cos\phi + \\
&\quad - \cos\gamma \sin\phi \cos\psi) \\
\dot{\gamma} &= \frac{L \cos\sigma}{V} + \left(\frac{V}{r} - \frac{g}{V}\right) \cos\gamma + 2\omega_E \cos\phi \sin\psi + \\
&\quad + \frac{\omega_E^2 r}{V} \cos\phi(\cos\gamma \cos\phi + \sin\gamma \sin\phi \cos\psi) \\
\dot{\psi} &= \frac{L \sin\sigma}{V \cos\gamma} + \frac{V}{r} \cos\gamma \sin\psi \tan\phi + \\
&\quad - 2\omega_E(\tan\gamma \cos\phi \cos\psi - \sin\phi) + \\
&\quad + \frac{\omega_E^2 r}{V \cos\gamma} \sin\phi \cos\phi \sin\psi
\end{aligned}
\tag{4.1}
$$

In this case, the state is $\boldsymbol{x} = [h, \theta, \phi, V, \gamma, \psi]^T \in \mathbb{R}^6$, constituted by the altitude (while the radial distance is $r = h + R_E$), longitude, latitude, co-rotating velocity modulus, FPA, and heading angle. ψ is 0° when the vehicle points the local north. σ is the bank angle, and typically it is the control variable with the AoA, for unpowered vehicles. In some problems, it could be useful to exploit the bank-rate as control variables. In this particular case, the state vector is augmented with the bank-angle, and $\dot{\sigma} = u_\sigma$ is added to the system of differential equations [52]. g is the gravity acceleration, while ω_E is the Earth angular rate, equal to 7.292115×10^{-5} rad/s. L and D are respectively the lift and drag accelerations, given by:

$$\begin{aligned} L &= \frac{1}{2}\rho V^2 S_{ref} \frac{C_L}{m} \\ D &= \frac{1}{2}\rho V^2 S_{ref} \frac{C_D}{m} \end{aligned} \tag{4.2}$$

This representation of the equations of motion allows for an easy interpretation of the results, due to the direct physical representation of the variables. On the other hand, this formulation may lead to singularities due to the presence of trigonometric terms at the denominator. For this reason, some problems requires a formulation with Cartesian coordinates.

3DoF equations of motion in rotating spherical Earth with spherical coordinates w.r.t. specific energy

The previous model exploits the time as independent variables. A good alternative is to use the specific energy [52]:

$$E = \frac{V^2}{2} - \frac{\mu_E}{h + R_E} \tag{4.3}$$

By differentiating this equation (Eq.(4.3)) with respect to time, it is possible to change the independent variable:

$$\dot{E} = V\dot{V} + \frac{\mu_E}{r^2}\dot{r} \tag{4.4}$$

By noting that for spherical Earth $\dot{r} = \dot{h}$, $g = -\mu_E/r^2$, and neglecting the term relative to the centripetal acceleration, if the equations of $\dot{h}$ and $\dot{V}$ are substituted in Eq.(4.4), the following result is obtained:

$$\dot{E} = -DV - gV\sin\gamma + \frac{\mu_E}{r^2}V\sin\gamma = -DV \tag{4.5}$$

Therefore, by combining Eq.(4.5) with Eq.(4.1), the following system of differential equations of motion expressed w.r.t. the energy is obtained [53]:

$$
\begin{aligned}
h' &= -\frac{\sin\gamma}{D} \\
\theta' &= -\frac{\cos\gamma\sin\psi}{Dr\cos\phi} \\
\phi' &= -\frac{\cos\gamma\cos\psi}{Dr} \\
V' &= \frac{1}{V} + \frac{g}{DV}\sin\gamma - \frac{\omega_E^2 r}{DV}\cos\phi(\sin\gamma\cos\phi + \\
&\quad - \cos\gamma\sin\phi\cos\psi) \\
\gamma' &= -\frac{L\cos\sigma}{DV^2} - \left(\frac{1}{r} - \frac{g}{V^2}\right)\frac{\cos\gamma}{D} - \frac{2\omega_E}{DV}\cos\phi\sin\psi + \\
&\quad - \frac{\omega_E^2 r}{DV^2}\cos\phi(\cos\gamma\cos\phi + \sin\gamma\sin\phi\cos\psi) \\
\psi' &= -\frac{L\sin\sigma}{DV^2\cos\gamma} - \frac{1}{Dr}\cos\gamma\sin\psi\tan\phi + \\
&\quad + \frac{2\omega_E}{DV}(\tan\gamma\cos\phi\cos\psi - \sin\phi) + \\
&\quad - \frac{\omega_E^2 r}{DV^2\cos\gamma}\sin\phi\cos\phi\sin\psi
\end{aligned}
\tag{4.6}
$$

This set of equations have been used to develop the estimation of the range capabilities within the Footprint Evaluation tool, by following the method reported in [54, 55]. However, within this work, Eq.(4.6) are augmented with correction terms for the presence of the Earth rotation as proposed in [52]. No practical difference has been observed in the results and from the computational perspective between the two formulations.

3DoF equations of motion in rotating spherical Earth with Cartesian coordinates

In a similar fashion, Eq.(4.7) describes the motion of a powered vehicle in planetary atmosphere with Cartesian coordinates [51, 56]:

$$
\begin{aligned}
\dot{\boldsymbol{r}} &= \boldsymbol{v} \\
\dot{\boldsymbol{v}} &= -\boldsymbol{g} - D\frac{\boldsymbol{v}}{||\boldsymbol{v}||} + L\frac{\boldsymbol{k}}{||\boldsymbol{k}||} + \frac{T_{amb}}{m}\boldsymbol{u} + \boldsymbol{a}_{rot} \\
\dot{m} &= -\frac{T_{nom}}{I_{sp}g_0}
\end{aligned}
\tag{4.7}
$$

In this case, the state vector is given by $\boldsymbol{x} = [\boldsymbol{r}, \boldsymbol{v}, m]^T \in \mathbb{R}^7$. T_{amb} is the thrust considering for the ambient pressure losses, D and L are the aerodynamic drag and lift accelerations. $\boldsymbol{u}$ is the control variable, and it defines the thrust orientation during the powered phases and the vehicle attitude during the unpowered phases. In a 3DoF model, the attitude can be, indeed, linked to the AoA by $\alpha = \arccos\left(-\boldsymbol{u} \cdot \frac{\boldsymbol{v}}{||\boldsymbol{v}||}\right)$. The vector $\boldsymbol{k}$ is defined by $\boldsymbol{k} = (\frac{\boldsymbol{v}}{||\boldsymbol{v}||} \times \boldsymbol{u}) \times \frac{\boldsymbol{v}}{||\boldsymbol{v}||}$, and it gives the direction of the lift. I_{sp} is the specific impulse. $\boldsymbol{a}_{rot}$ is the term relative to the acceleration due to the Earth rotation, and it is given by $\boldsymbol{a}_{rot} = -2\boldsymbol{\Omega}_E \times \boldsymbol{v} - \boldsymbol{\Omega}_E \times (\boldsymbol{\Omega}_E \times \boldsymbol{r})$, where $\boldsymbol{\Omega_E} = [0, 0, \omega_E]^T$.

The system of equations (Eq.(4.7)) includes the thrust because, within this work, this model has been used in the context of the powered landing of a reusable space launcher.

4.1.2 Environmental Models

This section characterises the environmental models included in the MA and GNC missionisation tool. In particular, it focuses on the gravity and atmospheric models.

Gravity Model

In first approximation, the gravity model can be formulated as a pure central field generated by a point with the mass of the Earth, or more in general the mass of the considered planet, located in its center. This model yields to a gravitational acceleration expressed by:

$$
g(r) = \frac{\mu_p}{r^2} \tag{4.8}
$$

In Cartesian coordinates Eq.(4.8) modifies in this way:

$$
\boldsymbol{g}(\boldsymbol{r}) = \frac{\mu_p}{||\boldsymbol{r}||^3}\boldsymbol{r} \tag{4.9}
$$

By focusing on the Earth, a more accurate model of the Earth gravity field can be obtained by modelling the mass distribution of the

Earth. For example, the oblateness of the Earth can be mathematically considered with the introduction of the zonal harmonic J_2 [51, 52, 57].

$$g(r,\phi) = \frac{\mu_E}{r^2}(1 + \frac{3}{2}J_2(\frac{r}{R_E})^2(1 - 3\sin^2\phi)) \tag{4.10}$$

In the equations above, the value of the standard gravitation parameter for Earth is $\mu_E = 3.986004418 \times 10^{14}$ m^3/s^2, Earth radius is $R_E = 6378.137 \times 10^3$ m, while $J_2 = 1.0826271 \times 10^{-3}$. However, for the mission scenarios analysed in this work, no significant difference have been observed. It worth mentioning that due to the modular nature of the proposed tool, any kind of gravity model can be added for future applications, as well as the high-fidelity WGS84 [58].

Atmospheric Model

Within the MA and GNC two atmospheric model have been implemented:

- **Exponential atmosphere:** This model estimates the density and the pressure variation with the altitude through an exponential law:

$$\begin{aligned} \rho(h) &= \rho_0 e^{\frac{-h}{H}} \\ P(h) &= P_0 e^{\frac{-h}{H}} \end{aligned} \tag{4.11}$$

  where ρ_0 and P_0 are the atmospheric density and pressure at sea level, and respectively equal to 1.225 kg/m^3 and 101325 Pa. H is the scale height, which can assume different values (typically 7200 m [12]). This profile is an approximation that is used from 0 to 86 km, while for higher altitude it may introduce non-negligible errors [12, 58].

- **US Standard 76:** This model has been developed by the U.S. Committee on Extension to the Standard Atmosphere [59]. The model assumes of dry, perfect gas mixture, and all the quantities depend only on the altitude. The density is modelled exploiting the ideal gas law:

$$\rho = \frac{PM_{mol}}{R_{gas}T} \tag{4.12}$$

where the pressure P and the temperature T are defined by several functions depending on the considered altitude regime. M_{mol} is the mean molecular weight of the gas mixture, while R_{gas} is the universal gas constant equal to 8.314462 $\mathrm{JK^{-1}mol^{-1}}$. The model estimates the properties of the atmosphere up to 1000 km from the surface according to [59].

The user, however, can provide a custom atmospheric model depending on the scenario to be analysed, as for instance the high-fidelity NRLMSISE-00 [60] or a model of a different planet.

Other aspects

Further models considered within the implementation of the missionisation tool and included in the analysed scenarios are:

- **Mechanical loads:** they consider the dynamic pressure, the axial and lateral accelerations load for the structural limitations of the re-entry vehicle and the payload, if present. The approach for the computation follows well-known equations [12, 52, 57].
- **Thermal load:** it consists in the heat flux at the stagnation point (typically the nose), which, for instance, it can be modelled with the Chapman's Equation [12].
- **Propulsion:** The thrust is modelled using the general rocket equations considering the expansion losses due to the change in the atmospheric pressure with the altitude [61].

The methodology used to compute these factors can vary in complexity from simple equations, as the ones cited here, to higher fidelity models. Depending on the analysis and simulation to be performed, more complex representation of the phenomena can be integrated, thank to the modular structure of the developed missionisation tool.

4.2 Modelling of the Disciplines

This section describes the engineering models of the disciplines included in the missionisation tool. This set of disciplines constitutes the core of the MDA framework of the tool. Each discipline has been modelled by a mathematical model to numerically assess a particular

Table 4.1: *Horus-2B parameters and boundary conditions.*

Parameter	Value	Unit
Mass (landing configuration)	26029	kg
L/D @ hypersonic regime	1.8	-
S_{ref}	110	m^2
L_{ref}	23	m
R_{nose}	0.8	m
Max dynamic pressure	10	kPa
Max heat flux	530	kW/m^2
Max axial load	2.5	-
Flap deflection range	[-20, 30]	◦
Initial altitude	100	km
Initial velocity	7.5	km/s

performance. This chapter reports a characterisation of the main assumptions, by highlighting the key parameters of each discipline, and qualitatively describing the inputs and the outputs. Moreover, an example of analysis is shown for each discipline.

Depending on the analysis that the user wants to perform, the disciplines can be called either independently or in sequence. As described in Section 3.3, the tool is highly modular, allowing the user to only select the required disciplines. The complete MDA cycle takes 10 seconds on average on an Intel®Core^{TM} i7-8750H processor.

The plots reported in this chapter have been computed by using Horus-2B as a baseline [62]. Its parameters and shape are stated in 4.1 and 4.1.

4.2.1 Geometry and Mass estimation tool

The geometry and mass estimation tool (GEOM) aims at obtaining a representative estimation of the reference surface and the entry dry

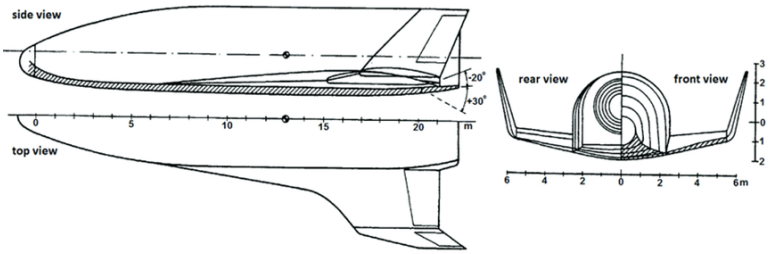

Figure 4.1: *Horus-2B vehicle.*

mass of the re-entry vehicle with respect to a minimum set of geometric parameters. The variables are the longitudinal length L_{ref}, the fuselage diameter $Diam$, the mean aerodynamic chord c, and the wing span b, if the vehicle is equipped with wings. At this stage, the GEOM tool does not address neither the design of complex shape nor the internal layout of the vehicle. The GEOM tool is, in fact, used when the missionisation aims at evaluating the mission capabilities of a re-entry vehicle with respect to the vehicle design and mission parameters. In this case, a parametric analysis concerning the geometry of different re-entry vehicles can be performed, in order to evaluate trade-off studies during the early phases of the design process.

When the missionisation process is performed in the latest phases of the mission design, the geometry and the mass of the vehicle are known and they are considered input parameters. In this case, the GEOM tool is not required.

The geometry and mass estimation (GEOM) tool is based on the following assumptions:

- The re-entry vehicles are subdivided into four main categories: Winged Re-entry Vehicles, Winged Lifting Body, Lifting Body and Vertical Landing Reusable Launcher Vehicle. The tool deals with the first three categories. A detailed explanation about the categories is given in Section 2.2.1.
- The reference surface is computed by considering a simplified geometry of the vehicle, and it refers to the planform area.
- The position of the Center of Gravity and the Moment Reference Center coincides.
- The mass of the vehicle is estimated through a simplified version of the Hypersonic Aerospace Sizing Analysis (HASA) tool documented by [63] and [64], which employs empirical equations.

The estimation of the dry mass of the vehicle is based on the four geometrical parameters reported above (L_{ref}, $Diam$, c and b), and the maximum aerodynamic and mechanical loads that the vehicle can withstands. The mass of the vehicle is computed by subdividing in parts and subsystems the re-entry vehicle. The mass of each component is estimated through empirical relations. Table 4.2 reports the equations for each considered element. In the equations, L_{body}, $S_{fus,tot}$, and V_{fus} are the length, the total surface and the volume of the fuselage, q_{dyn} is the dynamic pressure limit, while $S_{fus,bottom}$ is the bottom fuselage

surface. n_x is the load factor limit, b, c, λ, $\lambda_{1/2}$ are the wing span, the mean chord, the wing taper ratio, and the mid-chord sweep angle, while S_w is the wing surface. η_{TPS} is the area density parameters, a typical value is 3lb/ft^2. C_{eq} is a constant depending on the vehicle category. The relations use imperial units and not SI units [63]. The dry mass is the sum of each components by also considering the payload mass.

$$m_{dry} = m_{pay} + m_{fus} + m_{TPS} + m_w + m_{gear} + m_{hyd} + m_{av} + m_{el} + m_{prop} + m_{eq} \tag{4.13}$$

As it can be noted, the equations in Table 4.2 are function of the dry mass itself, thus the final solution is to be solved iteratively. Table 4.3 summarises the input and output parameters for this discipline.

4.2.2 Aerodynamic Database tool

The Aerodynamic Database tool (AEDB) aims at estimating the longitudinal aerodynamic coefficients and building a representative database

Table 4.2: *Empirical relations for the mass estimation of the components.*

Component mass	**Equation**
Fuselage (m_{fus})	$0.3819 \left[\left(\frac{L_{body}}{\sqrt{\frac{V_{fus}}{0.35 L_{body}}}} \right)^{0.15} q_{dyn}^{0.16} S_{fus,tot}^{1.05} \right]$
Wings (m_w)	$0.3313 \left(\left(\frac{m_{dry} n_x}{1000} \right)^{0.52} S_w^{0.7} \left(\frac{b}{c} \right)^{0.47} \left(\frac{1+\lambda}{t/c} \right)^{0.4} \left(0.3 + \frac{0.7}{\cos(\lambda_{1/2})} \right) \right)^{1.017}$
TPS (m_{TPS})	$\eta_{TPS}(S_w + S_{fus,bottom})$
Landing gear (m_{gear})	$0.00916 m_{dry}^{1.124}$
Hydraulic (m_{hyd})	$2.64 \left(\frac{1.1 S_w q_{dyn}}{1000} \right)^{0.334} (L_{body} + b)^{0.5}$
Avionics (m_{av})	$66.37 m_{dry}^{0.361}$
Electrical subsystem (m_{el})	$1.167 m_{dry}^{0.5} L_{body}^{0.25}$
Propulsive subsystem (m_{prop})	$0.2 m_{dry}$
Auxiliary equipment (m_{eq})	$C_{eq} + 0.01(m_{dry} - 0.0000003)$

Table 4.3: *Input and Output parameters for the Geometry and Mass estimation tool.*

	Parameter	Description
Input	$L, Diam, b, c$	geometric parameters
	q_{dyn}, n_x	Sizing constraints
	Vehicle Category	Flag for the class of the re-entry vehicle
Output	S_{ref}	Reference surface of the vehicle
	m	Estimated mass of the vehicle
	$L_{ref}/Diam$	Fineness ratio
	b/c	Modified wing aspect ratio

for a wide range of re-entry vehicles. The tool can be used for the preliminary phases of the design of a re-entry mission. As for the GEOM tool, the AEDB tool is called when the missionisation objective is to evaluate the mission capabilities of a re-entry vehicle with respect to the vehicle design and mission parameters, during the early phases of the design process. The tool, in fact, does not address an accurate aerodynamic characterisation, but computes a low-fidelity aerodynamic database of the considered vehicle. When the MA and GNC missionisation is carried out during the last phases of the mission design, in fact, a high-fidelity aerodynamic database of the vehicle must be provided as an input of the missionisation tool, and the AEDB tool is not considered.

The estimation of the aerodynamic coefficients of the vehicle with the proposed AEDB tool is performed instantaneously, and it eliminates the computational burden of the classical methods [65, 66]. This feature makes this tool suitable for MDA-MDO application, when multiple evaluation has to be performed. The aerodynamic coefficients, $C_L(M, \alpha, \delta)$, $C_D(M, \alpha, \delta)$ and $C_m(M, \alpha, \delta)$, of a specific vehicle is obtained by evaluating the stored interpolating functions in the desired geometrical parameters. The AEDB tool includes, in fact, an aerodynamic database constituted by a set of interpolating functions obtained from several datasets of aerodynamic coefficients. These functions depends on a predefined set of geometrical parameters, which are the fineness ratio ($L_{ref}/Diam$) and the modified wing-aspect ratio (b/c), if the vehicle is equipped with wings or fins. The AEDB tool stores five interpolating functions, thus the same number of classes of re-entry vehicles considered in this work (Section 2.2.1) [21]. Figure 4.2 illustrates the creation of the interpolating function for one category [67].

The datasets used to obtain the interpolating functions have been

computed by varying a prescribed number of geometrical parameters with two tools provided by the German Aerospace Center (DLR). The tools are CAC and HOTSOSE. The former is a DATCOM-like method [66], and it has been used for a Mach regime $\in$ [0.25, 4]. The latter is based on shock expansion methods [68], and it has been employed for the estimation of the coefficients at hypersonic regime (Mach $>$ 5). The Moment Reference Frame (MRC) has been assumed to coincide with the CoG of the vehicle.

Figure 4.3 shows the block diagram of the AEDB tool, while Table 4.4 summarizes the input and outputs parameters.

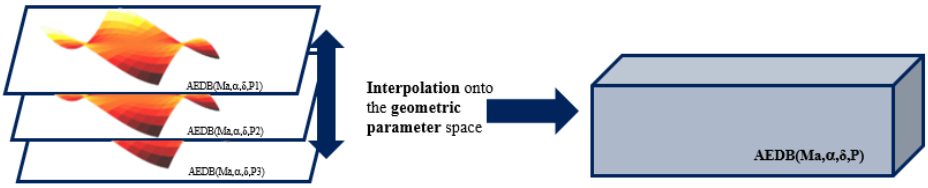

Figure 4.2: *High-Level concept for the creation of one interpolating function, P_i are the geometrical parameters.*

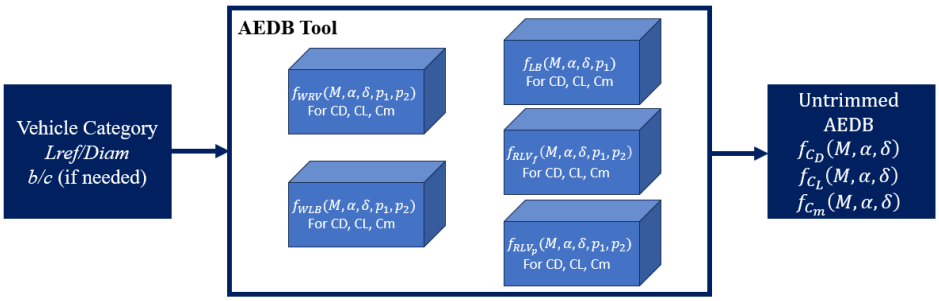

Figure 4.3: *Block Diagram of the AEDB Tool, p_1 and p_2 are the geometrical parameters.*

Table 4.4: *Input and Output parameters for the Aerodynamic Database tool.*

	Parameter	Description
Input	$L_{ref}/Diam$	Fineness ration
	b/c	Modified wing aspect ratio
	Vehicle Category	Flag for the class of the re-entry vehicle
Output	$C_D(M,\alpha,\delta)$	Untrimmed drag coefficient
	$C_L(M,\alpha,\delta)$	Untrimmed lift coefficient
	$C_m(M,\alpha,\delta)$	Pitching moment coefficient

4.2.3 Flying Quality Analysis tool

The Flying Quality Analysis (FQA) tool evaluates the trim and static longitudinal stability of the vehicle [69, 13]. The FQA provides the stability domain, so-called Angle-of-Attack entry corridor, and assesses the thickness of this corridor. Moreover, the tool automatically selects the Angle-of-Attack trim line within the stability domain. The implementation of the tool assumes the following:

- The tool is limited to the longitudinal trim and static stability analysis;
- The aerodynamic of the control surfaces is described by an unique equivalent aerodynamic surface;
- The aerodynamic surface deflection is limited by user's define bounds;
- The tool deals with unpowered phases of the mission. It can handle WRV, WLB, LB, and VL-RLV;

The tool evaluates the required deflection of the aerodynamic surface to trim the vehicle, if exists, and then computes the static longitudinal stability of the found equilibrium point, in the specified α-Ma domain. The FQA tool takes in input the untrimmed AEDB of the vehicle, which can be provided by the user or given by the AEDB tool.

Generally, the AEDB of a vehicle is given by a function of the Mach number, Angle-of-Attack, and the control surface:

$$\begin{aligned} C_D(M,\alpha,\delta) &= C_{D,clean}(M,\alpha) + \Delta C_D(M,\alpha,\delta) \\ C_L(M,\alpha,\delta) &= C_{L,clean}(M,\alpha) + \Delta C_L(M,\alpha,\delta) \\ C_m(M,\alpha,\delta) &= C_{m,clean}(M,\alpha) + \Delta C_m(M,\alpha,\delta) \end{aligned} \tag{4.14}$$

The trim condition is given when the torques acting on the vehicles are zero, so when:

$$\exists \quad \hat{\delta} \quad \text{for given} \quad [M,\alpha] \quad \text{such that} \quad C_m(M,\alpha,\hat{\delta}) = 0; \tag{4.15}$$

As introduced above, only the longitudinal equilibrium is studied, thus the analysis is done by considering the pitching moment coefficient. When Eq.(4.15) cannot be found in specific flight conditions, the vehicle is said to be untrimmable. Equation (4.15) is valid when

CoG and the MRC coincide. If this is not the case, Equation (4.15) must be modified, by considering the transport terms:

$$\begin{aligned} C_m(M,\alpha,\delta) &= C_{m,clean}(M,\alpha) + \Delta C_m(M,\alpha,\delta) \\ &+ C_N(M,\alpha,\delta)\Delta X + C_A(M,\alpha,\delta)\Delta Z \end{aligned} \tag{4.16}$$

where C_N and C_A are the normal and axial force coefficients defined by:

$$\begin{aligned} C_A(M,\alpha,\delta) &= C_D \cos\alpha - C_L \sin\alpha \\ C_N(M,\alpha,\delta) &= C_D \sin\alpha + C_L \cos\alpha \end{aligned} \tag{4.17}$$

The additional torques generated by the transport terms are ruled by the definition of ΔX and ΔZ, so the difference between the CoG and the MRC position in x-axis and z-axis:

$$\begin{aligned} \Delta X &= -\frac{X_{CoG} - X_0}{L_{ref,FQA}} \\ \Delta Z &= \frac{Z_{CoG} - Z_0}{L_{ref,FQA}} \end{aligned} \tag{4.18}$$

Equation (4.16) and (4.18) refer to the reference frame and conventions reported in Figure 4.4. $L_{ref,FQA}$ is the reference dimension of the vehicle: typically is the longitudinal length or the diameter. It can be noted, that the CoG position directly influence the trimmability and the stability of the vehicle.

Once a trim point has been found, the static longitudinal stability is evaluated by computing the static margin. If the static margin is positive, then the vehicle is flying in a longitudinal static stable configuration. The static margin is given by Equation (4.19):

$$SM = -\frac{C_{m,\alpha}}{|\frac{C_N C_{A,\alpha}}{C_A} - C_{N,\alpha}|} \tag{4.19}$$

where $C_{(.),\alpha}$ stands for the derivative of the considered aerodynamic coefficient with respect to the AoA.

After having computed the static margin, it is possible to characterise the AoA entry corridor, i. e. the domain in which the AoA trim line can be defined. This procedure is done automatically by the FQA tool. The selection is ruled by a logic in order to set the AoA close to the maximum C_L condition. This selection allows having a wider entry corridor at a high Mach number, due to the minimisation of the

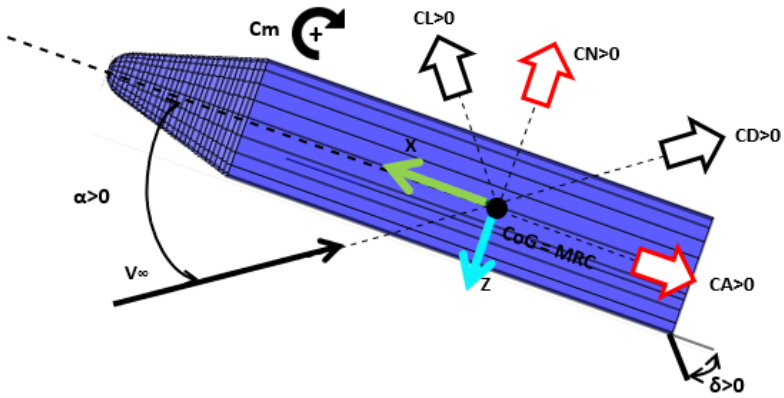

Figure 4.4: *Conventions for angles, forces and torques considered within the FQA tool. In this case, the CoG and the MRC coincide.*

heat flux at the stagnation point [12]. Different logic may be considered for future development. The trim line is crucial for the design of the entry corridor (Section 4.2.4), and thus the achievement of a safe re-entry trajectory for the aerothermal-mechanical view point. Figure 4.5 reports an example of the FQA performed for Horus-2B. The analysis have been carried out by considering a Mach of [0, 25], and an AoA between 0° and 45°. The range of deflection of the body flap is limited from -20° to 30°. In particular, Figure 4.5a shows the required body flap deflection to trim the vehicle. Figure 4.5b displays the static margin computed in the trim point. The void area is the region where the trim in unfeasible. The stability domain is delimitated by the red lines. Below, Figure 4.5c shows the resulting AoA entry corridor (in green) and the selected trim line in blue. In this case, a feasible AoA entry corridor can be defined for the whole Mach-AoA domain.

Table 4.5 gives an overview of the inputs and outputs parameters of the FQA tool.

4.2.4 Entry Corridor tool

The Entry Corridor (EC) tool computes the domain where the vehicle can fly without violating the aerothermal-mechanical loads bounds. This analysis is crucial for designing safe re-entry trajectories. The entry corridor is commonly obtained in the drag-energy space, by using the energy as the independent variable, or in the altitude-velocity space, with the velocity as the independent variable.

Table 4.5: *Input and Output parameters for the Flying Qualities Analysis tool.*

	Parameter	Description
Input	AoA, Mach	Flight conditions domain
	δ_{min}, δ_{max}	Aerodynamic surface deflection limits
	X_{cog}, Z_{cog}	CoG position displacement concerning the MRC
	C_D, C_L, C_m	Untrimmed AEDB
	$L_{ref,FQA}$	Reference length
Output	δ_{trim}	Required trim deflection
	SM	Static Margin
	AoA entry corridor	Trimmability and stability domain
	AoA line	Selected AoA trim line
	$C_{D,trim}$, $C_{L,trim}$	Trimmed AEDB

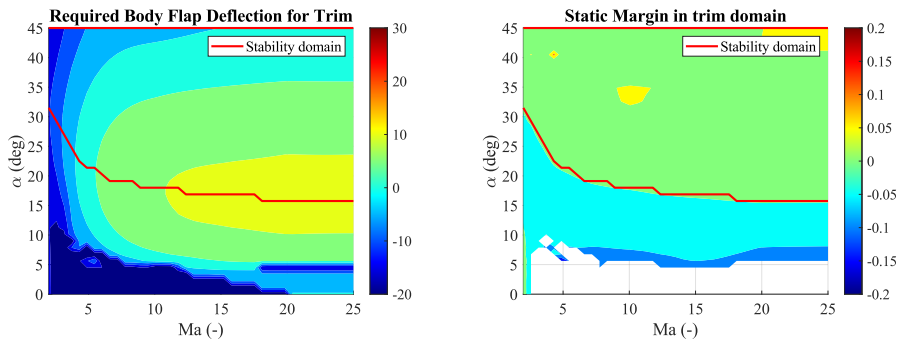

(a) *Required trim deflection in the Mach-AoA domain.* **(b)** *Static margin in the Mach AoA domain.*

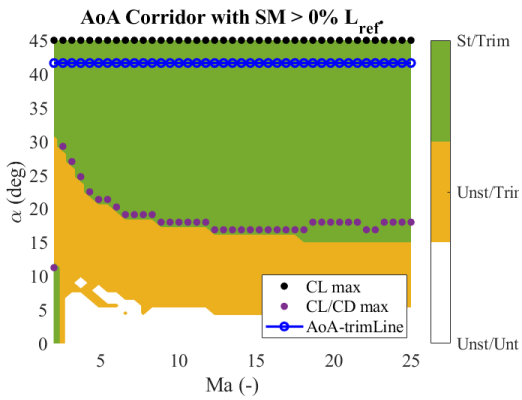

(c) *AoA Entry Corridor.*

Figure 4.5: *Example of FQA outputs obtained using Horus-2B as baseline.*

For the implementation of this discipline, the following assumptions have been considered [12, 70, 71]:

- The tool estimates the entry corridor for the aerodynamic phase of the flight. In this phase, the vehicle is unpowered;
- The specific energy is the independent variable (as said previously, the co-rotating velocity can be used alternatively);
- The aerothermal-mechanical constraints included within the analysis are:
  - Maximum dynamic pressure;
  - Maximum heat flux at stagnation point (Chapman's Equation [12]);
  - Maximum acceleration load;
  - Equilibrium glide or terminal velocity for vehicle characterised by low L/D;

When the energy is used as the independent variable, a set of systems of nonlinear equations can be solved to obtain the bounds of the entry corridor. The energy and the aerothermal-mechanical constraints equations, in fact, are both functions of the velocity and the altitude. Therefore, it is possible to solve the system of nonlinear equations, to get the altitude and velocity couple which generates the maximum value of a specific constraint, by fixing a prescribed level of specific energy. The system of nonlinear equations is constituted by the equation of the specific energy, expressed by Eq. (4.20), and the equation of the considered aerothermal-mechanical constraint. The equations of the loads are reported in Table 4.6, while the specific energy is given by:

$$\frac{V^2}{2} - \frac{\mu}{h + R_E} = \bar{E} \tag{4.20}$$

where $\bar{E}$ is the prescribed energy value. It is possible to add other aerothermal-mechanical loads, for instance the heat flux at the flap, by including in the analysis a new system of nonlinear equations with the correspondent constraints formulation.

One of the drawbacks of the equilibrium glide condition presented is given by the fact that it does not take into account the terms relative to the planet rotation, and the Flight-Path-Angle (FPA) and the bank angle are considered equal to zero. An alternative approach for

the formulation of the equilibrium glide drag profile consists of the implementation of a Flight-Path-Angle tracking control. The feedback controller schedules the bank angle to track a reference FPA. The reference profile can be considered relatively small to increase the range capabilities. This approach accounts for planet rotation and reduces phugoid motion. The feedback controller is given by the first-order dynamics [54]:

$$(\gamma'_{ref} - \gamma') + K_\gamma(\gamma_{ref} - \gamma_{ref}) = 0 \tag{4.21}$$

Replacing Eq.(4.21) in the dynamic equation of motion of the FPA written in function of the specific energy, the following equation is obtained:

$$\frac{L}{D}\cos\sigma = \left(g - \frac{V^2}{r}\right)\frac{\cos\gamma}{D} + V^2(C_\gamma - K_\gamma(\gamma_{ref} - \gamma) - \gamma'_{ref}) \tag{4.22}$$

where $C_\gamma = -(\frac{2\omega_E}{VD})\cos\phi\sin\psi$ includes the Coriolis effect due to planet rotation, while K_γ is a constant for the feedback control [54]. After propagating the equations of motion with Eq. 4.22, it is possible to get the equilibrium glide trajectory and the associated drag profile.

Once the four systems of equations given by Eq.(4.20), and the equations in Table 4.6 are solved, the altitude and velocity profiles associated to the constraints are obtained. From these profiles, the corresponding drag accelerations are recovered:

$$D_{qdyn,max} = \frac{1}{2}\rho(h_{qdyn})V_{qdyn}^2\frac{S_{ref}}{m}C_D(M(h_{qdyn}, V_{qdyn}), \alpha) \tag{4.23}$$

$$D_{qheat,max} = \frac{1}{2}\rho(h_{qheat})V_{qheat}^2\frac{S_{ref}}{m}C_D(M(h_{qheat}, V_{qheat}), \alpha) \tag{4.24}$$

Table 4.6: *Equations of the aerothermal-mechanical loads considered within the tool.*

Aerothermal-mechanical load	Equation
Dynamic pressure [12, 71]	$\frac{1}{2}\rho(h)V^2 = \bar{q}_{dyn,max}$
Heat flux at the stagnation point [12]	$\frac{C_0}{\sqrt{R_{nose}}}\sqrt{\rho(h)}V^{3.15} = \dot{\bar{q}}_{heat,max}$
Acceleration load [12, 71]	$\frac{\sqrt{L^2+D^2}}{g_0} = \bar{n}_{g,max}$
Equilibrium glide [12, 71]	$(g(h) - \frac{V^2}{h+r_p}) - L = 0$
Terminal velocity [12]	$W = D$

$$D_{g,max} = \frac{1}{2}\rho(h_g)V_g^2\frac{S_{ref}}{m}C_D(M(h_g, V_g), \alpha) \tag{4.25}$$

$$D_{eg} = \frac{1}{2}\rho(h_{eg})V_{eg}^2\frac{S_{ref}}{m}C_D(M(h_{eg}, V_{eg}), \alpha) \tag{4.26}$$

where $h_{(.)}$ and $V_{(.)}$ are the altitude and velocity profiles associated to the different loads. The lower bound of the the entry corridor in drag-energy space is defined by the equilibrium glide drag profile, while the upper bound is given by the minimum value for each energy level between the aerothermal-mechanical constraints:

$$u_{b,ec} = \min(D_{qdyn,max}, D_{qheat,max}, D_{g,max}) \tag{4.27}$$

Figure 4.6a shows the entry corridor for Horus-2B with the parameters and entry conditions specified in Table 4.1 from EIP to TAEM.

Table 4.7 summarizes the input and output parameters associated to this discipline.

The shape of the entry corridor is directly affected by the AoA line selected within the FQA. If the provided AoA trim line generates an unfeasible entry corridor, the missionitation tool enters in a loop constituted by the FQA tool and the Entry Corridor tool in order to evaluate different AoA line defined within the feasible AoA corridor. In the case in which a feasible solution is not found, the simulation is stopped. This result conveys that the vehicle is not able to perform a safe re-entry and a feasible trajectory cannot be defined with the considered conditions (boundary conditions and loads limits).

Table 4.7: *Input and Output parameters for the Entry Corridor tool.*

	Parameter	**Description**
Input	AoA profile	Angle-of-Attack trim line
	$C_{D,trim}$, $C_{L,trim}$	Trimmed AEDB
	Vehicle dimensions	Reference dimensions of the vehicles (S_{ref})
	m	Mass of the vehicle
	Loads limits	Max values of the aerothermal-mechanical loads
	Environment	Environmental properties of the planet
	EIP and TAEM point	Boundary Conditions
Output	Entry Corridor bounds	Upper and lower feasible drag profiles
	AoA trim line	Updated trim line if the corridor is closed

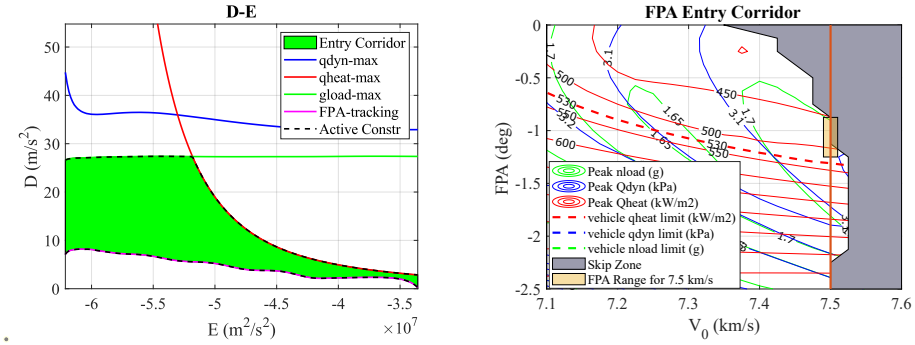

(a) *Entry Corridor analysis for Horus-2B.* **(b)** *FPA entry corridor analysis for Horus-2B.*

Figure 4.6: *Example of Entry Corridor outputs obtained using Horus-2B as baseline.*

Initial Flight-Path-Angle computation

A secondary functionality of the Entry Corridor tool is the automatic computation of the initial FPA, if the user does not set up it in the input file. For specific entry conditions (velocity and altitude), the tool evaluates the minimum FPA to avoid skipping trajectories (grey-zone in Figure 4.6b), and the maximum FPA to avoid trajectories that would violate the aerothermal-mechanical constraints. The tool will use this information for the computation of the equilibrium glide profile, and for the estimation of the range capabilities.

Figure 4.6b shows an example of this kind of analysis for Horus-2B. The figure reports the feasible range of FPA for the prescribed velocity. The analysis also yields the initial FPA and velocity sensitivity for the entry corridor performance. The yellow band has the scope to highlight the feasible region. This analysis can be also carried out by considering different variables, for instance the ballistic coefficient.

4.2.5 Footprint Evaluation tool

The Footprint Evaluation (FE) tool predicts the feasible range capability of a re-entry vehicle, or landing footprint, from any initial entry condition [12, 54, 72]. The tool estimates the reachable area without violating the aerothermal-mechanical constraints defined by the Entry Corridor tool. The landing footprint conveys critical information about the mission planning and the selection of possible landing sites.

The range capability area is defined by the set of boundary points

of the landing footprint. In the literature, the boundary points are computed in two ways. The first approach involves solving a family of optimal trajectories to obtain the optimal bank profile which maximise the crossrange for a given downrange [72]. This way allows to include several constraints in the prediction of the end points. On the other hand, the efficient computation of a set of optimal control problem is a burdensome task. The second approach entails the simulation of a group of re-entry trajectories at different constant bank angles. This method results to be more efficient with respect the first one, however, due to the fact that the aerothermal-mechanical constraints are not imposed, some of the trajectory may not be feasible.

Within this work, the estimation of the landing footprint has been done by implementing an algorithm based on the Evolved Acceleration Guidance Logic (EAGLE) [54, 55]. The EAGLE planner designs feasible trajectories, accounting the vehicle aerothermal-mechanical loads and Coriolis effects. This approach predicts the range capabilities of the vehicle by involving the results obtained within the Entry Corridor tool. Each trajectory is generated through a prescribed drag profile defined within the entry corridor bounds and in the function of the specific energy E. From the drag profile, a bank profile is scheduled to propagate the equations of motion and obtain the trajectory. From different drag profiles, different trajectories are given.

A step forward with respect to the state-of-the-art was to generalise the algorithm concerning the atmospheric model. In this work, any kind of atmospheric model can be used, while in [54] an exponential model was assumed.

The drag profiles are computed by interpolating the lower bound drag profile (D_{min}) and the upper bound drag profile (D_{max}). The former yields the far-edge end point of the footprint, while the latter provides the near-edge end point. The interpolation is defined by Eq. (4.28):

$$D(E) = D_{max}(E) + c(D_{min}(E) - D_{max}(E)) \tag{4.28}$$

with $c \in [0,1]$. Figure 4.7a shows an examples of feasible drag profiles used to get the footprint. The minimum and maximum drag profile have been modified in order to match the boundary conditions. Moreover, the maximum drag profile has been smoothed in the proximity of the point in which the active constraint changes.

The bank profiles have been scheduled with the following equations (Eqs. 4.29, 4.30), obtained by differentiating two time the drag with

respect to the specific energy [52, 55]:

$$\frac{L}{D}\cos\sigma = \frac{1}{b}(D'' - a) \tag{4.29}$$

where

$$\begin{aligned} a &= D(\frac{C_D''}{C_D} - \frac{C_D'^2}{C_D^2}) + D'(\frac{C_D'}{C_D} + \frac{2}{V^2}) - \frac{4D}{V^4} \\ &+ \frac{1}{DV^2}(\frac{\rho_h}{\rho} - 2\frac{g}{V^2})(\frac{V^2}{R_E + h} - g) + (\frac{2g}{V^2} - \frac{\rho_h}{\rho})C_\gamma \\ b &= \frac{1}{V^2}(\frac{\rho_h}{\rho} - \frac{2g}{V^2}) \end{aligned} \tag{4.30}$$

C_γ is the term related to the rotation of the planet [54], while the terms $(.)'$ and $(.)''$ stands for a differentiation with respect to the specific energy. The complete derivation of these terms is available in [52, 71]. ρ_h is the derivative of the density with respect to the altitude. Thus, the bank angle is:

$$|\sigma| = \cos^{-1}(\frac{D}{bL}(D'' - a)) \tag{4.31}$$

Equation 4.31 computes only the magnitude of the bank angle, thus the right and the left-edge of the footprint are estimated by banking always positive and negative during the flight (Figure 4.7b). To define the farthest and the nearest edges, reversal bank maneuvers may be considered, however, for preliminary analysis, a possible simplification is to assume them as straight lines. Figure 4.8 shows an example where bank reversal manoeuvres are either considered or not. It can be noted, that in first approximation the results are very similar, especially for what it concerns the definition of the far-edge. Moreover, the FE tool can evaluate the minimum distance between the footprint bound and the prescribed target point, if it has been specified in the input file.

4.2.6 Trajectory Optimisation tool

The Trajectory Optimisation (TO) tool is a modular framework developed for the mission analysis of any re-entry vehicle, even if it can also manage optimal control problem of different nature. The TO tool can handle both single phase and multiphase problem (Section 2.4), and trajectory optimisation with parameters. Moreover, the TO tool can

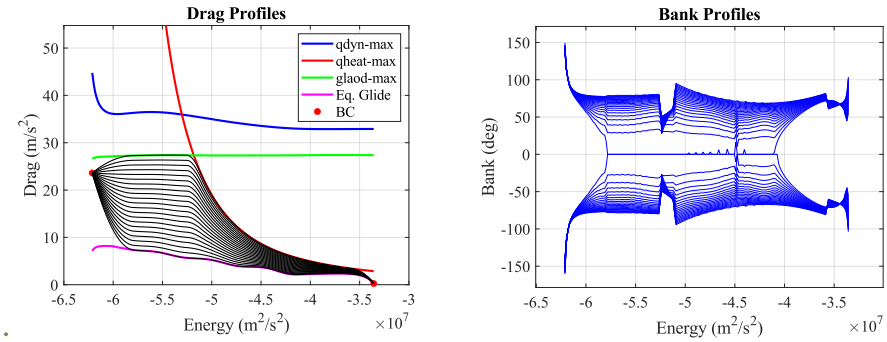

(a) *Interpolated drag profiles.*

(b) *Bank profiles associated to the drag profiles.*

Figure 4.7: *Example of drag profiles and scheduled bank angle profiles for Horus-2B, with initial condition reported in Table 4.1, 0° latitude, 0° longitude and 60° heading angle.*

be used whenever the missionisation process requires the definition of a new reference trajectory.

The tool has been developed in `MATLAB`, and it is constituted by two major components: the user interface, and the optimisation core. The first one is used to set up the user-inputs to describe the problem to be analysed. This operation can be directly done within the input file of the missionisation tool. It is based on a set of structure and user customisable `MATLAB` functions in which the physical problem is defined with the required constraints and cost function. The optimisation core performs two operation. Firstly it automatically translates the problem defined in the input file into the form required by the optimisation

Table 4.8: *Input and Output parameters for the Footprint Evaluation tool.*

	Parameter	**Description**
Input	AoA profile	Angle-of-Attack trim line
	$C_{D,trim}$, $C_{L,trim}$	Trimmed AEDB
	Vehicle dimensions	Reference dimensions of the vehicles (S_{ref})
	m	Mass of the vehicle
	Entry Corridor bounds	Upper and lower feasible drag profiles
	Environment	Environmental properties of the planet
	EIP and Final point	Boundary Conditions
	Target point	Longitude and Latitude of the target
Output	Range capabilities	Feasible footprint domain
	Bank profiles	Scheduled bank profiles
	Min distance	Footprint-target min. distance

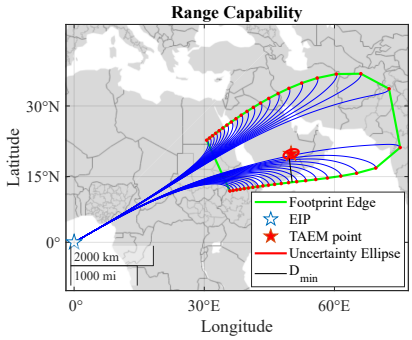

(a) *Estimated range capability without considering bank reversals. D_{min} in the minimum distance between the target point and the footprint edge.*

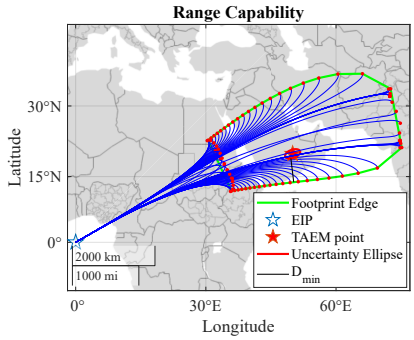

(b) *Estimated range capability with bank reversals. D_{min} in the minimum distance between the target point and the footprint edge*

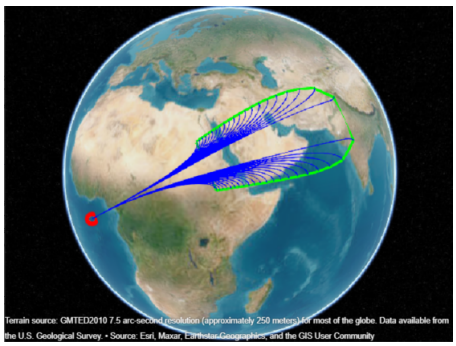

(c) *3D representation of the range capability.*

Figure 4.8: *Example of range capability estimation for Horus-2B, with initial condition reported in Table 4.1, 0° latitude, 0° longitude and 60° heading angle.*

algorithm. Then, it passes the problem and the decision vector to the optimisation algorithm which solves the problem. The output of the TO tool is a structure array containing the optimised variables and parameters.

The TO tool employs local algorithm to solve the trajectory optimisation problem [30, 31, 32]. The original continuous problem is transformed into a finite problem with K nodes through a direct transcription method. In particular, the Hermite-Simpson scheme has been implemented, even if in future work, different collocation methods may be included [73]. Then, the obtained NLP is solved by using a Sequential Quadratic Programming (SQP) algorithm [74] available in `MATLAB` toolbox within `fmincon` [75].

The decision vector of the trajectory optimisation problem typically includes the following variables:

- The state nodes: $\{\boldsymbol{x}_1^{(p)}, ..., \boldsymbol{x}_N^{(p)}\}$, for $p = 1, ..., P$;
- The control nodes: $\{\boldsymbol{u}_1^{(p)}, ..., \boldsymbol{u}_N^{(p)}\}$, for $p = 1, ..., P$;
- The final time of each phase $t_f^{(p)}$ for $p = 1, ..., P$;

Additional parameters may be added to the optimisation vector if required. The number of the nodes N can be different between the phases.

4.2.7 GNC tool

The GNC tool is an user customisable framework to include a GNC model within the missionisation process. The models of the GNC system commonly includes hardware and software which are dependent on the re-entry vehicle itself and the mission to be performed. The implementation of a general fully functional GNC may result into a hard task. For this reason, the GNC tool allows to interface external GNC models depending on the analysed case. This operation is done by two user-defined functions. The first one is used to define the parameters needed by the external GNC model, while the second function translates the outputs of the other disciplines in a format readable by the GNC. In the context of re-entry vehicles, typically, the outputs needed by a classical GNC model are the profiles of the reference trajectory computed by the TO tool, and the AoA trim line obtained by the FQA tool. More novel GNC appraoches, such as the optimal on-board guidance [26, 71, 76, 77], may require only the reference profiles for the generation of the guess solution to initialise the process.

Figure 4.9 shows an example of translation process performed by the GNC tool. In this example, the GNC module requires the drag-energy profile, obtained from the TO tool, and the AoA trim line, computed in the FQA tool. The GNC tool fits the discrete profiles with a cubic spline in a set of breakpoints. The selection of the breakpoints is automatically performed by the tool in order to minimise the RMSE. Figures 4.9a and 4.9b report the reference data points, the selected breakpoints and the obtained splines. Moreover, the figures shows the residuals between the interpolated splines and the reference data points. Figures 4.9c and 4.9d display the convergence of the RMSE during the selection of the breakpoints. For both cases the obtained

splines are featured by a low RMSE and coefficient of determination R^2 equal to 1, meaning that the reference profiles are well replicated by the splines.

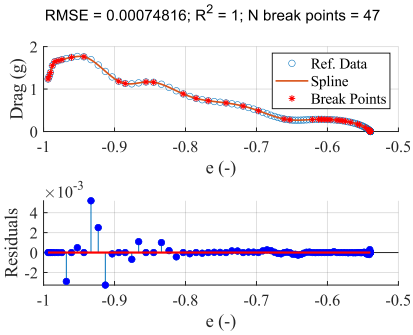

(a) *Drag-energy reference profile (blue circles) fitted by the GNC tool. The selection of the fitting point (red dots) is performed automatically to minimise the RMSE.*

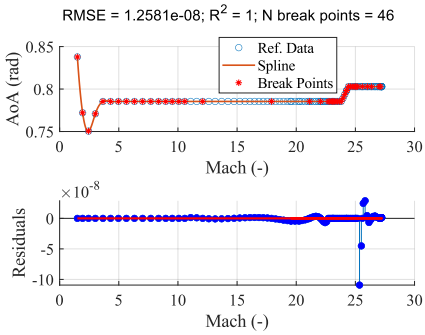

(b) *AoA-Mach reference profile (blue circles) fitted by the GNC tool. The selection of the fitting points (red dots) is performed automatically to minimise the RMSE*

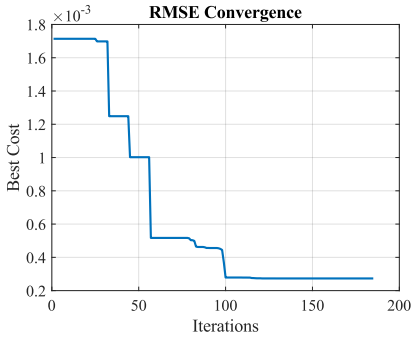

(c) *RMSE convergence for the translation of the drag-energy profile.*

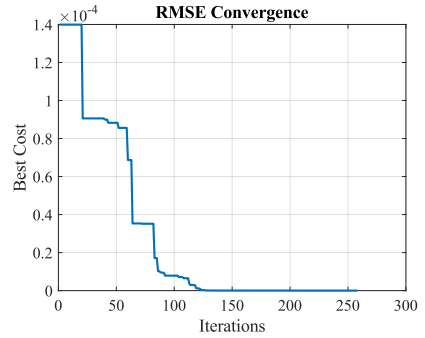

(d) *RMSE convergence for the translation of the AoA-Mach profile.*

Figure 4.9: *Example of fitting of the reference profiles performed by the GNC tool.*

"Okay, Houston ... we've had a problem here"
Jack Swigert - Apollo 13

CHAPTER 5

Validation

The objective of this chapter is to report the validation process followed during the development of the missionisation tool. The validation has the goal to check that the code achieves its purpose. Due to the extension of the work, the chapter shows the validation of the disciplines, while the tests performed for the environmental models and equations of motion are not reported.

The chapter is organised as follow: Section 5.1 gives an overview of the validation process for the GEOM, AEDB, FQA, EC, and FE tool. In Section 5.2, a preliminary analysis regarding the error propagation is performed, while Section 5.3 reports the validation of the TO tool considering the results of the RETALT(Retro Propulsion Assisted Landing Technologies) project [78].

5.1 Validation of the Disciplines

The general logic followed during the validation process was to compare the results obtained with the developed tool against the data available in the literature and the outcomes achieved with validated models.

For what concerns the GNC tool, its validation is not reported here

because it depends on the specific analysed case. However, the example reported in Section 4.2.7 exploits validated `MATLAB` functions, so further validation actions are not needed. Moreover, the inspection of the RMSE underscores the process was executed with success.

5.1.1 GEOM tool validation

The GEOM tool has been validated by computing the mass of several re-entry vehicles and comparing the results with the data available in the literature [13, 15]. Table 5.1 reports the comparison and the associated errors. The overall model accuracy is ±10%, which is the typical value for semi-empirical methods and the preliminary design [63]. For this reason, the results have been deemed acceptable within this research. Only X34 has a larger error, but it was designed for sub-orbital applications to demonstrate key technologies for RLV, so a bigger error was expected.

Regarding the reference surface, it was difficult to gather data. The GEOM tool, in fact, estimates the planform area of the vehicle, however in the literature it is often not specified whether the reference surface is the planform area or not. Moreover, the GEOM tool computes a reference area following the guidelines used for the development of the AEDB tool, so a difference with respect to the literature value is expected. For instance, the reference area computed for the Space Shuttle is 309 m^2, while in the literature is 249 m^2. For Hermes, the values are 74.4 m^2 and 84.7 m^2, while for Horus-2B, the estimation is 108.2 m^2, while the real value is 110 m^2. [13, 15, 62]. For the purpose of the research, these value have been considered acceptable, since the proposed GEOM tool shall be used only during the early phase of the design process for preliminary analysis.

Table 5.1: *Mass estimation assessment.*

Name	Category	Mass tool [kg]	Mass Reference [kg]	Error %
Space Shuttle	WRV	75662	78000	-3.00
Horus-2B	WRV	27397	26029	5.25
Hopper	WRV	63680	60200	5.78
X34	WRV	10363	8200	26.38
Hermes	WRV	15945	15000	6.30
X38	WLB	11430	10659	7.23
HL-20	WLB	11881	10884	9.16
IXV	LB	2002	1900	5.37
Space Rider	LB	2714	2900	-6.41

5.1.2 AEDB tool validation

The AEDB tool has been validated by comparing the aerodynamic coefficients estimated with the AEDB tool against the data available in literature computed with CFD and wind tunnel tests [13, 15, 62].

Figure 5.1 shows the literature data (full line) and the ones obtained with the proposed tool (dashed lines) for Horus-2B. Figure 5.2, instead, reports the aerodynamic coefficients for X38. Generally speaking, the discrepancies increase by reducing the Mach number and by increasing the angle-of-attack. This behavior is due to the fact that when the angle-of-attack is increased nonlinear phenomena arise. These phenomena are difficult to predict with semi-empirical approach and simplified methods, resulting in a loss of accuracy. Moreover, by decreasing the Mach number, the aerodynamic performance is more sensitive to every feature of the geometry of the vehicle [79]. The same discussion can be done for the prediction of the pitching moment coefficient (here not reported). The AEDB tool can only approximate the trends for hypersonic regime, and the more complex the geometry is, the more the discrepancies increase. However, the trends of the drag and lift coefficients are catch and the L/D is estimated with good performance. This behavior is due to the fact that simplified methods exploits the lift for the estimation of the drag (lift-induced drag), so given a specific geometry, an overestimation (or underestimation) of the lift creates an overestimation (or underestimation) of the drag, resulting to a mitigation of the L/D error. This also reduces the impact on the mission performance.

It is reminded that the scope of the AEDB tool is to have a representative estimation of the aerodynamic coefficients in real-time (less than 1 second in a consumer hardware) to be used for preliminary analysis, and not an accurate aerodynamics characterisation of the vehicle, thus the achieved accuracy has been deemed acceptable for this research. Future work will address an improvement of this discipline.

5.1.3 FQA tool validation

The FQA tool has been validated by performing the FQA of past projects. Here, the FQA of RETALT have been reported and compared against the results obtained by the DEIMOS validated tool [25, 80]. The analyses have been carried out with a high-fidelity aerodynamic database of RETALT obtained from a dataset provided by DLR [81, 82, 83].

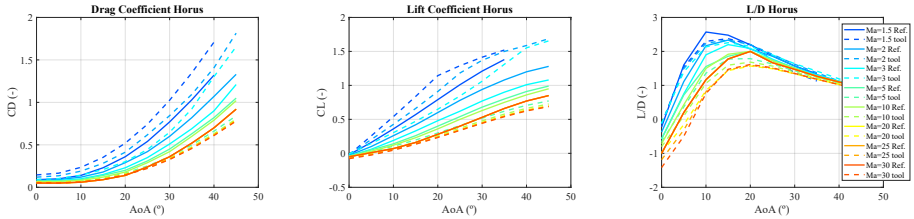

(a) *Lift coefficient.* **(b)** *Lift coefficient.* **(c)** *Lift to drag ratio.*

Figure 5.1: *Aerodynamic coefficients with $\delta = 0°$ for the Horus-2B. The full lines are the literature data, while the dashed lines are the profiles computed with the AEDB tool.*

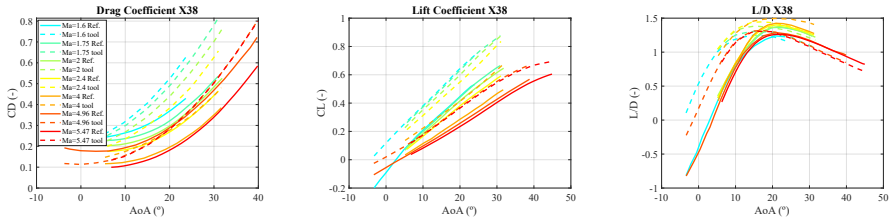

(a) *Lift coefficient.* **(b)** *Lift coefficient.* **(c)** *Lift to drag ratio.*

Figure 5.2: *Aerodynamic coefficients width $\delta = 20°$ for the X38. The full lines are the literature data, while the dashed lines are the profiles computed with the AEDB tool.*

Figure 5.3 shows the comparison of the outcomes. Due to a different convention used within the FQA tool and the RETALT consortium, the AoA is defined with a difference of 180°. Moreover, the accessible dataset is limited to +10° of AoA, so the results have been compared till this value (red box in Figures 5.3c and 5.3d). The reference cases are available in [25, 84].

The visual comparison of Figures 5.3a and 5.3c shows very similar results for the analysed case. The fin deflections required for the trim are practically the same for each AoA-Ma couple. Moreover, both figures detects an untrimmable area in the region around M=4 and AoA=10°. The same discussion can be done for the evaluation of the AoA Entry Corridor, by looking Figures 5.3b and 5.3d. The only difference is given by an unstable area around AoA=10° at M=0.9 obtained with the FQA tool. This discrepancy can be dictated by the assumption done for the creation of the aerodynamic database from the dataset.

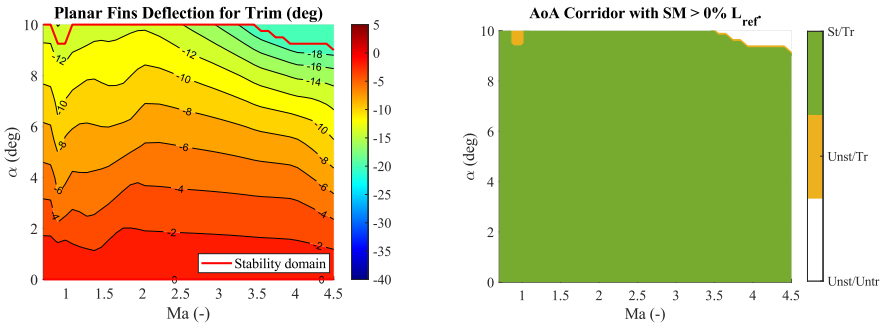

(a) *RETALT trim analysis with FQA tool.* **(b)** *RETALT AoA corridor with FQA tool.*

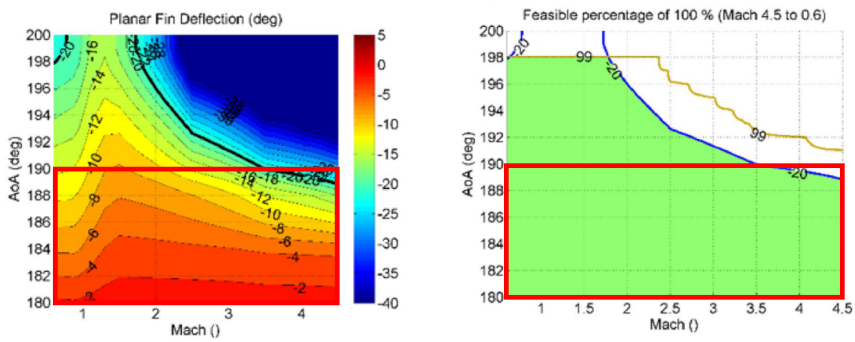

(c) *RETALT reference trim analysis [25].* **(d)** *RETALT reference AoA corridor analysis [25].*

Figure 5.3: *Comparison of FQA results obtained with the FQA tool with respect to the reference (red boxes).*

5.1.4 EC tool validation

The EC tool has been validated by comparing the entry corridor in the drag-energy domain of the spaceplane Horus-2B obtained with the proposed tool and the outcomes reported in [71].

For the evaluation of the validation tests, it has been considered the mission scenario reported in [71]. Table 4.1 reports Horus-2B the geometric features and peak loads, while the boundary conditions have been changed such that the initial conditions are given by $h_{EIP} = 122$ km, $V_{EIP} = 7435.5$ m/s, and $\gamma_{EIP} = -1.43°$. The terminal conditions, instead, are $h_{TAEM} = 25$ km and $M_{TAEM} = 2.5$. Figures 5.4 shows the comparison between the two entry corridor. The results (Figures 5.4a and 5.4b) are visually very similar and there are not significant differences.

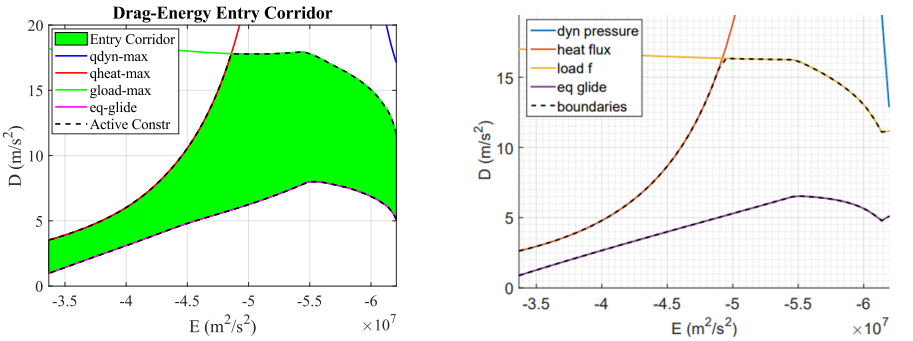

(a) *HORUS-2B Entry Corridor computed with the EC tool.*

(b) *HORUS-2B reference Entry Corridor [71].*

Figure 5.4: *Comparison of EC results obtained with the EC tool with respect the reference.*

5.1.5 FE tool validation

The FE tool has been validated by comparing the range capability estimated by the FE tool with the landing footprint computed by solving a family of maximum crossrange problem with the TO tool [31, 72, 85].

The maximum crossrange problem have been formulated in a rotating frame with Eq. (4.1) and the aerothermal-mechanical constraints have been imposed to obtain feasible trajectories. The control variable is the bank angle, and the landing footprint have been obtained by varying the downrange. For the sake of simplicity, the problem has been solved at the Equator with initial heading equal to 90°, so due to East. In this particular case, in fact, the crossrange is directly given by the latitude, so the cost function of the problem is the latitude at the final time. The complete formulation of the problem can be seen in [31, 72].

Figure 5.5 visualises the landing footprint obtained with the two methods considering Horus-2B. As expected, the optimised landing footprint is larger than the one obtained by the FE tool [72]. The optimiser, in fact, can find better solutions in terms of bank profiles, especially for high-drag trajectories. However, the absolute maximum crossrange is well described by the FE tool, as well as the maximum downrange attainable by the vehicle. Moreover, the FE tool is more efficient in terms of computational demand: it requires roughly 5 seconds to generate the footprint, while the TO tool employs about 1 minute per trajectory (the performance considers an Intel®Core^{TM} i7-8750H processor).

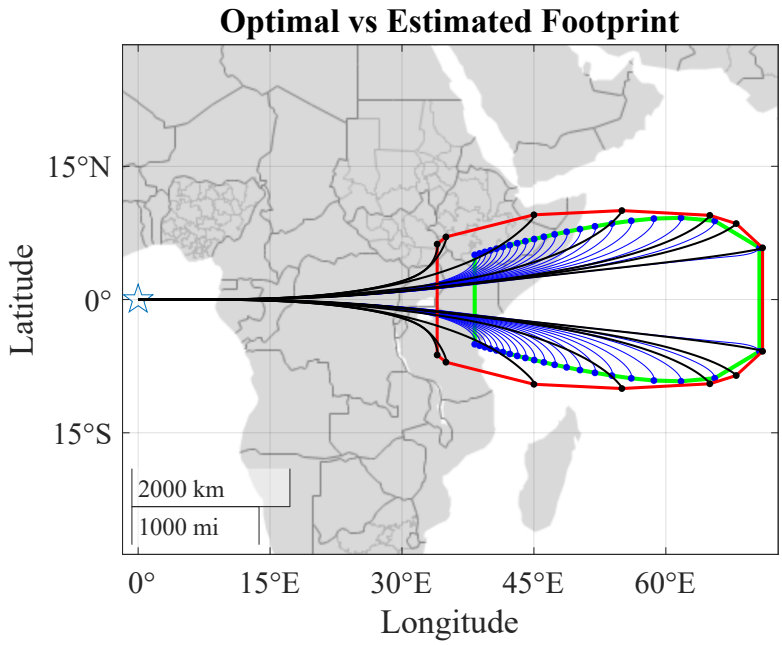

Figure 5.5: *Optimal (red) and estimated (green) range capability. The initial point is defined by the start.*

5.2 Sensitivity Analysis

The validation process of the disciplines has identified the GEOM tool and the AEDB tool as two possible critical factors. In order to better assess how the errors introduced by these disciplines impact on the output of the missionisation tool, a preliminary sensitivity analysis has been performed by perturbing the parameters computed within the GEOM and the AEDB disciplines.

The considered parameters are the dry mass and the reference surface of the vehicle, and the drag and lift coefficients. An *One-variable-at-a-time* analysis has been carried out, where one parameters is perturbed by a percentage of ($\pm 10\%$), while all the others are kept fixed [39]. The objective of this analysis is to assess which discipline may determine the largest error in the output of the missionisation tool. In this way, it is possible to identify where to pinpoint the attention for future improvements and developments.

The analysis considers two outputs of the missionisation tool, which have been used as performance indices for the application case in Section 6.2. The former is the edge distance (D_{min}), that is defined as the

minimum distance between the target point and the landing footprint edge. The latter is the deflection margin (Δ_δ), which is the minimum excursion of the aerodynamic surface that is still available to control the vehicle after achieving the trim. For an extensive definition of these performance parameters see Section 6.2.2.

Table 5.2 shows the results of the *One-variable-at-a-time* analysis for a variation of the parameters equal to +10%. The re-entry vehicle is Horus-2B, with the nominal parameters expressed in Table 4.1. The mission scenario considers an equatorial re-entry with the TAEM interface at 0° and 50° longitude. The influence of the mass and S_{ref} on the D_{min} is less than ±4%. As expected, an increase of the mass caused a decrease of the D_{min}, due to an higher ballistic coefficient. On the other hand, a bigger S_{ref} is translated into a smaller ballistic coefficient that caused a larger D_{min}. However, the impact of these two parameters is limited because they affect in the same way the accelerations due to the aerodynamics forces. Moreover, the mass and S_{ref} do not have an influence on the Δ_δ, since this output does not depend on these parameters (Table 4.5).

Concerning the influence of C_D and C_L on the outputs, as expected they have a larger impact, since they caused a variation of the two outputs around the ±10%, for the analysed case. A variation of one of these parameters, in fact, leads to a modification of the L/D of the re-entry vehicle, in one case a decrease in the L/D of approximately -10% (ΔC_D +10%), and in the other case +10% (ΔC_L +10%). This effect has a direct impact on the flying capability of the vehicle itself, and so on the D_{min}. However, as reported in Section 5.1.2, the estimation of the C_D and C_L are mutually connected, leading to a mitigation of the L/D error. If both C_D and C_L are increased by +10%, the percentage variation of D_{min} lowers to +3%. A similar discussion can be done for Δ_δ, where a modification of the aerodynamic database yields to different trim conditions.

The results of this analysis shows that the AEDB tool has the largest influence on the considered outputs of the missionisation tool. However, so far the AEDB tool has been developed only for preliminary analysis, where large uncertainties are still accepted. Further improvements and future work will address the definition of a more accurate AEDB tool. As reported, in Section 4.2.2, the computation of an complete aerodynamic characterisation of the vehicle is out of the scope of this research. Whenever more accurate analysis must be performed, the user can provide a high-fidelity aerodynamic database.

Table 5.2: *Preliminary sensitivity analysis of the error for WRV with Horus-2B. The nominal value of D_{min} is 910 km, while for Δ_δ it is 6.4°.*

	Mass [kg]	$\boldsymbol{S_{ref}}$ [m^2]	$\boldsymbol{C_D}$ [-]	$\boldsymbol{C_L}$ [-]
Ref. Value	26029	110	0.918	0.851
Δ Value (+10%)	2602.9	11	0.0918	0.0851
$\boldsymbol{D_{min}}$ [km]	877.7	940.3	820.4	1031.8
$\boldsymbol{\Delta D_{min}}$ [%]	-3.55	3.33	-9.85	13.38
$\frac{\Delta D_{min}}{\Delta Param.}$	-0.01 [km/kg]	2.75 [km/m^2]	-976.93 [km]	1431.26 [km]
$\boldsymbol{\Delta_\delta}$[◦]	6.4	6.4	5.7	5.9
$\boldsymbol{\Delta(\Delta_\delta)}$ [%]	0	0	-10.94	-7.81
$\frac{\Delta(\Delta_\delta)}{\Delta Param.}$	0 [◦/kg]	0 [◦/m^2]	-7.63 [◦]	-5.88 [◦]

5.3 RETALT Missionised Solution

In order to validate the TO tool, this section reports the missionisation of the DRL trajectory of RETALT from the MECO condition [78, 86, 87]. The objective is to test the TO tool in a representative reference scenario, in which the preliminary design of the mission was performed.

5.3.1 Problem parameters and formulation

To implement this test case, the first stage features of RETALT1 have been considered [86]. The system is characterised by a length of 71.2 m and a body diameter of 6 m. It has nine engines, with liquid oxygen and hydrogen (LOX/LH2) with a specific impulse at sea level of 372.2 s, but only three of them are used during the re-entry burn, and one during landing manoeuvre. Each engine can provide 1179 kN of thrust. The gross mass at MECO is 116.288 tons, with 57 tons of propellant. The first stage is equipped in planar fins, and the high-fidelity aerodynamic database has been provided by the DLR. This database has been used also to perform and validate the FQA, as reported in Section 5.1.3. The environment is modeled by considering the US76 atmospheric model and spherical Earth.

The optimisation problem is modelled by considering four phases, as shown in Section 2.5. The equation of motion are expressed in Cartesian coordinates and the system is modelled as a 3DoF point mass (Eq. 4.7). The cost function is the maximisation of the final mass, while typical aerothermal-mechanical constraints and control limits are taken into accounts. As explains Eq. (4.7) in Section 4.1.1, the control variables describes the thrust magnitude and direction during the propulsive phase, otherwise it enters in the definition of the AoA. Equa-

tion (5.1) presents the formulation of the optimisation problem. The boundary conditions and the path constraints value are reported in Table 5.1, the boundary conditions are given in spherical coordinates for an easier physical visualisation.

$$
\begin{aligned}
&\text{minimize} \quad J = -m(t_f^{(4)}) \\
&\text{subject to} \\
&\quad \dot{\boldsymbol{x}}^{(p)}(t) = \mathbf{f}^{(p)}(\boldsymbol{x}^{(p)}(t), \boldsymbol{u}^{(p)}(t), t) \qquad \text{Equation (4.7)} \\
&\quad \boldsymbol{x}^{(1)}(t_0^{(1)}) = \boldsymbol{x}_0 \\
&\quad \boldsymbol{x}^{(4)}(t_f^{(4)}) = \boldsymbol{x}_f \\
&\quad ||\boldsymbol{u}^{(p)}(t)|| = 1 \\
&\quad 0 \leq T_{nom}^{(k)}(t) \leq \bar{T} \qquad\qquad \text{p} \in [1,2,3,4] \\
&\quad r_E \leq ||\boldsymbol{r}^{(p)}(t)|| \qquad\qquad \text{k} \in [2,4] \\
&\quad q_{dyn}^{(j)} \leq q_{dyn,max} \qquad\qquad \text{j} \in [2,3,4] \\
&\quad \dot{q}_{heat}^{(j)} \leq \dot{q}_{heat,max} \qquad\qquad \text{s} \in [1,2,3] \\
&\quad n_x^{(j)} \leq n_{x,max} \\
&\quad n_z^{(j)} \leq n_{z,max} \\
&\quad \alpha^{(j)} \leq \alpha_{max} \\
&\quad \boldsymbol{x}(t_f^{(s)}) = \boldsymbol{x}(t_0^{(s+1)})
\end{aligned}
\tag{5.1}
$$

Table 5.3: *Problem parameters and boundary conditions.*

Parameter	Value	Units	Parameter	Value	Units
ϕ_{MECO}	5.211	∘	$m_0^{(1)}$	116288	kg
θ_{MECO}	-51.974	∘	$\bar{T}$ (1 engine)	1179	kN
ψ_{MECO}	94.640	∘	$q_{dyn,max}$	80	kPa
h_{MECO}	93.057	km	$\dot{q}_{heat,max}$	200	kW
V_{MECO}	2217.203	m/s	$n_{x,max}$	6.4	g
ϕ_f	4.743	∘	$n_{z,max}$	1.6	g
θ_f	-46.506	∘	α	10	∘
ψ_f	118.549	∘	$\|\|\boldsymbol{u}(t)\|\|$	1	-
h_f	0.020	m	V_f	2.051	m/s

5.3.2 Results

Figure 5.6 shows the results of the TO tool with the reference trajectory computed within the RETALT project. Figure 5.6a visualises the trajectory in the altitude-velocity domain, reporting also the entry corridor of the aerodynamic phase (green region). The trajectories are very similar, especially concerning the aerodynamic and the landing phases. The differences in the entry burn phase are due to the fact that the TO tool found a solution in which the engine is ignited approximately 5 km above the point in the reference trajectory, as also reported in Figure 5.6c. However, the altitude variation with the time is practically the same, as shown in Figure 5.6d. Moreover, both trajectories lie within the entry corridor, underlying the coherency among the results. The discrepancies between the two solutions may depends by several factors including the modeling of the environment, the post processing of the aerodynamic database, and the formulation of the optimisation problem.

Table 5.4 reports the values of the state variables at the beginning of each phase and at the touchdown. As it is possible to note, the errors between the obtained solution and the reference trajectory is negligible for most of the cases (<3%). The comparison of the two trajectories leads to a precise match between the results, both in terms of state variables and time schedule of the phases. In particular, the ratio between the final masses is 1.0004, meaning that the optimisation processes converge to the same cost value. Furthermore, the peak loads are well predicted. The obtained results provide confidence in the implementation of the TO tool, showing that the validation process has been satisfactorily accomplished.

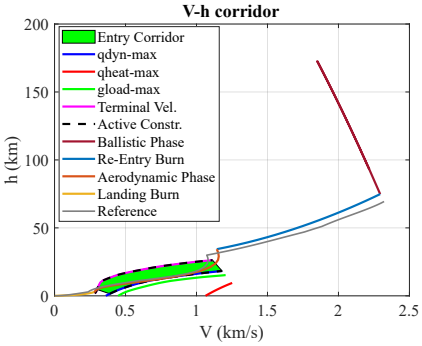

(a) *RETALT trajectory in the Altitude vs Velocity plane.*

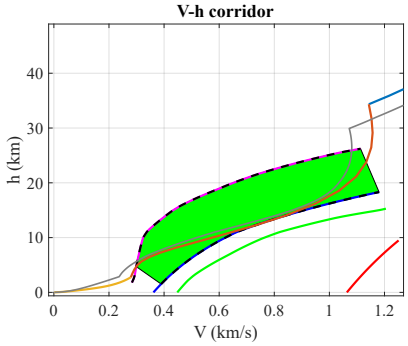

(b) *RETALT trajectory in the Altitude vs Velocity plane: aerodynamic and landing phases inspection. Same legend of Figure 5.6a.*

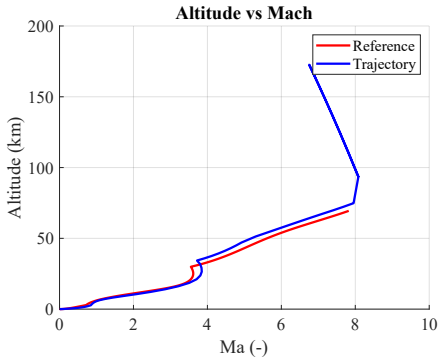

(c) *RETALT Altitude-Mach profiles comparison.*

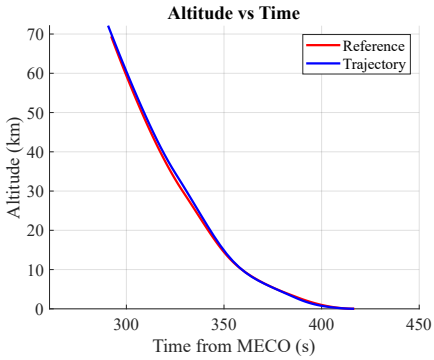

(d) *RETALT altitude histories comparison.*

Figure 5.6: *Comparison of results obtained within the RETALT project (red) and the ones obtained with the TO tool.*

Table 5.4: *RETALT trajectory comparison for TO tool validation.*

Parameter	Value	Ref. Value	Error [%]	Constraint
Re-entry Burn Start				
Time [s]	288.52	291.80	-1.1	
Altitude [km]	74.85	69.94	7.0	
Co-rotating velocity [m/s]	2293.88	2314.09	-0.9	
Longitude [◦]	-47.25	-47.195	0.1	
Latitude [◦]	4.80	4.79	0.2	
Mass [t]	116.29	116.29	0.0	
FPA [◦]	-34.39	-35.03	-1.8	
Heading [◦]	95.28	95.30	0.0	
Downrange flown [km]	525.86	532.04	-1.2	
Aerodynamic Phase Start				
Time [s]	325.33	328.9	-1.1	
Altitude [km]	34.34	29.92	14.8	
Co-rotating velocity [m/s]	1143.11	1080.39	5.8	
Longitude [◦]	-46.80	-46.75	0.1	
Latitude [◦]	4.76	4.75	0.2	
Mass [t]	80.61	80.35	0.3	
FPA [◦]	-43.24	-43.74	-1.1	
Heading [◦]	95.11	95.35	-0.3	
Downrange flown [km]	575.78	582.20	-1.1	
Landing Burn Start				
Time [s]	386.98	387.8	-0.2	
Altitude [km]	2.75	2.87	-4.5	
Co-rotating velocity [m/s]	279.12	242.99	14.9	
Longitude [◦]	-46.53	-46.52	0.0	
Latitude [◦]	4.74	4.74	0.0	
Mass [t]	80.61	80.35	0.3	
FPA [◦]	-51.80	-51.40	0.8	
Heading [◦]	88.75	86.38	2.7	
Downrange flown [km]	605.79	607.33	-0.3	
Touchdown				
Time [s]	416.7	416.8	0.0	
Altitude [km]	0.02	0.02	0.0	
Co-rotating velocity [m/s]	2.05	2.05	0.0	
Longitude [◦]	-46.51	-46.51	0.0	
Latitude [◦]	4.74	4.74	0.0	
Mass [t]	71.01	70.98	0.0	
FPA [◦]	-89.94	-89.94	0.0	
Heading [◦]	88.95	89.94	-1.1	
Downrange flown [km]	608.62	608.61	0.0	
Max Loads and Constraints				
Body Pitch at Landing [◦]	88.95	89.94	-1.1	>85
Max Q [kPa]	80.0	79.7	0.4	<80.0
Max normal load [g]	4.72	4.9	-3.67	<6.4
Max lateral load [g]	1.16	1.56	25.6	<1.6

"This is not flying, it's falling with style!"
Buzz Lightyear - Toy Story

CHAPTER 6

Test Cases

THIS chapter reports the application cases developed within this research work, that are used to validate the proposed missionisation tool and to evaluate its flexibility in diverse scenarios and analyses.

6.1 Lifting Body Missionised Solution: Mission Design and Verification from EIP to TAEM

Commonly, a reusable re-entry vehicle needs to perform a range of different missions during its operational life. In this case, the missionisation is the recurrent activity to tailor the mission analysis and GNC solution for the particular mission that must be fulfilled. The test case presented in this section shows an application of the MA and GNC missionisation tool for the optimal adaptation of the mission analysis solution and the GNC parameters concerning a specific mission scenario and re-entry vehicle.

The presented test case consists in the design of an end-to-end re-entry mission from the de-orbiting manoeuvre to the TAEM interface point, by considering specific mission requirements and constraints. In

particular the followed approach is constituted by these steps:

- Assessment of the longitudinal FQA within the range of entry conditions of the considered re-entry vehicle.
- Definition of the EIP conditions by coupling the performance and the feasibility of both the de-orbiting manoeuvre and the range capability of the considered vehicle.
- Computation of the reference optimal trajectory from the EIP to the TAEM interface point.
- Tuning of the GNC parameters based on the obtained reference trajectory.
- Assessment of the reference trajectory in a high-fidelity simulator with the closed-loop guidance in nominal conditions, in order to define the nominal trajectory.
- Verification of the missionised MA and GNC solution through a Montecarlo campaign within the high-fidelity simulator.

The high-fidelity simulator used within this application case is ENDOSIM, developed by DEIMOS Space S.L.U [80]. This methodology has been applied to a lifting body vehicle similar to the Space Rider (Space Reusable Integrated Demonstrator for Europe Return) and the Intermediate eXperimental Vehicle (IXV) [8, 18], but it can be employed for any user-defined case.

6.1.1 Objectives

The objectives of this test case are the following:

- Optimal tuning of the end-to-end mission analysis solution and the GNC parameters for the specific mission scenario.
- Validation and verification of the obtained solution with DEIMOS high-fidelity simulator.

The overall goal is to show the capability of the MA and GNC missionisation tool and how it can be used for the missionisation process.

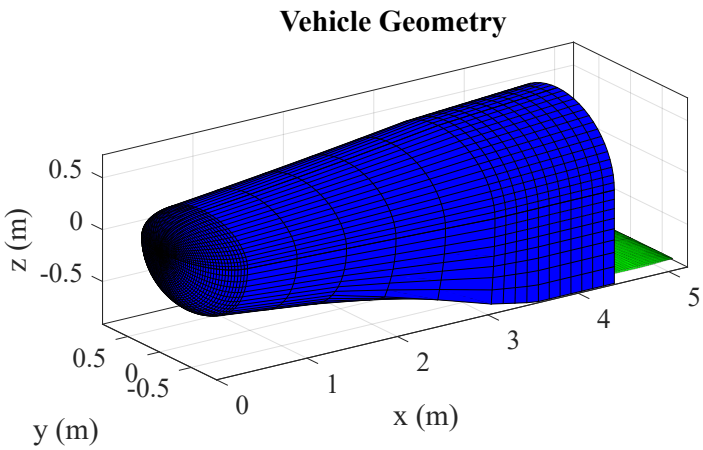

Figure 6.1: *Geometry representation of the considered lifting body.*

6.1.2 Problem Modelling

Vehicle Design

The vehicle is composed by an expendable AVUM Orbital Module (AOM) used for the orbital operations and the de-orbiting manoeuvres [8, 88], and a reusable re-entry module.

The re-entry module is a lifting body with similar size and shape to Space Rider [8, 18, 89]. The vehicle is characterised by a longitudinal length of 4.4 m, and a mean fuselage diameter of 1.8 m, it has a re-entry mass of 2950 kg. The re-entry vehicle is equipped with two body flaps that are used to trim and control the vehicle on the longitudinal axis with symmetrical deflections, and lateral axis with unsymmetrical deflections during the re-entry phase. Figure 6.1 shows the geometry of the vehicle

The AVUM has a dry mass 590 kg and it loads 740 kg of propellant to perform the de-orbiting. The engine can develop a maximum thrust of 2.42 kN with a specific impulse in vacuum of 315.5 s [88].

Aerothermodynamics

The aerodynamics of the vehicle has been computed by exploiting the DLR porperty tool HOTSOSE with the geometry reported in Figure

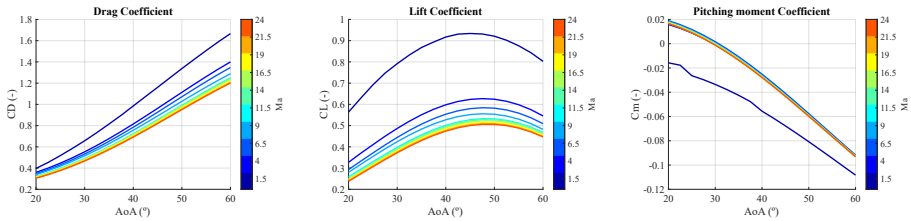

(a) *Drag coefficient.* **(b)** *Lift coefficient.* **(c)** *Pitching moment coefficient.*

Figure 6.2: *Aerodynamic coefficients for $\delta = 0°$ for the considered vehicle.*

6.1. The datasets of the untrimmed aerodynamics coefficients C_D, C_L and C_m have been defined by considering a Mach number range of $1.5 \leq M_a \leq 24$, an AoA variation between $20° \leq \alpha \leq 60°$, and flaps deflection within $-30° \leq \delta \leq 30°$. Then, the datasets have been used both to create interpolation functions and look-up tables. The former have been used as input for the missionisation tool, while the latter have been employed for the simulation with ENDOSIM. Figure 6.2 show the aerodynamics variation with respect to the AoA, for different Mach number, while considering $\delta = 0°$.

For what concerns the thermodynamics model, it has been modelled with the Chapman equation (or Sutton Graves equation) [12] within the analyses performed with the missionisation tool. This equation estimates the heat flux at the stagnation point of the vehicle, that typically is at the nose. Regarding the simulation with ENDOSIM, a more accurate thermal model has been used, that takes into account both the radiative and the convective heat flux [57].

Mission Scenario

The test mission analysed within this application case assumes that the vehicle has a circular operational orbit characterised by an altitude of 400 km and an inclination of 4°. The landing point is close to the ESA Kourou Centre Spatial Guyanais launch site. For this reason, the target TAEM interface point is at 52.69027° W longitude and 5.1689° N latitude. Table 6.1 reports the complete orbital parameters and the TAEM conditions.

The mission is composed by two main phases. The first one consists in the de-orbit manoeuvre, which is a controlled manoeuvre to change the trajectory of the re-entry vehicle in such a way that it starts its

Table 6.1: *Operational orbit and TAEM interface point parameters.*

Parameter	Value	Unit
a_{orbit}	$400 + R_E$	km
e	0	-
i	4	◦
Ω_{orbit}	255.42	◦
ω_{orbit}	29.11	◦
h_{TAEM}	25	km
θ_{TAEM}	-52.69027	◦
$\phi TAEM$	5.1689	◦
V_{TAEM}	448	m/s
$M_{a,TAEM}$	1.5	-

re-entry into the planet atmosphere. The second phase is characterised by the atmospheric reentry, in which a controlled trajectory is defined in order to bring the vehicle towards the target TAEM (or landing) point. The de-orbit and the re-entry trajectory have been computed separately.

De-Orbit Modelling

The de-orbit problem has been modelled with point mass 3DoF equations of motion in Cartesian coordinates with respect to the ECEF reference frame. The gravity model assumes spherical Earth with standard gravitational parameters $\mu = 3.986 \times 10^{14}$ m^3/s^2 and a radius $R_E = 6378.137$ km. The manoeuvre have been computed by formulating the problem into three phases: two coast arcs, where the engine of the AVUM is switched off, and one burning arc. The dynamics equations are the ones reported in Section 4.7, but assuming the absence of atmosphere and the presence of the thrust term only during the powered phase. Thus, it has been solved a multiphase optimal control problem to minimise the propellant used to perform the manoeuvre. The optimisation problem has been treated as explained in Section 4.2.6, so the decision vector includes the state variables $\boldsymbol{x}^{(p)}(t) = [\boldsymbol{r}(t), \boldsymbol{v}(t), m(t)] \in \mathbb{R}^7$, the control variables $\in \mathbb{R}^4$, and the final time of each phase, with $p \in [1, 2, 3]$. The control is given by the thrust magnitude $T^{(2)}_{nom}(t)$ and its direction $\boldsymbol{u}^{(p)}(t)$. For this case, the problem has been discretised in 90 nodes, 30 for each phase, thus the optimisation variables are 933. Table 6.2 summarised the formulation of the minimum-propellant de-orbit problem.

Table 6.2: *Minimum-propellant de-orbit manoeuvre formulation.*

	Equations	Comments
Cost Function	$-m(t_f^{(3)})$	
Dynamics Constraints	$\dot{\boldsymbol{x}}^{(p)}(t) = \mathbf{f}^{(p)}(\boldsymbol{x}^{(p)}(t), \boldsymbol{u}^{(p)}(t), t)$	p ∈ [1,2,3]; Equation (4.7) without atmosphere
Boundary Conditions	$\boldsymbol{x}^{(1)}(t_0^{(1)}) = \boldsymbol{x}_0$ $\boldsymbol{x}^{(3)}(t_f^{(3)}) = \boldsymbol{x}_f$	$\boldsymbol{x}_0$ s.t. $\nu_{orbit} = 90°$ $\boldsymbol{x}_f = \boldsymbol{x}_{EIP}$
Path Constraints	$\|\|\boldsymbol{u}^{(2)}(t)\|\| = 1$ $0 \leq T_{nom}^{(2)}(t) \leq \bar{T}$ $r_E \leq \|\|\boldsymbol{r}^{(p)}(t)\|\|$ $\|\|\boldsymbol{r}^{(p)}(t)\|\| \leq 400 + R_E$	p ∈ [1,2,3] $\hat{T} = 2.42$ kN
Linkage Constraints	$\boldsymbol{x}(t_f^{(s)}) = \boldsymbol{x}(t_0^{(s+1)})$	s ∈ [1,2]

Atmospheric Re-entry Trajectory Modelling

The atmospheric re-entry has been modelled with the general assumptions presented in Section 4.1.1. Thus, the vehicle has been represented as 3DoF point mass in an ECEF reference frame with spherical coordinates. The re-entry trajectory problem has been formulated considering only one phase from the EIP to the TAEM interface point. Thus, an optimal control problem has been solved in order to obtain a feasible trajectory that targets the TAEM point, while a set of path and control constraints is imposed. In this case, the dynamics of the problem are given by Equation (4.1). However, they have been modified in order to use the bank rate as control variables to obtain a smoother control law. So, for this problem, the state variables is given by $\boldsymbol{x}(t) = [h(t), \theta(t), \phi(t), V(t), \gamma(t), \psi(t), \sigma(t)] \in \mathbb{R}^7$, while the control is $\dot{\sigma}(t) = u(t)$. Here, 100 discretisation points have been used, such that the problem has 801 variables. Table 6.3 summarises the formulation of the atmospheric re-entry trajectory problem.

Regarding the optimisation problem, the gravity model has been formulated by assuming spherical Earth with the same parameters reported for the de-orbit problem. The atmosphere has been modelled with the U.S. Standard Atmosphere 1976 model. As introduced in Section 6.1, the solution of the trajectory optimisation has been assessed and verified with DEIMOS high-fidelity simulator with a closed-loop guidance strategy. For this operation, the simulator employs the WGS84 geodetic system to model the Earth geometric parameters and

Table 6.3: *Atmospheric re-entry trajectory problem formulation.*

	Equations	Comments
Cost Function	$(h(t_f) - h_{TAEM})^2 + (\theta(t_f) - \theta_{TAEM})^2 +$ $+(\phi(t_f) - \phi_{TAEM})^2 + (V(t_f) - V_{TAEM})^2$	
Dynamics Constraints	$\dot{\boldsymbol{x}}(t) = \mathbf{f}(\boldsymbol{x}(t), \boldsymbol{u}(t), t)$	Equation (4.1) with bank rate
Boundary Conditions	$\boldsymbol{x}(t_0) = \boldsymbol{x}_0$ $\boldsymbol{x}(t_f) = [\,]$	$\boldsymbol{x}_0 = \boldsymbol{x}_{EIP}$
Path Constraints	$-5° \leq \dot{\sigma} \leq 5°$ $-90° \leq \sigma \leq 90°$ $q_{dyn}(t) \leq q_{dyn,max}$ $\dot{q}_{heat}(t) \leq \dot{q}_{heat,max}$ $n_{load}(t) \leq n_{load,max}$ $D_{glide} \leq D(t)$	$q_{dyn,max} = 8$ kPa $\dot{q}_{heat,max} = 670$ kW/m^2 $n_{load,max} = 4$ g

the EGM2008 for the gravity model [90]. Moreover, it uses the NRLMSISE00 model for the Earth atmosphere [60].

The output of the optimisation routine has been used for tuning of the GNC parameters. The guidance technique used for this application is similar to the one used by Space Rider and IXV [89, 91]. Briefly, it is based on the update of the nominal drag profile to cope with discrepancies between the on-board estimation of the range-to-go and the available range capability. The range-to-go prediction is performed considering the current drag profile and the actual state of the vehicle. Then, the drag profile is used to schedule bank manoeuvres. The guidance also employs a lateral corridor to handle the azimuth error. This guidance strategy requires the drag profile in a spline-format, so for this case, the tuning GNC parameters are the coefficient of the spline to fit the reference trajectory. This operation is automatically performed by the missionisation tool within the GNC tool (Section 4.2.7). Moreover, the simulator employs a navigation performance model complaint with the one used by Spacer Rider to estimate the state along the simulation of the re-entry trajectory, while the control is not considered, and so the dynamics of the system is directly fed with the guidance commands.

Approach for the definition of the EIP

As described in the previous sections, the end-to-end mission is composed by the de-orbit manoeuvre and the atmospheric re-entry. The connecting point between these two phases is the Entry Interface Point.

The definition of a such point affects the mission performance and feasibility of both phases. Concerning the de-orbit manoeuvre, the selection of the EIP has to take into account the propellant budget constraint, while for what regards the atmospheric re-entry phase, the selection of the EIP directly influence the reachable area. In order to have a feasible re-entry mission, the target point must be included in the range capability of the vehicle.

According to the mission scenario described in Section 6.1.2, a coupled parametric analysis has been performed to select the coordinates of the EIP. This analysis aim at finding the longitude θ_{EIP} and the latitude ϕ_{EIP} of the EIP such that the feasibility of both the de-orbit manoeuvre and the atmospheric re-entry is granted. The other variables have been prescribed using typical LEO re-entry values and geometric constraints [8, 92]. Thus, the EIP altitude is $h_{EIP} = 120$ km, the EIP co-rotating velocity is $V_{EIP} = 7.429$ km/s, the EIP flight-path-angle is $\gamma_{EIP} = 1.20°$, and the EIP heading angle is $\psi_{EIP} = 86°$.

The analysis has the following steps:

- Evaluation of the minimum distance between the target point and the range capability edge with respect to the θ_{EIP} and ϕ_{EIP};
- Selection of the EIP coordinates by inspecting the ground track of the operational orbit and the maps obtained in the previous step;
- Evaluation of the de-orbit manoeuvre performance to reach the selected EIP point;

This search study has been performed through a parametric analysis. In future work, it may be embedded within a unique optimisation process to obtain more refined and accurate results, however the computational effort to solve this kind of problem might be intensive.

6.1.3 Results

Longitudinal Trimmability and Stability analysis

One of the requirements needed to obtain a feasible re-entry mission is the definition of a trim strategy. This analysis is supported by the Flying Quality Analyses, through the identification of the AoA Entry Corridor and the AoA trim line (Section 4.2.3). Since the trimmability and the stability performance are influenced by the CoG location, an analysis has been carried out in order to identify a CoG position that

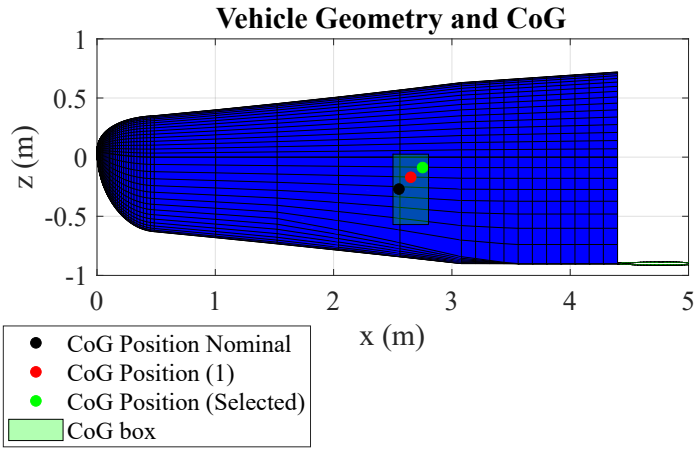

Figure 6.3: *Example of CoG locations within the CoG Box.*

guarantees the existence of AoA entry corridor with good properties. The features that have been evaluated are the minimum thickness of the AoA corridor and the minimum flap deflection margin. A better description of these figures of merit is given in Section 6.2.2.

Figure 6.3 shows three CoG positions within the identified CoG box. The CoG box has been defined through a parametric analysis to define the boundaries in terms of CoG locations that ensure the existence of a AoA corridor. Figure 6.4 reports the associated trim and AoA corridor analysis for the different CoGs. From these figures, it is possible to note how the trimmability and the AoA entry corridor change. For this case, with the available AEDB, the selected CoG (green point), with coordinates [2.752,0,0.088] m, allows to trim the vehicle for a broader range of AoA-Mach conditions, resulting also in a wider AoA entry corridor. Table 6.4 reports the values of the two figure of merits. It is clear that the selected CoG has better performance, by allowing more flexibility for the design of the AoA trim line and leaving more control authority to the GNC to cope with the disturbances, since the flaps still have around 9° of excursion available. Within this test case, the selection of the CoG has been performed through a parametric analysis, however the missionisation tool can manage this process with an optimisation routine. In future work, this solution has to be verified considering the internal layout of the vehicle. However, it is beyond the scope of this research work.

Table 6.4: *FQA performance with respect to the CoG locations in Figure 6.3.*

CoG position [m]	Deflection margin	AoA corridor thickness
Nominal ([2.552,0,-0.27])	1.364°	5°
(1) ([2.652,0,-0.17])	2.245°	2°
Selected ([2.752,0,-0.088])	8.979°	11°

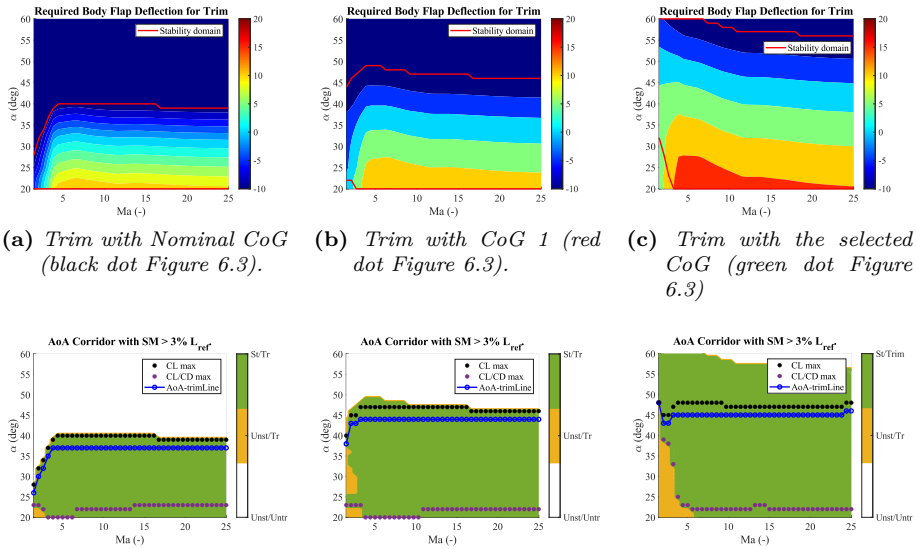

(a) *Trim with Nominal CoG (black dot Figure 6.3).*

(b) *Trim with CoG 1 (red dot Figure 6.3).*

(c) *Trim with the selected CoG (green dot Figure 6.3)*

(d) *AoA corridor with Nominal CoG (black dot Figure 6.3).*

(e) *AoA corridor with CoG 1 (red dot Figure 6.3).*

(f) *AoA corridor with the selected CoG (green dot Figure 6.3).*

Figure 6.4: *FQA with respect to CoG locations considered in Figure 6.3.*

EIP Selection: de-orbit manoeuvre design and re-entry mission engineering

This section reports the results of the analysis carried out for the selection of the EIP. The search space considered in this analysis spans the longitude from -92° to -142°, and the latitude from -5° to 15°.

Figure 6.5 shows the maps obtained by evaluating the minimum distance between the target point and the footprint edge. In particular, Figure 6.5a reports the value of this performance with respect to the EIP conditions. The void region corresponds to EIP conditions for which the target point is not included in the range capability. By looking the figure, it can be noted that the selected EIP (red star) stays on the ground track of the operational orbit (black line). In fact, even if there are EIP coordinates that allow to obtained better

solutions in terms of minimum distance (yellow region of the map), these would require a prohibitive de-orbit manoeuvre concerning the propellant consumption due to the necessary change of plane. Figures 6.5b and 6.5c also show the downrange and the crossrange variation from the EIP to the target point in the feasible region. They give useful information for the trajectory design with regard to expected drag and bank profiles.

The selected EIP is at 120.786° W and 0.923° S, corresponding to a downrange and a crossrange to target about 7600 km and 200 km. The minimum distance between the target point and the range capability edge is 260 km, leaving enough margin to cope with the uncertainties. Moreover, the de-orbit manoeuvre required to reach this point consumes 438.5 kg of propellant, considerably low with respect to the propellant budget constraint. Figure 6.6 shows the results of the de-orbit manoeuvre: Figures 6.6a and 6.6b report a visualisation of the manoeuvre, while Figure 6.6c, 6.6d and 6.6e show the altitude, the mass and the thrust profiles with respect to the time. From these figures, it can be noted that the manoeuvre is performed with only one burn. During the first coast arc, the spacecraft follows the orbital motion till the burn is performed around 2000 s from t_0 (Figure 6.6c). The complete trajectory lasts about one hour.

Future development may account also a phasing strategy in order to have a more complete analysis with the possibility to define better EIP conditions.

Reference Trajectory, GNC Tuning, and Nominal Trajectory definition

The atmospheric re-entry trajectory has been optimised to reach the target TAEM interface point while satisfying all the constraints. The solution has been obtained by accounting 100 discretisation nodes.

Figure 6.7 shows the plots of the solution. The figures reports also the profiles of the nominal solution, so the simulation performed with DEIMOS high-fidelity simulator with the closed-loop guidance. Figure 6.7d reports the bank angle with respect to the non-dimensional specific energy ($E/(R_E g_0)$). The final result is a smooth bank angle profile (blue line), characterised by flat zone around -25° during the hypersonic phase. This feature allows to have good controllability to cope with the uncertainties. The bank reference manoeuvre generates a re-entry trajectory which brings the vehicle to a negligible error at the target point (Figure 6.7b), while keeping the aerothermal-mechanical loads under control (Figure 6.7c, 6.7e, and 6.7f). Figures 6.8a and 6.8b

show the resulting ground track of the trajectory and a visualition of the end-to-end mission.

Consequently, the reference trajectory has been used to tune the required GNC parameters, which in this case consists on the creation of fitting curve for the drag and the AoA line (Figure 6.8c and 6.8d). This operation has been done with the GNC tool. Then, the obtained solution has been simulated in nominal condition within ENDOSIM, the DEIMOS proprietary high-fidelity simulator. Figure 6.7 shows the reference and the nominal trajectory profiles. From the figures, it is possible to note that the results are very similar, meaning that the designed reference trajectory is flyable and it is well-defined. The profiles have practically the same histories, and the accuracy at the target is granted. The main discrepancies are due to the different environmental models used with the two tools. Moreover, the closed loop guidance employs a correction of the azimuth error to deal with the lateral motion. This feature has not been implemented within the optimisation problem, so the behavior of the bank angle in Figure 6.7d was expected. Future work foresees to embed the lateral strategy in the definition of the reference. The results convey that the missionisation tool can used for the definition of reference trajectory for real-case scenario in nominal conditions. The obtained missionised MA and GNC solution has been assessed through a Montecarlo campaign in the next section to verify its the robustness.

Mission Verification

In this section, the results of the Montecarlo campaign with 500 shots. The dispersion have been applied to the mass, the atmospheric properties, the aerodynamic database of the vehicle, and the initial conditions. Table 6.5 reports the considered dispersion. Concerning the atmospheric properties, it has been used tables developed for the Space Rider project. In future work, larger dispersion and other contributions (like winds) could be considered.

Figures 6.9 and 6.10 show the results of the Montecarlo verification. In particular, Figure 6.9 reports the dispersion at TAEM interface point. The outcome conveys that the guidance strategy is able to cope with the applied dispersion, since for the 99% of the cases the final position error is less than 2 km, which is a very good achievement for this phase of the mission. Figures 6.10a and 6.10b show the dispersed trajectories.

Moreover, Figures 6.10e and 6.10f indicate that the aerothermal-

Table 6.5: *Applied dispersion for the Montecarlo campaign.*

Variable	Dispersion	Distribution	Unit
Δm	[-73.75 73.75]	U	kg
$\Delta C_L(M_a, \alpha, \delta)$	[-5% 5%]	3-σ	-
$\Delta C_D(M_a, \alpha, \delta)$	[-5% 5%]	3-σ	-
Δh_{EIP}	[-3000 3000]	3-σ	m
$\Delta \theta_{EIP}$	[-2.5 2.5]	3-σ	$\circ$
$\Delta \phi_{EIP}$	[-0.5 0.5]	3-σ	$\circ$
ΔV_{EIP}	[-20 20]	3-σ	m/s
$\Delta \gamma_{EIP}$	[-0.05 0.05]	3-σ	$\circ$
$\Delta \psi_{EIP}$	[-0.3 0.3]	3-σ	$\circ$

loads are kept under control and the limits are not overtaken. This result can also be seen also in Figure 6.10c, where the complete spectrum of the drag profiles remain within the Entry Corridor bounds, underlying coherence between the outcomes. This also implies that the designed reference trajectory is robust with respect to the considered uncertainties.

The results convey that the missionisation strategy and solution developed in this application case can be applied to the missionisation process of a real-world MA and GNC scenario.

6.1.4 Summary and Comments

This application case shows how the MA and GNC missionisation tool can be used within the missionisation process for the design of an end-to-end re-entry mission, in particular from the operational orbit to the TAEM interface point. This tool allows to handle multiple analysis in a unique framework.

The test case considers the definition of a strategy that couples the performance of the de-orbit manoeuvre with the mission engineering of the atmospheric re-entry for the selection of the EIP. This allows to target a promising EIP both in terms of propellant budget constraints for the de-orbit, and range capability margin at the TAEM interface point.

Then, the FQA, the reference trajectory and the tuning of the GNC parameters have been performed by exploiting the develped missionisation tool in order to obtain a tailored solution for the analysed mission scenario. Consequently, the solution has been tested in the DEIMOS proprietary high-fidelity simulator with a closed-loop guidance. The

objective was to assess the flyability of the obtained solution. Moreover, a Montecarlo campaign has been performed for the verification of the solution.

The results convey that the MA and GNC missionisation tool is able to compute an end-to-end missionised solution for a real-case scenario, allowing to handle a complex multidisciplinary problem.

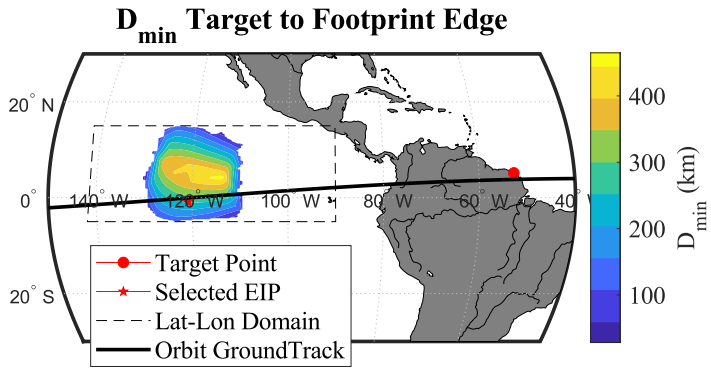

(a) *Feasible minimum distance between the target point and the footprint edge with respect to the EIP coordinates.*

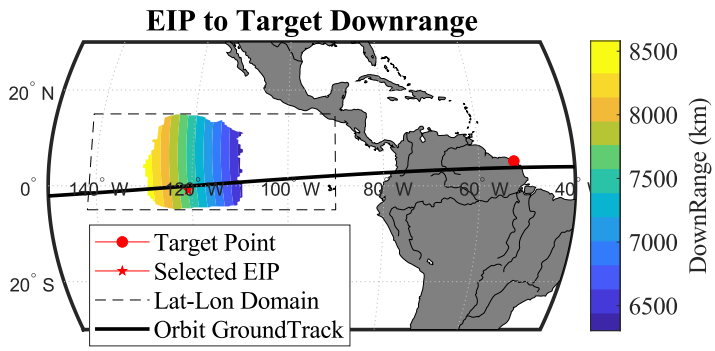

(b) *Feasible EIP to target downrange distance with respect to the EIP coordinates.*

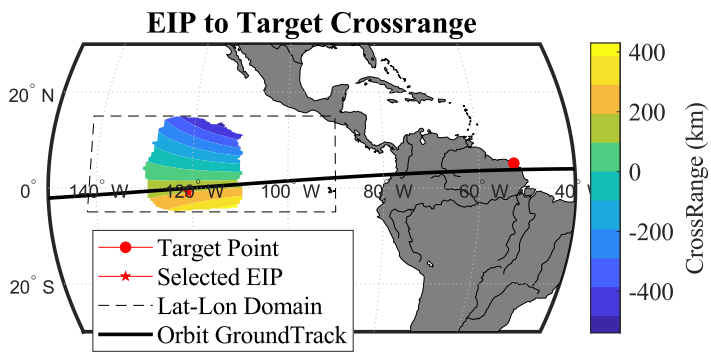

(c) *Feasible EIP to target crossrange distance with respect to the EIP coordinates.*

Figure 6.5: *Maps for the EIP selection analysis.*

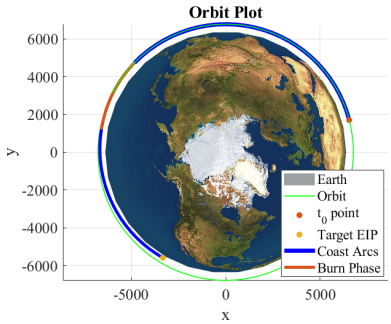

(a) *2D visualisation of the de-orbit manoeuvre.*

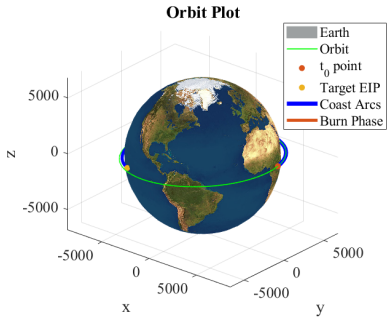

(b) *3D visualisation of the de-orbit manoeuvre.*

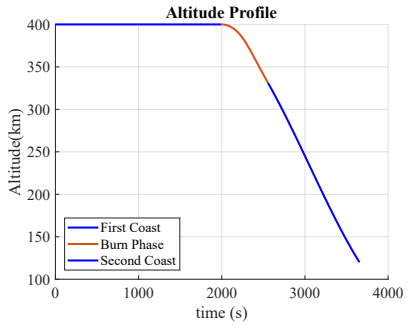

(c) *Mass profile with time of the de-orbit manoeuvre.*

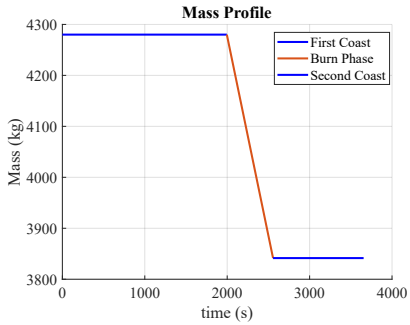

(d) *Altitude profile with time of the de-orbit manoeuvre.*

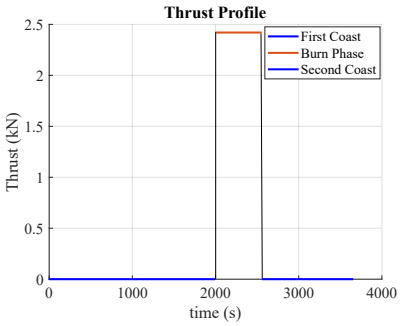

(e) *Thrust profile with time of the de-orbit manoeuvre.*

Figure 6.6: *De-orbit manoeuvre design results.*

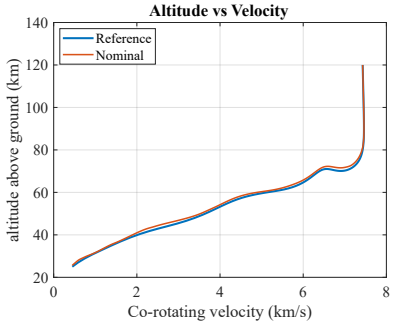

(a) *Altitude-velocity profile of the reference trajectory (blue) and the nominal one (orange).*

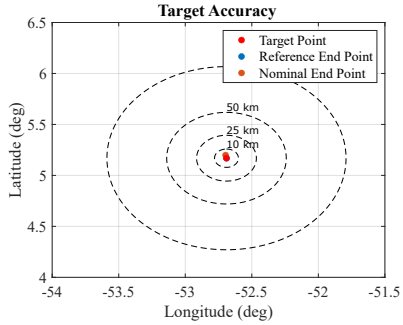

(b) *Target accuracy of the reference trajectory (blue) and the nominal one (orange).*

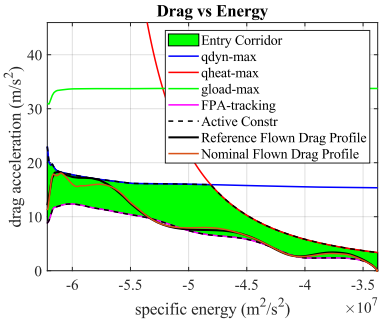

(c) *Reference and nominal drag profiles plotted within the Entry Corridor.*

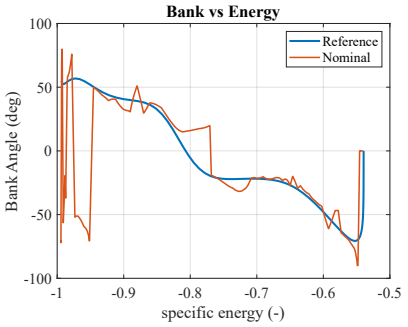

(d) *Reference bank profile, and flown bank profile with the guidance in the loop in nominal conditions.*

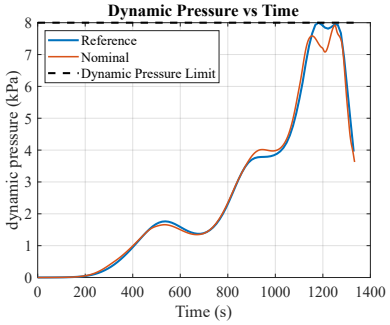

(e) *Dynamic pressure history.*

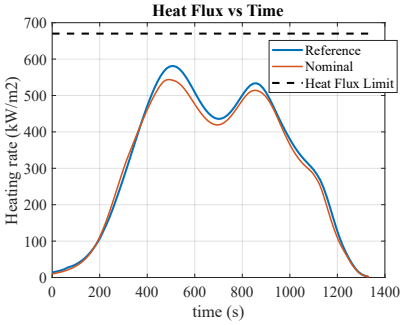

(f) *Heat flux at the stagnation point history.*

Figure 6.7: *Reference and nominal trajectory profiles. The nominal has been simulated with DEIMOS high-fidelity simulator with the closed-loop guidance.*

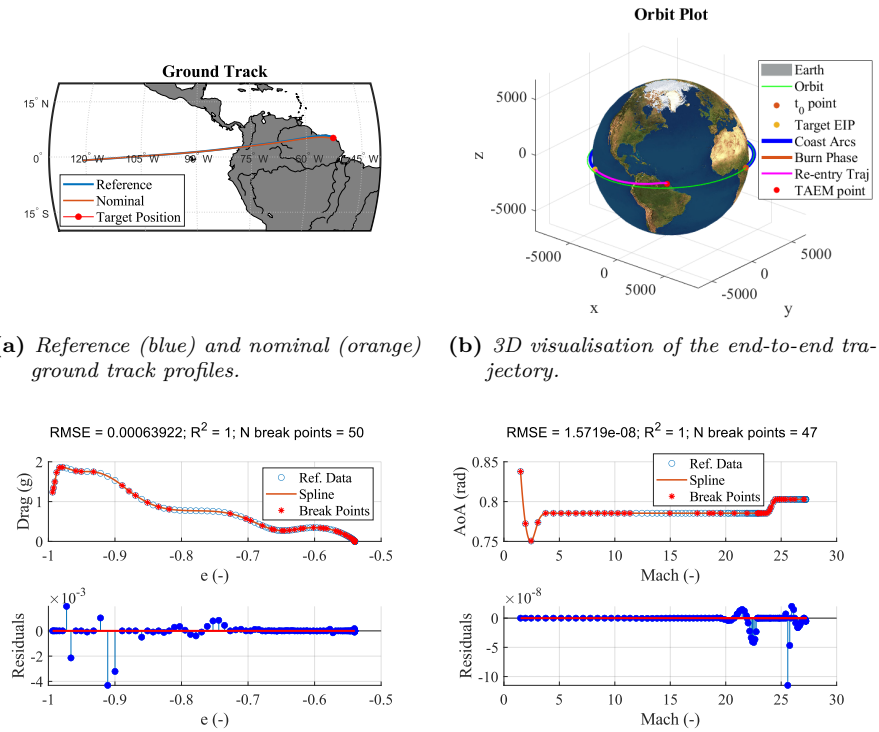

(a) *Reference (blue) and nominal (orange) ground track profiles.*

(b) *3D visualisation of the end-to-end trajectory.*

(c) *Fitting of the drag profile for the GNC.*

(d) *Fitting of the AoA profile for the GNC.*

Figure 6.8: *Trajectory design and GNC tuning results.*

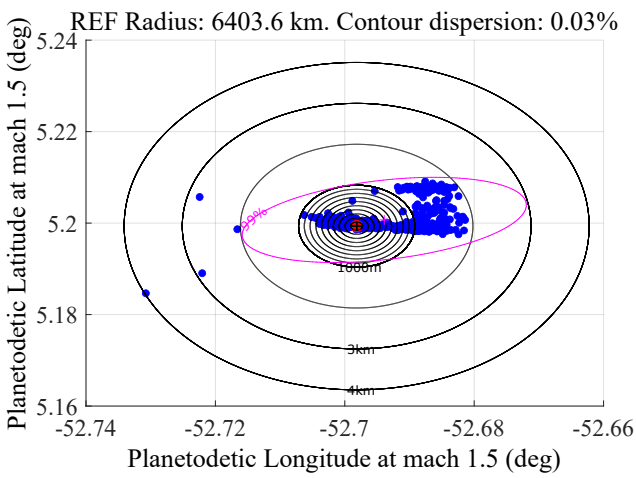

Figure 6.9: *Montecarlo campaign dispersion.*

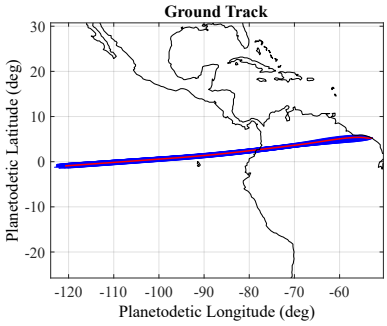

(a) *Ground track.*

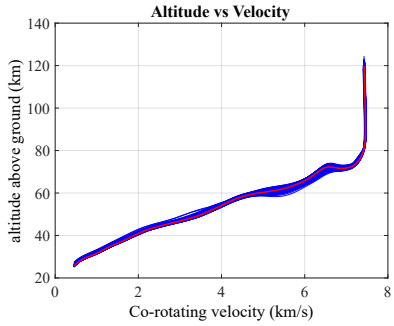

(b) *Altitude vs velocity profiles.*

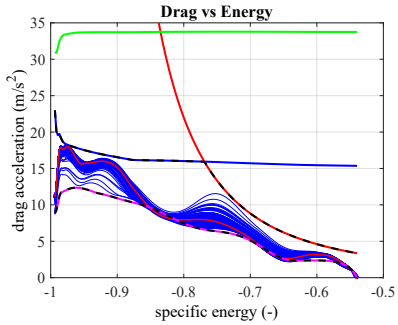

(c) *Drag vs non-dimensional energy profiles.*

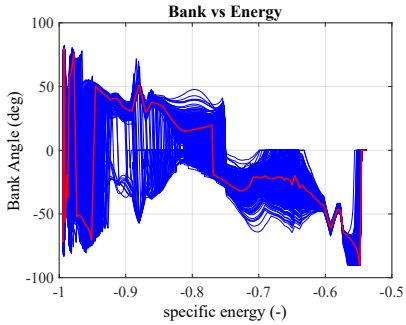

(d) *Bank vs non-dimensional energy profile.*

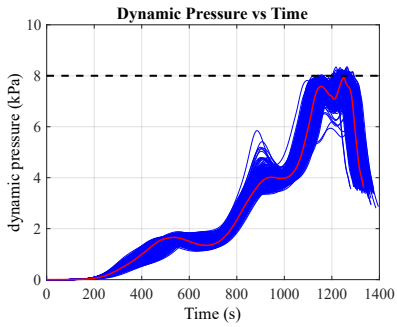

(e) *Dynamic pressure vs time profiles.*

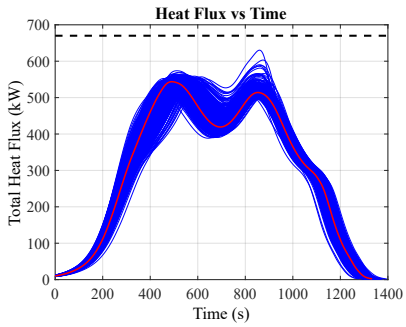

(f) *Heat flux at the stagnation point vs time profiles.*

Figure 6.10: *Results of the Montecarlo campaign. The nominal profiles are highlighted in red.*

6.2 WRV Preliminary Mission Design and Mission Capabilities Evaluation

The application case presented in this section shows how the concept of missionisation can be considered during the early phases of the design process. Whenever a space vehicle has to perform a set of multiple missions, such as in the case of a reusable re-entry vehicle, a crucial analysis consists in the evaluation of its mission capability. This process can be performed since the early phase of the design process in order to evaluate how the design parameters of a vehicle impact on its performance. The optimisation of the performance with respect to these parameters allows to determine and evaluate different design solutions that are more robust from a mission analysis view point. This feature leads to a re-entry vehicle solution that is more flexible and adaptable to several mission scenarios, and so it can be missionised more efficiently [93].

In order to perform this analysis, an MDO approach has been followed. By using this technique, the goal is to evaluate different design options to perform trade-off studies and identify the optimal designs, especially when a multi-objectives approach is considered and nondominated optimal Pareto solutions are obtained. This study is performed to assess promising design solutions within the scope of the WRV category, in a nominal mission which maximise prescribed performances, without violating a set of system and mission constraints. The considered mission performances assess the flying capability, the controllability and the static longitudinal stability of the vehicle along the nominal trajectory, while considering both system and mission design parameters.

The analysis is supported by the MDA framework of the missionisation tool, while the optimisation process is solved by exploiting two complementary approaches embedded in the Missionisation Layer of the tool. The former uses the MOPSO algorithm, while the latter makes use of a metamodelling technique (Section 3.1.3).

6.2.1 Objectives

The objectives of this test case are:

- Assess the mission capability of a re-entry vehicle with respect to system and mission design parameters to obtain robust solutions from the mission analysis perspective.

- Evaluate different design solutions to perform trade-offs studies and identify promising regions of the search domain.

6.2.2 Problem Modelling

MDA-MDO set up

As reported in in Figure 3.6 of Section 3.3, within this study case, five disciplines have been involved: GEOM, AEDB, FQA, EC and FE. Figure 6.11 shows the DSM for this case. With this set-up the tool takes 10 seconds on average for each MDA cycle. Table 6.6 reports the qualitative definition of the design variables and the paramters involved. In particular, the design variables are six and consist in the EIP FPA γ_{EIP}, the length of vehicle L_{ref}, the fuselage diameter $Diam$, the wing span b, and the delta position of the Centre of Gravity (X_{cog} and Z_{cog}) with respect to the nominal condition, which coincides with the MRC for the conventions used within the AEDB tool. The chord is linked to the diameter to avoid unfeasible geometries.

The optimisation of the design variables and the prescribed mission performance have been done by using both MOPSO and ESAT (Section 3.1.3). The two strategies have been compared both in term of accuracy and computational performance. The analyses are applied to the WRV category.

Performance Indices

The exploration of the solution space domain, the trade-off analysis and the evaluation of the best design solutions have been performed by considering three performance indices:

- Edge distance (D_{min}): defined as the minimum distance between the target point (in this case TAEM interface point) and the edge of the landing footprint. D_{min} considers a margin given by a prescribed uncertainty ellipse centred in the target. The D_{min} provides a representation of the flying capability of the vehicle in nominal conditions.

- Deflection margin (Δ_δ): it is the difference between the trim aerodynamic surface deflection and the maximum deflection attainable. The minimum value along the trajectory is considered for the evaluation of the performance index. This parameter represents the control authority available to the GNC to compensate disturbances along the trajectory. It is defined by:

Configuration	C1	C2	C3	C4	C5	OUTPUTS
System and mission (variant/invariant)	P1	P2	P3	P4	P5	
System and Mission Optimization	X1	X2	X3	X4	X5	
	GEOM(1)	X12		X14	X15	Y1
		AEDB(2)	X23			Y2
			FQA(3)	X34	X35	Y3
			X43	EC(4)	X45	Y4
					FE(5)	Y5
						FoM, performance

MDA Core

Missionisation Layer

Figure 6.11: *DSM of the involved disciplines for the analysed test case.*

Table 6.6: *Qualitative definition of the parameters for the DSM in Figure 6.11*

ID	Parameters	ID	Parameters
$\boldsymbol{P}_1$	Vehicle class, Aero-mechanical loads, Payload mass, Vehicle dimensions	$\boldsymbol{X}_{14}$	Reference surface, Mass
$\boldsymbol{P}_2$	Vehicle class	$\boldsymbol{X}_{15}$	Reference surface, Mass
$\boldsymbol{P}_3$	Max and Min flap deflection, MRC position, CoG position w.r.t. MRC	$\boldsymbol{X}_{23}$	Untrimmed AEDB
$\boldsymbol{P}_4$	Aerothermal-mechanical loads, Environment parameters, Boundary conditions	$\boldsymbol{X}_{34}$	Trimmed AEDB AoA trim line
$\boldsymbol{P}_5$	Environment parameters, Boundary conditions	$\boldsymbol{X}_{35}$	Trimmed AEDB AoA trim line
$\boldsymbol{X}_1$	L_{ref}, $Diam$, b	$\boldsymbol{X}_{43}$	AoA trim line
$\boldsymbol{X}_2$	-	$\boldsymbol{X}_{45}$	Entry corridor bounds
$\boldsymbol{X}_3$	X_{cog}, Z_{cog}	$\boldsymbol{Y}_1$	Trimmed AEDB, AoA trim line
$\boldsymbol{X}_4$	γ_{EIP}	$\boldsymbol{Y}_2$	Untrimmed AEDB
$\boldsymbol{X}_5$	γ_{EIP}	$\boldsymbol{Y}_3$	Trimmed AEDB, AoA trim line
$\boldsymbol{X}_{12}$	Slenderness ratio, Wing aspect ratio	$\boldsymbol{Y}_4$	Entry corridor bounds
$\boldsymbol{X}_{13}$	Reference length for C_m	$\boldsymbol{Y}_5$	Landing Footprint

$$\begin{aligned} \Delta_\delta &= \delta_{max} - \delta_{trim} \quad \text{if} \quad \delta_{trim} \geq 0 \\ \Delta_\delta &= |\delta_{min} - \delta_{trim}| \quad \text{if} \quad \delta_{trim} < 0 \end{aligned} \tag{6.1}$$

- Angle-of-Attack corridor thickness (Δ_{AoA}): this parameter assesses the minimum width of the stable region of the Angle-of-Attack entry corridor. It can be considered as a preliminary stability performance index of the vehicle in nominal conditions.

These three performance indices have been maximized along the optimisation process in order to obtain robust solution options from the mission analysis view point. Figure 6.12 reports an example of the three performance indices considered in this context, obtained with a dummy solution X = [-1° 25m 5m 20m 0m 0m]. The performance indices are 674.76 km for D_{min}, 4.43° for Δ_δ, and 10° for Δ_{AoA}.

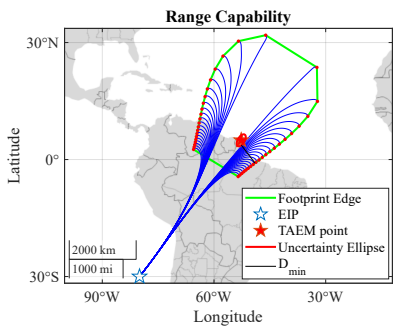

(a) *Minimum edge distance (black line).*

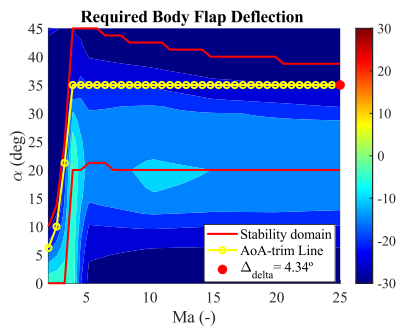

(b) *Minimum deflection margin (red dot).*

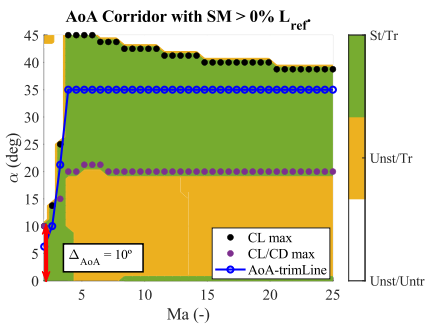

(c) *Minimum AoA entry corridor thickness.*

Figure 6.12: *Performance indices example considered for this test case.*

Analysed scenario and Problem parameters

The considered scenario is a nominal descent mission from the Entry Interface Point (EIP, here assumed at 90 km of altitude) to the Terminal Area Energy Management (TAEM, here assumed at Mach around 2, and at 27 km of altitude) interface point of an unpowered winged re-entry vehicle. The chosen entry coordinates are set at 30° S, 80° W latitude and longitude, and initial heading angle of 38.4° (from the local North). The final point is at 5.2° N and 52.7° W latitude and longitude, characterized by an uncertainty ellipse of 400x200 km. The scenario simulates a descent mission from a LEO orbit with an inclination of 51.6° with a scheduled landing at the Centre Spatial Guyanais. The entry vehicle is assumed to carry a payload mass of 1000 kg.

During the descent, the re-entry vehicle can withstand a set of maximum aerothermal-mechanical loads: a maximum dynamic pressure of 10 kPa, a heat flux at the stagnation point of 530 kW/m^2, and a total acceleration load of 4 g. The excursion of the aerodynamic surface is within -30° and +30°.

The analysis considers the US76 atmospheric model for the estimation of the atmospheric pressure, density and Mach number. The gravity assumes a spherical Earth with a radius of 6371 km. Table 6.7 reports the problem parameters, while the research space of the design variables is bounded with the ranges defined in Table 6.8.

6.2.3 Results

This section reports the results of the test case presented in this section. Firstly, the solution obtained with both ESAT and MOPSO are compared. Then, the optimum solution space domain is explored and the preliminary system and mission design solutions are analysed.

Comparison of ESAT and MOPSO solutions

Considering the optimisation process performed with ESAT, the RBFs metamodel has been built by calling the MDA in 1064 points (1000 plus 64 hypervertices) generated with Latin Hypercube Sampling (LHS) within the research space domain. The optimal Pareto-Front is given by evaluating the metamodel in 70000 query points. The whole process takes about 1 hour and 30 minutes on Intel®Core™ i7-8750H processor, by using five cores in parallel. With these parameters, the metamodel describes the output of the MDA for the analysed case, with the errors shown in Figure 6.13. For this case, the surrogate can

Table 6.7: *Problem paramters: boundary conditions, aerothermal-mechanical loads, flaps deflection constraints.*

Paramter	Value	Unit
EIP/TAEM altitude (h_{EIP}, h_{TAEM})	[90, 27]	km
EIP/TAEM velocity (V_{EIP}, V_{TAEM})	[7.5, 0.6]	km/s
EIP/TAEM latitude (ϕ_{EIP}, ϕ_{TAEM})	[-30, 5.2]	◦
EIP/TAEM longitude ($\theta_{EIP}, \theta_{TAEM}$)	[-80, -52.7]	◦
EIP/TAEM FPA ($\gamma_{EIP}, \gamma_{TAEM}$)	[- , -]	◦
EIP/TAEM Heading angle (ψ_{EIP}, ψ_{TAEM})	[38.4, -]	◦
Max dynamic pressure($q_{dyn,max}$)	10	kPa
Max acceleration load (n_{max})	4	g
Max heat flux ($\dot{q}_{heat,max}$)	530	kW/m^2
Flap range ($\delta_{min}, \delta_{max}$)	[-30, 30]	◦

Table 6.8: *Design variables upper and lower bounds.*

Variable	Range	Unit
EIP FPA (γ_{EIP})	[-1.2, -0.8]	◦
Longitudinal Length (L_{ref})	[24, 35]	m
Fuselage diameter ($Diam$)	[5, 6]	m
Wing span (b)	[18, 35]	m
Longitudinal CoG shift (X_{cog})	[-1.5, 1.5]	m
Vertical CoG shift (Z_{cog})	[-0.5, 0.5]	m

approximate the performance indices with a good accuracy, in fact, the error of the predictions are < 50 km for D_{min}, $< 6°$ for Δ_δ, and $< 3°$ for Δ_{AoA}. These values are deemed acceptable for this test case. Regarding the MOPSO, the analysis accounts for a population of 50 particles with a maximum of 100 generations, thus a total of 5000 evaluations of the MDA. The MOPSO routine takes approximately 6 hours and a half to complete the process, on the same computer. In future research the drawback and benefit of using less generations will be studied.

Figure 6.14 shows the input distribution of the Pareto solutions obtained with ESAT (Figure 6.14a) and MOPSO (Figure 6.14b). The comparison of the plots shows similar patterns in the optimal solutions found by the two methods. The position of the Pareto solutions within the research space domain predicted by ESAT is visually similar to the results obtained with the MOPSO. The main difference are present in the FPA domain, where ESAT found Pareto solutions also for higher values of the FPA, while in MOPSO the particles migrate to the lower bound of the domain. This behaviour is given by the approximation

introduced by the metamodel, whose accuracy depends on the number of sampling points used for its construction. In contrast, MOPSO directly explores the search space and computes solutions based on the objectives without approximations. The accuracy of the metamodel method may be improved by both using more sample points and exploiting more advanced techniques for the generation of the surrogate [38]. However, the lack of accuracy is balanced by the higher computation efficiency of the metamodel approach (in this case, about 80% of run time reduction). The results show that the metamodeling MDO is a valuable approach for the preliminary mission capability evaluation for the analysed scenario during preliminary studies, so ESAT outcomes have been used for the solution analysis in the next section.

Solution Analysis: Preliminary System and Mission Design

Optimisation tools can greatly enhance the multidisciplinary design process by harnessing the synergies across different disciplines. Nevertheless, it is crucial for engineers to maintain an active role in the design process, using their experience to maintain control over the outcomes and results.

Exploring the solution space domain offers a valuable analytical approach to trade-off the optimal solutions achieved in the preceding

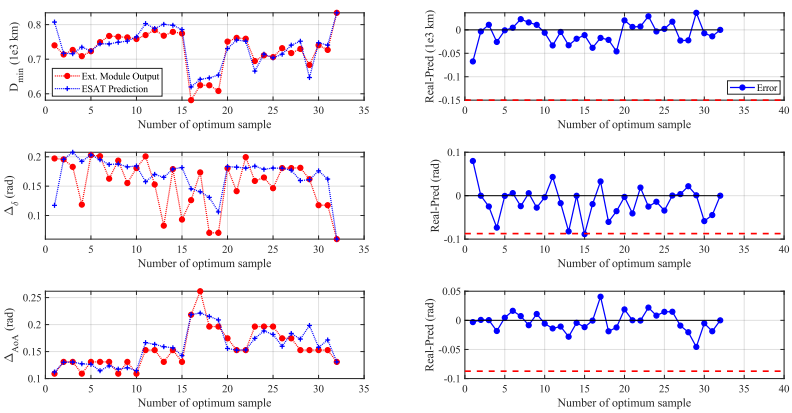

Figure 6.13: *ESAT prediction of the optimum solutions and validation with the MDA. In the figure on the left, the ESAT predictions (blue) are compared with the exact MDA evaluations (red), while on the right the correspondent errors are reported.*

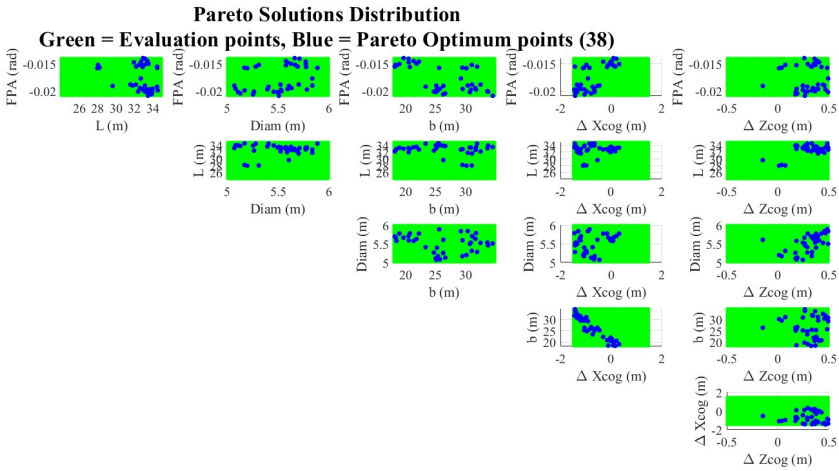

(a) *Inputs distribution of the Pareto solutions obtained with ESAT.*

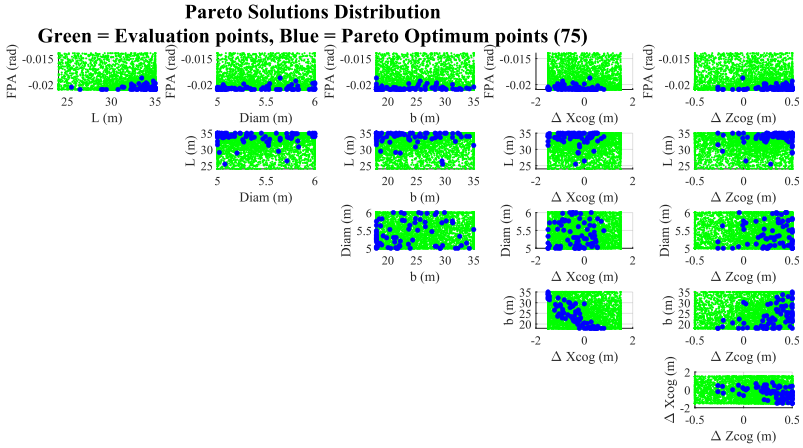

(b) *Inputs distribution of the Pareto solutions obtained with MOPSO.*

Figure 6.14: *Comparison of the inputs distribution of the Pareto solutions computed with ESAT (a) and MOPSO (b).*

subsection. This technique involves the analysis of the relationship between input and output variables, such as I/O correlation and sensitivity analyses on performance indices relative to the inputs. The goals are to gain a deeper comprehension of the entire problem and pinpoint promising areas warranting more comprehensive analysis throughout the iterative design process. The efficacy of the research space exploration analysis is boostered by the computational efficiency of the metamodel throughout the creation of performance maps.

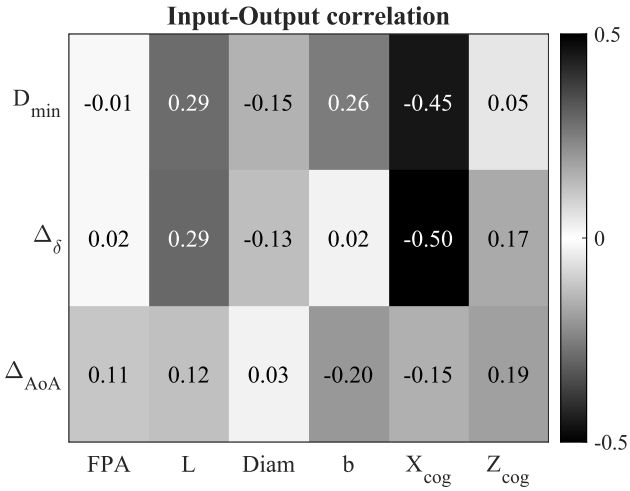

Figure 6.15: *Input-Output correlation for the WRV mission capability test case. Color scale is set between -0.5 and 0.5 for visualisation purposes.*

An example of this analysis applied to the test case is reported in this section. Figure 6.15 shows the correlation between the input-output. For the test case, the correlation between the length L_{ref}, the wing span b, and the X_{cog} is clear, when the minimum edge distance (D_{min}) and the minimum deflection margin (Δ_δ) are taken into account. L_{ref} and b, in fact, play a crucial role for the definition of the AEDB, while X_{cog} is a key parameters for the trim and stability, and so the definition of the AoA trim line. Even Z_{cog} enters in the definition of the AoA line, as X_{cog}, but it has a smaller impact. This is due to the fact that typically the re-entry is performed at high AoA, and so the normal force is larger than the axial one. On the other hand, $Diam$, and FPA have a relatively small correlation regarding all the outputs. For these reasons, in the analysis that follows, these last three parameters have been set to 0.25 m for Z_{cog}, 5.4 for $Diam$, and -1.2 for FPA. These values have been chosen from Figure 6.14.

In this way, the problem have been reduced from six to three variables. So a further step consists in the visualisation of the dependency of the performance indices with respect to the three input variables (Figure 6.16). Moreover, by looking Figures 6.12a, 6.16c, and 6.16e, that show the performance indices maps with respect to L_{ref}, X_{cog}, and b, it is possible to note that the three performance indices are maximised in the region where the L_{ref} is larger than 30 m. For this reason, the original problem has been further reduced by setting the

longitudinal length of the vehicle equal to 34 m. Figures 6.16b, 6.16d, and 6.16f report the resulting two-dimensional maps, that have been extracted by the plots on the left. The white areas identify non-feasible regions, while the dots are the subset of the Pareto solutions characterized by FPA, length, diameter and Z_{cog} equal to the fixed values. These performance maps are crucial inputs for the engineers during the design process, in order to identify promising research space areas where more accurate analyses and local optimisation can be carried out.

Out of 11 Pareto points found of the reduced problem, three of them are chosen as representative candidates. The first one is taken from the left part of the domain (blue dot, Figure 6.16). The second solution is the one in the middle of the research space (red dot), while the third one is in the right part of the map (green dot). These three points approximately span the whole feasible domain. Table 6.9 lists the values of the design variables and the associated performances. Figure 6.17 shows the variation of the geometries of the three design solutions and the associated mission analysis performance. The plots illustrate the aerodynamic surfaces deflection required to trim the vehicle, the associated AoA corridor, and the estimated landing footprint. The performance are well represented by the metamodel, except for the D_{min} for the third candidate. It is, in fact, a special case where the minimum edge distance is given by the nearest edge, and not by one of the sides. This case underlines the fact that the engineers must remain in the loop and check the obtained results. The solution, however, may be improved by changing the FPA at EIP, or other mission parameters. The selection of the best solution is not a trivial task, because several objectives must be considered and other drivers and requirements must to be taken into account. For instance, a larger wing span (candidate 1 and 2) implies a larger mass of the system, and so higher launch performance and costs. Moreover, such concepts can be more difficult to build from a technological and structural view point. Additional constraints, in fact, can be set by the customer, the launcher provider and more detailed analysis carried out along the design process.

6.2.4 Summary and Comments

This test case shows how the missionisation of a re-entry vehicle can be taken into account from the early phase of the design process. This is addressed by evaluating the mission capability of the vehicle with

respect to the design parameters and assessing the preliminary robustness of the solution from the mission analysis view point. The methodology used to pursue the objective of such analyses is based on MDO. The MDO, in fact, can manage simultaneously several design variables and multi-objective performance indices, while satisfying a broad set of mission and system requirements.

The application case presents two MDO approaches to handle the evaluation of the mission performance of WRVs with respect to a set of design parameters. In particular, the study demonstrates that a metamodeling MDO approach can achieve complementary results of the MOPSO algorithm for the optimisation routine in terms of accuracy, for the considered test case. The enhanced computational efficiency of the metamodel MDO activity can be exploited for the rapid generation and exploration of the solution space domain. The surrogate can be probed practically in real time on consumer hardware. This process aids the engineers during the design process to identify and assess interesting regions, where more accurate optimisation and in-depth analysis can be conducted. The solutions obtained with the metamodel, in fact, can be used within an iterative design process as warm start guess solutions for local optimisation. The selection of the best design solution is not a trivial work, especially in the initial stages of the design where preliminary analyses are performed, and additional constraints may be added along the process. However, an MDO approach coupled with a critical examination of the solution space domain can drive the engineers towards good designs solutions even in the early phases of the design. In future work, the analysis may be extended by including other re-entry categories.

Table 6.9: *Three example of optimal solutions. Both the real and predicted performance indices are reported.*

		Candidate 1	**Candidate 2**	**Candidate 3**
Variables	b, [m]	31.95	25.77	21.85
	X_{cog}, [m]	-1.42	-0.67	-0.02
Output ESAT	D_{min}, [km]	742.1	792.5	685.1
	Δ_{δ}, [$\circ$]	10.43	9.47	5.91
	Δ_{AoA}, [$\circ$]	6.50	7.01	11.64
Output MDA	D_{min}, [km]	751.5	781.9	344.7
	Δ_{δ}, [$\circ$]	12.32	6.13	4.18
	Δ_{AoA}, [$\circ$]	6.25	7.50	8.75

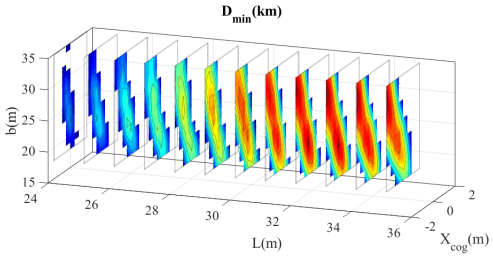

(a) *Minimum edge distance with respect to L_{ref}, X_{cog}, and b.*

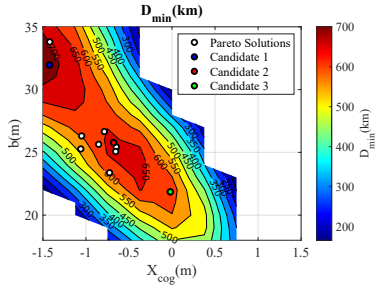

(b) *Minimum edge distance with respect to X_{cog}, and b, and L_{ref} set equal to 34 m.*

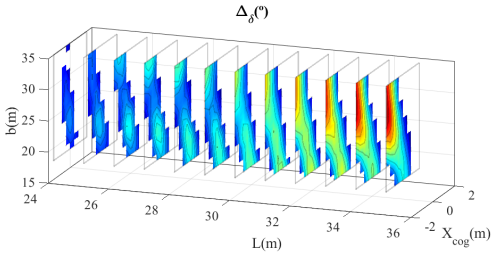

(c) *Minimum deflection margin with respect to L_{ref}, X_{cog}, and b.*

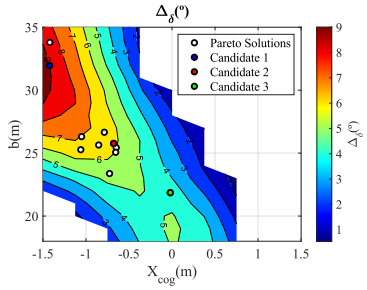

(d) *Minimum deflection margin with respect to X_{cog}, and b, and L_{ref} set equal to 34 m.*

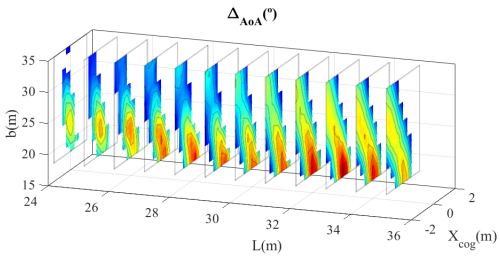

(e) *Minimum AoA corridor thickness with respect to L_{ref}, X_{cog}, and b.*

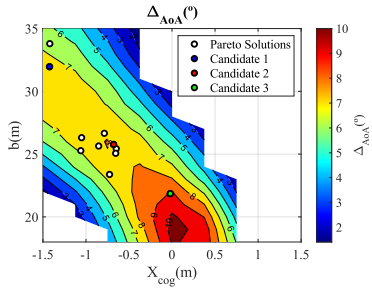

(f) *Minimum AoA corridor thickness with respect to X_{cog}, and b, and L_{ref} set equal to 34 m.*

Figure 6.16: *Performance indices maps with respect to L_{ref}, X_{cog}, and b (left). Corresponding two-dimensional maps with L_{ref}=34 m (right).*

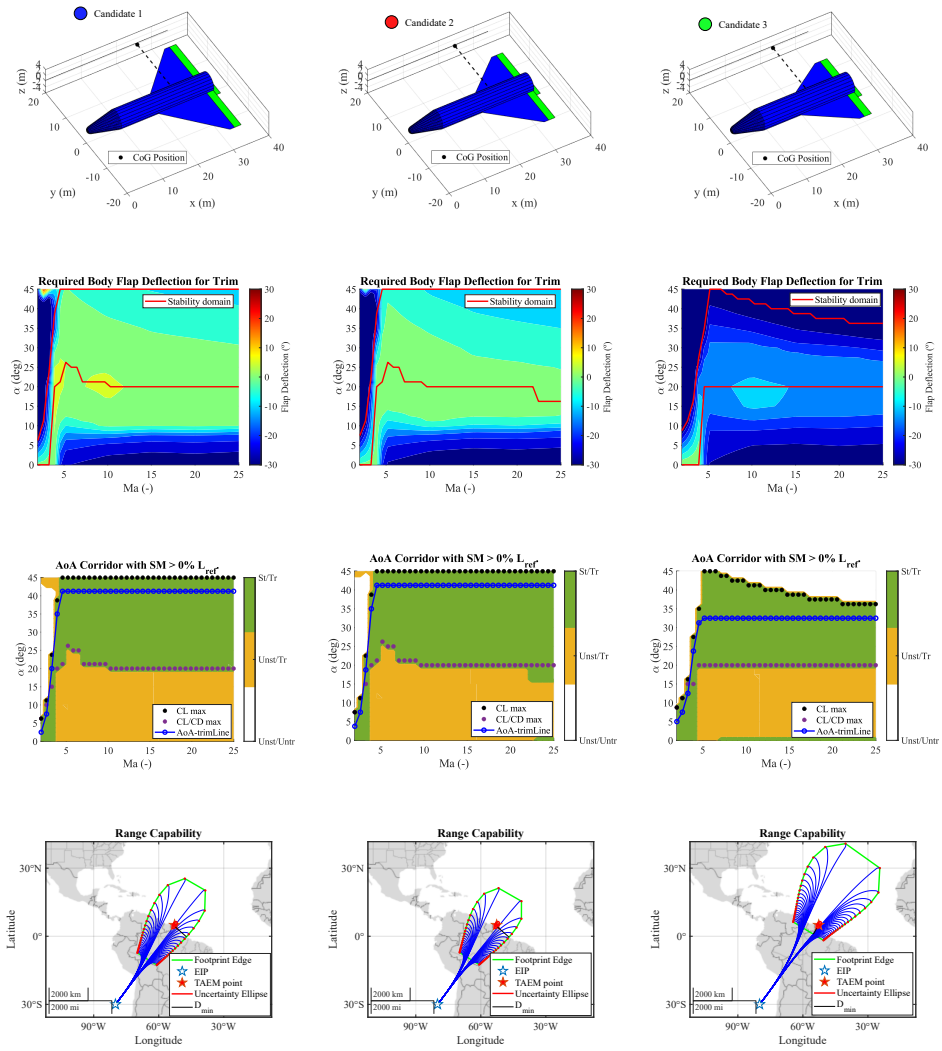

Figure 6.17: *Geometries and mission analyses performance associated to the three selected candidates. The results of each candidate are organised in column.*

6.3 Mission Analysis and GNC Missionisation of a VL-RLV

The test case focuses on the mission analysis missionisation of the propellant-optimal return trajectory of a VL-RLV. In particular, the goal is to obtain performance envelopes and the mission feasibility region by considering a wide range of conditions at MECO without violating propellant budget, aerothermal-mechanical, and path constraints. The analysis aims at estimating the propellant needed to perform RTLS and DRL recoveries for a representative variability of the MECO conditions. The objective of these maps is to provide the launcher flexibility and capabilities, as well as estimating the propellant consumption concerning different mission scenarios. This analysis represents a crucial tool for an efficient missionisation of the mission analysis solution for a specific mission. Characteristics conditions for LEO and GTO missions, indeed, can be mapped in terms of velocity and Flight-Path-Angle (FPA) at MECO [25] [94].

The missionisation tool is exploited to perform the analysis and to build the maps. A set of multi-phase trajectory optimisation problems characterized by different MECO conditions is solve by using the TO discipline (Section 4.2). Due to the high computational effort, a predefined number of optimal control problems are solved. Then, the process employs a metamodeling technique to create the surrogate of the original problem and estimates the output. Consequently, the missionisation tool evaluates the metamodel in the domain of interest to build the performance maps.

6.3.1 Objectives

The objectives of this application case are the following:

- Assess the performance envelopes of both RTLS and DRL recovery strategies in term of required mass propellant with respect to the MECO conditions.
- Definition of the feasibility region map to evaluate which recovery strategy is more efficient from the propellant mass consumption with respect to the MECO conditions.

6.3.2 Problem Modelling

The vehicle is a small-lift space launcher with similar size and performance to the Electron of RocketLab [95]. Since the analysis focuses

on the entry descent and landing phase, only the first-stage features are used. The launcher has a longitudinal length of 12 m and a base diameter of 1.2 m. The rocket is equipped at the top of the first stage with planar fins used for the longitudinal trim during the aerodynamic phase of the trajectory. The fins have a mean aerodynamic chord of 0.5 m and, a wing span of 0.5 m. At the MECO, the first stage has a gross mass of 2000 kg and a dry mass of 950 kg. The propellant needed for the recovery is about 10% used by the first stage during the ascent.

The vehicle is equipped with nine engines but is assumed to use only three during the recovering manoeuvres and landing. Each engine has a specific impulse of 311 s, with a nominal thrust of 25 kN. The nozzles are adapted at an altitude of 8 km from the ground, and each nozzle has an external area of 0.26 m^2. The thrust is modelled using the general rocket equations considering the expansion losses due to the change in the atmospheric pressure with the altitude [61].

Aerodynamics and Trimmability

The untrimmed aerodynamic database of the launch vehicle has been computed with the AEDB tool to obtain the variation of the coefficients C_D, C_L, and C_m in the function of the Angle-of-Attack, the Mach number, and the deflection of the planar fins [21]. For VL-RLV, the database is defined within a Mach number range of $0.25 \leq M \leq 7$, an AoA of $-15° \leq \alpha \leq 15°$ considering the nozzle base plate directed against the flow, and the fins deflection within $-20° \leq \delta \leq 20°$. The output of the AEDB tool are three functions $C_L = f_{C_L}(\alpha, M, \delta)$, $C_D = f_{C_D}(\alpha, M, \delta)$, and $C_m = f_{C_m}(\alpha, M, \delta)$ that are employed for the FQA and the estimation of the aerodynamic forces along the simulation. During the retro-propulsive manoeuvres, the effect of aerodynamic forces is reduced due to the interaction of the plume with the external flow, according to [56, 82, 81, 83].

The longitudinal trimmability and static stability analysis of the aerodynamic model is performed to assess the existence of a feasible Angle-of-Attack (AoA) Entry Corridor during the aerodynamic phase of the descent. The analysis is performed by considering a CoG location towards the engines, at 4 m from the nozzle base plate, as reported in Figure 6.18. During the aerodynamic phase, indeed, the first stage is characterized by a low propellant load.

Figure 4.5 shows the result of the FQA. In particular, Figure 4.5a and Figure 4.5b outline the existence of a trim solution in the entire $\alpha - M$ domain of interest. Moreover, each trim point is also stable.

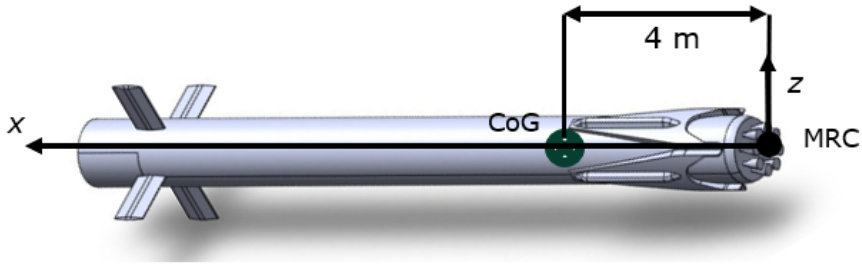

Figure 6.18: *Visualisation of the geoemtry and the CoG position during the aerodynamic phase. Credit [25, 78, 96]*

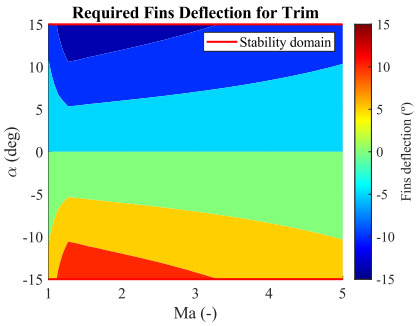

(a) *Required trim deflection in the Mach-AoA domain.*

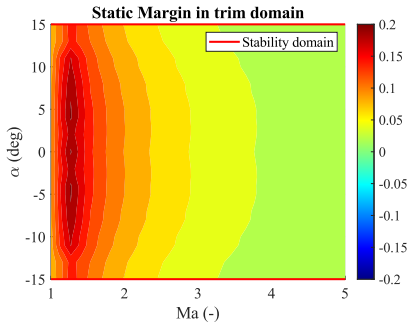

(b) *Static margin in the Mach AoA domain.*

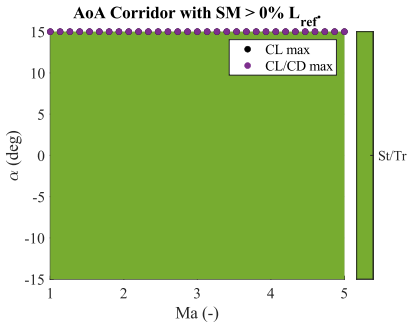

(c) *AoA Entry Corridor.*

Figure 6.19: *FQA for the considered vehicle during the aerodynamic phase.*

Thus, based on the models available, the planar fins can fully trim the rocket during the aerodynamic phase, and a feasible AoA entry corridor can be defined (green region Figure 4.5c).

Dynamics and Environment model

The dynamics of the problem are formulated with point-mass 3DoF equations of motion expressed with Cartesian coordinates in ECEF reference frame as reported in Section 4.1 with Eq. (4.7).

The gravity assumes a spherical Earth with a standard gravitational parameter $\mu = 3.986 \times 10^{14}\text{m}^3/\text{s}^2$ and a mean radius R_E of 6378 km, as stated in Section 4.1 in Eq. (4.9). The rotation of the Earth is $\omega_E = 7.2921150 \times 10^{-5}\text{rad/s}$. The atmosphere is modelled with the US76 model.

6.3.3 Propellant-optimal Problem formulation

The RTLS multiphase optimal control problem is formulated in five phases, while the DRL is in four according to Section 2.3.2. The objective of the optimal control problem is to find the control vector $\boldsymbol{u}^{(p)}(t)$, the thrust magnitude $T_{nom}^{(k)}(t)$, and the final time of each phase $t_f^{(p)}$ which maximise the final mass $m(t_f^{(P)})$, while a set of constraints are satisfied. The control $\boldsymbol{u}(t)$ gives the direction of the thrust when the engine is running, otherwise, it simulates the attitude of the rocket. The model, indeed, assumes that the x-axis of the vehicle is aligned with the thrust. The state variable is $\boldsymbol{x}^{(p)}(t) = [\boldsymbol{r}(t), \boldsymbol{v}(t), m(t)]^T$. The apexes p and k stand for the phase id: it is $p \in [1, 5]$ for RTLS, and $p \in [1, 4]$ for DRL. P refers to the last phase of the mission, so 5 and 4, respectively for RTLS and DRL. It worth highlighting, that the thrust magnitude is considered only in phases 1,3,5 for RTLS, while 2 and 4 for DRL. Table 6.10 summarises the formulation of the optimisation problem both for RTLS and DRL, highlighting the constraints considered. It can be noted that for the DRL case, the final conditions are not imposed as a constraint, while the cost function is augmented with penalty terms to only ensure that the final altitude is equal to the Earth surface, and the final velocity is a desired value. In this way, the optimisation algorithm can select the best landing location on the Earth surface. For the RTLS, instead, the final conditions must be strictly satisfied, since the landing site is prescribed. Moreover, the final time of each phase is an optimisation variable. This means that the optimisation process may find a solution that skips one phase of the return mission. For instance, the entry burn manoeuvre may not be performed, because the ballistic and aerodynamic phases are sufficient to slow down the launch vehicle before performing the landing burn.

Table 6.10: *Propellant-optimal problem formulation for RTLS and DRL.*

	RTLS	DRL	Comments
Cost Function	$-m(t_f^{(5)})$	$-m(t_f^{(4)}) + w_1(\|\|\boldsymbol{r}(t_f^{(4)})\|\| - r_E)^2$ $+w_2(\|\|\boldsymbol{v}(t_f^{(4)})\|\| - \bar{v}_f)^2$	
Dynamics Constraints	$\dot{\boldsymbol{x}}^{(p)}(t) = \mathbf{f}^{(p)}(\boldsymbol{x}^{(p)}(t), \boldsymbol{u}^{(p)}(t), t)$		p ∈ [1,2,3,4,5] RTLS; p ∈ [1,2,3,4] DRL Equation (4.7)
Boundary Conditions	$\boldsymbol{x}^{(1)}(t_0^{(1)}) = \boldsymbol{x}_0$ $\boldsymbol{x}^{(5)}(t_f^{(5)}) = \boldsymbol{x}_f$	$\boldsymbol{x}^{(1)}(t_0^{(1)}) = \boldsymbol{x}_0$ $\boldsymbol{x}^{(4)}(t_f^{(4)}) = [\ ]$	
Path Constraints	$\|\|\boldsymbol{u}^{(p)}(t)\|\| = 1$ $0 \leq T_{nom}^{(k)}(t) \leq \bar{T}$ $R_E \leq \|\|\boldsymbol{r}^{(p)}(t)\|\|$ $q_{dyn}^{(j)}(t) \leq q_{dyn,max}$ $\dot{q}_{heat}^{(j)}(t) \leq \dot{q}_{heat,max}$ $n_x^{(j)}(t) \leq n_{x,max}$ $\alpha^{(j)}(t) \leq \alpha_{max}$		p ∈ [1,2,3,4,5] RTLS; p ∈ [1,2,3,4] DRL; k ∈ [1,3,5] RTLS; k ∈ [2,4] DRL; j ∈ [2,3,4,5] RTLS; j ∈ [2,3,4] DRL
Linkage Constraints	$\boldsymbol{x}(t_f^{(s)}) = \boldsymbol{x}(t_0^{(s+1)})$		s ∈ [1,2,3,4] RTLS; s ∈ [1,2,3] DRL

Problem parameters

The analysed cases consider the Centre Spatial Guyanais as the launch site. This means that this location is the targeted landing site for the RTLS strategy. On the other hand, the DRL does not account for a specific landing location. Table 6.11 summarises the problem parameters, the values of the path constraints, and the final conditions considered along the optimisation.

For creating the performance envelopes, three variables are considered to define the variation of the MECO conditions. For what concerns the RTLS, the variables are the norm of the MECO velocity, the FPA at MECO, and the downrange distance between the MECO and the launch site, which is a function of the longitude at MECO [97]. Regarding the DRL, the decision parameters are the altitude at MECO, the norm of the MECO velocity, and the FPA. Table 6.11 also reports the variables at MECO that are considered fixed. These have been selected through preliminary dry runs to understand their effects on the final mass. Table 6.12 reports the variables at MECO and their ranges of variation.

In Table 6.11 and 6.12, the variables are expressed in spherical coordinates to ease the physical representation. However, the transformation into Cartesian coordinates can be done by exploiting the relations

Table 6.11: *Problem parameters and path constraints values.*

Parameter	Value RTLS	Value DRL	Units
Gross Mass at $t_0^{(1)}$	2000	2000	kg
Max Thrust (T)	75	75	kN
Max dynamic Pressure ($q_{dyn,max}$)	150	150	kPa
Max heat flux ($\dot{q}_{heat,max}$)	200	200	kW
Max axial load ($n_{x,max}$)	7.5	7.5	g
Angle-of-Attack (α)	$0 \leq \alpha \leq 15$	$0 \leq \alpha \leq 5$	$\circ$
$\|\|\boldsymbol{u}(t)\|\|$	1	1	-
Initial Latitude (ϕ_{MECO})	5.2	5.2	$\circ$
Initial Longitude (θ_{MECO})	-	-51.974	$\circ$
Initial Heading (ψ_{MECO})	94.640	94.640	$\circ$
Initial Altitude (h_{MECO})	85	-	km
Touchdown Velocity ($\|\|v_f\|\|$)	2	2	m/s
Final Latitude (ϕ_f)	5.169	-	$\circ$
Final Longitude (θ_f)	-52.690	-	$\circ$

Table 6.12: *Domain of interest for MECO conditions. Ranges defined from [25, 94]*

Variable	Range for RTLS	Range for DRL	Units
Initial Longitude (θ_{MECO})	[-52.5, -52.1]	-	$\circ$
Downrange Distance	$\sim$[20, 70]	-	km
Initial Altitude (h_{MECO})	-	[80, 95]	km
Initial Velocity (v_{MECO})	[1400, 2000]	[1400, 2400]	m/s
Initial FPA (FPA_{MECO})	[60, 80]	[20, 80]	$\circ$

in [51]. The values of the dispersion at MECO are defined from [25, 94]. However, these ranges can be accordingly tuned depending on the specific case and through the design of the ascent phase.

6.3.4 Results

Return-to-launch-site

Figure 6.20 shows the map of the minimum propellant mass required to perform RTLS trajectories with respect to the variations of the velocity norm, the FPA, and the downrange at MECO within the range reported in Table 6.12. For this case, the other variables (altitude, latitude, and heading angle) are kept fixed (Table 6.11). For RTLS, the metamodel is created by solving the optimisation problem with 429 variables in 123 sample points (100 samples generated with LHS,

8 hypervertices, and 15 tests points). This operation is done in about 6 hour in an Intel® Core™ i7-8750H processor. The presence of "bubbles" in the plot is due to the behavior of the metamodel. The results may be improved by adding more samples points or using a different distribution of the sampling population.

The results of the analysis show that the required propellant mass has the following general pattern:

- The required propellant mass increases as the downrange between the MECO and the launch site grows. This trend is expected since the engine must run longer in order to cope with a greater distance, during the boost-back manoeuvre.
- The propellant mass decreases as the FPA increases. This behavior is explained by the fact that less propellant is needed to invert the vehicle velocity when the horizontal velocity is lower (high FPA) during the boost-back manoeuvre.
- The required propellant mass increases as the norm of the velocity grows since the system must use more propellant both during the boost-back manoeuvre to invert the speed, and during the entry burn, if present, and landing burn to slow down.

Moreover, the results show that RTLS is not feasible within the full domain of interest. For these MECO conditions, the propellant budget is not sufficient to obtain a trajectory that satisfies both the aerothermal-mechanical loads limits and the final conditions (void regions). Furthermore, it can be noted how the feasible domain shrinks with respect to the increasing downrange. This behavior indicates that this variable has a crucial role in obtaining a feasible and efficient RTLS trajectory.

Figure 6.21 shows the obtained feasible trajectories in the altitude-velocity domain (Figure 6.21a) and in the altitude-downrange domain (Figure 6.21b), outlining the variability of the solutions with respect of the MECO conditions. From Figure 6.21a, it can be noticed that in some case, the optimiser has found a solution with only two burning manoeuvres by skipping the entry burn. This result is different from the typical mission performed by Falcon 9. For this reason, further analyses are foreseen in future for these cases. Moreover, the figure shows that aerthermo-mechanical loads limits are respected, since the trajectories are within the entry corridor.

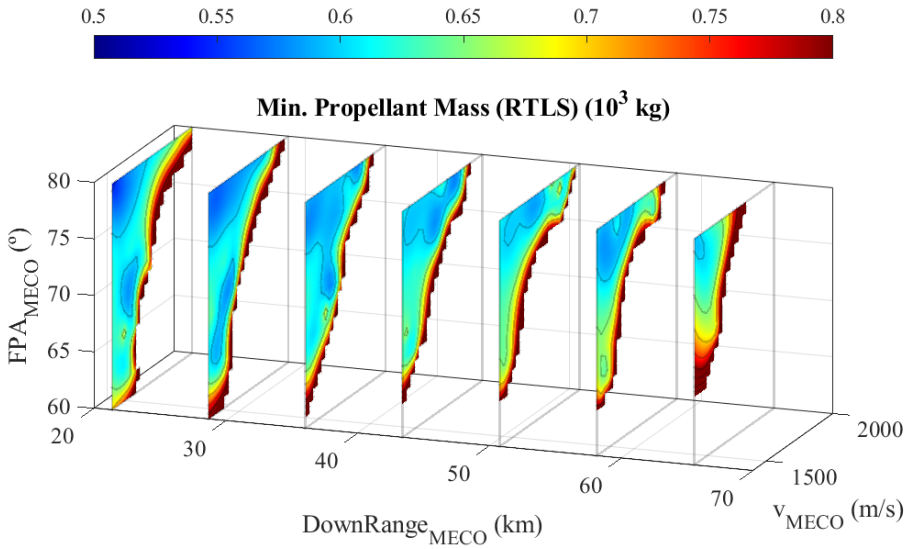

Figure 6.20: *Expected minimum propellant mass consumed for RTLS recovery strategy.*

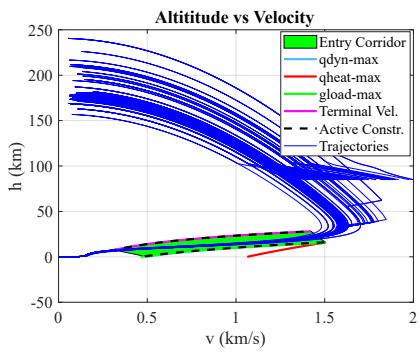

(a) *Generated RTLS trajectories in Altitude-Velocity domain for different MECO conditions. All trajectories are within the entry corridor.*

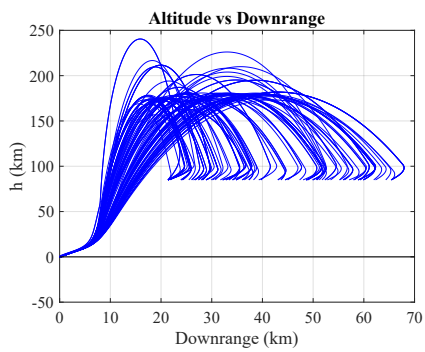

(b) *Generated RTLS trajectories in Altitude-Downrange domain for different MECO conditions.*

Figure 6.21: *RTLS trajectories dispersion.*

Downrange landing

Figure 6.22 reports the performance map obtained for the DRL strategy. In this case, the required propellant mass is obtained in function of the norm of the velocity, the FPA, and the altitude at MECO, as reported in Table 6.12. For the DRL, the fixed variables are the latitude,

the longitude, and the heading angle (Table 6.11). For this case, the optimisation problem is solved in 250 points (200 samples, 16 hyper-vertices and 34 test points) to compute the metamodel. The operation is done in about 5 hours in the same processor. In this case, each optimisation problem has 340 variables.

As in the RTLS case, the results of the analysis for DRL convey the following general pattern:

- The consumed propellant mass increases as the FPA grows, especially at higher velocity. This behavior is explained by the fact that a larger FPA at MECO generates a steeper trajectory during the descent phase, which requires longer retro-propulsive manoeuvres to reduce the aerothermal-mechanical loads and slow down the rocket. A shallower FPA, instead, leads to smoother trajectories with lower loads.
- Increasing the velocity at the MECO is associated with an increase of the required propellant mass since longer burns are needed to slow down the launch vehicle to reduce the aerothermal-mechanical loads and meet the desired touchdown conditions.
- The altitude at MECO does not have a primary effect on mass consumption.

The results show that DRL is feasible within the complete domain of interest for the analysed case. This means that for each MECO condition within the range in Table 6.12, it is possible to define a return trajectory that satisfies the propellant budget, the aerothermal-mechanical loads limits, and the touchdown conditions.

Even in this case, Figure 6.23 shows the feasible trajectories in the altitude-velocity domain (Figure 6.23a) and in the altitude-downrange domain (Figure 6.23b), outlining the variability of the solutions with respect of the MECO conditions. For this reason, further analyses are foreseen in future for these cases. Moreover, Figure 6.23b highlights that the aerothermo-mechanical loads limits are respected, since the trajectories are included in the entry corridor.

Recovery feasibility region analysis

In light of the results obtained in Section 6.3.4 and 6.3.4, an overall feasibility region is determined considering both the RTLS and the DRL recovery strategies with respect to the velocity and FPA conditions at

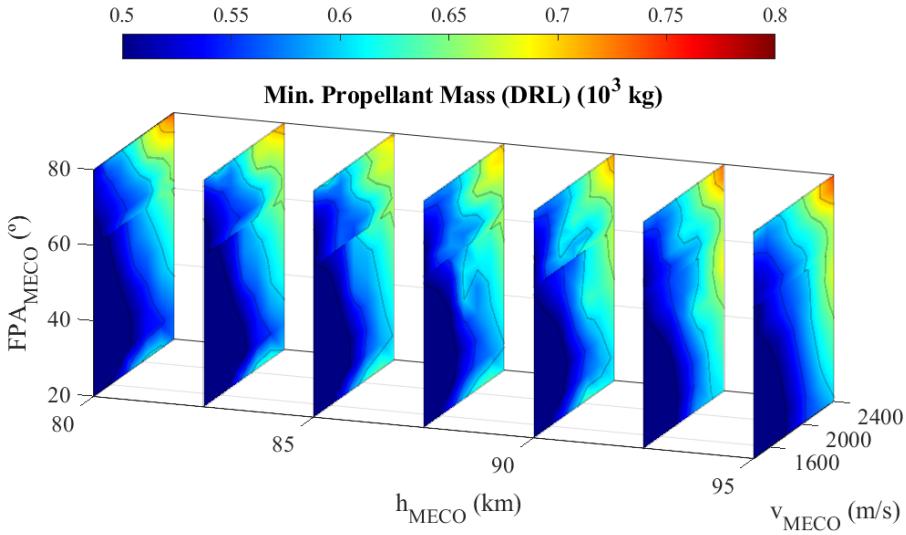

Figure 6.22: *Expected minimum propellant mass consumed for DRL recovery strategy.*

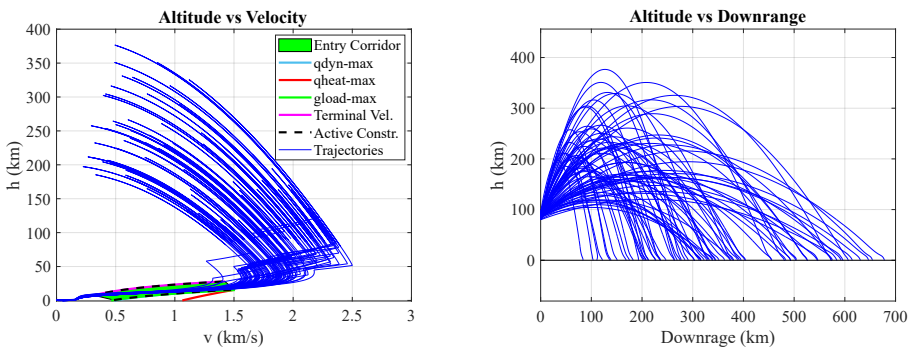

(a) *Generated DRL trajectories in Altitude-Velocity domain for different MECO conditions. All trajectories are within the entry corridor.*

(b) *Generated DRL trajectories in Altitude-Downrange domain for different MECO conditions.*

Figure 6.23: *DRL trajectories dispersion.*

MECO. From the performance maps obtained in the previous sections, the feasibility region is created by considering a downrange between MECO and the landing site of about 35 km for RTLS, and an altitude

at MECO of 85 km for DRL. This operation has been done to reduce the dimension of the problem and obtain a two-dimensions maps.

Figure 6.24 shows the recovery feasibility map of the considered launch vehicle for the range of MECO velocity and FPA analysed in this mission feasibility analysis. This single plot compares which recovery strategy is feasible depending on specific MECO conditions. Moreover, it highlights which strategy is more efficient from the propellant-consumption point of view. In particular, for this case, Figure 6.24 reports in yellow where RTLS is feasible and more efficient than DRL, while in blue the region where DRL is feasible and more efficient than RTLS. Lastly, the intersected in violet highlights the area in which both strategies are feasible, but DRL is more efficient than RTLS.

This analysis shows that DRL is more flexible and efficient than RTLS if only the required propellant mass is considered as performance. However, if different parameters are taken into account, for instance, refurbishment, barge operations, and transportation time and costs, the analysis may lead to different results. It worth mentioning that, for what concerns RTLS, in several case, the optimiser finds a solution with only two burns (boost-back and landing burn). These solutions can be further analysed in future work since the consumed propellant is comparable with DRL solutions.

The feasibility region analysis may be exploited along the missionisation process to select the most efficient recovery strategy concerning the mission requirements and objectives, such as target orbit and payload mass, which can be translated into MECO conditions.

6.3.5 Summary and Comments

This test case has been studied the mission performance in terms of propellant mass with respect to a wide range of MECO conditions for a VL-RLV, considering RTLS and DRL recovery strategies. Moreover, the feasibility region to compare the two recovery strategies has been obtained. The results show the influence of different MECO conditions on the consumed propellant mass while considering budget-propellant, and aerothermal-mechanical loads constraints for a small-lift launch vehicle. The results of the analysis convey that DRL is a more flexible and efficient solution than RTLS concerning the performance and the parameters considered.

The test case outlines the capability of the missionisation tool for the definition of an automated design framework, in fact, the achieved

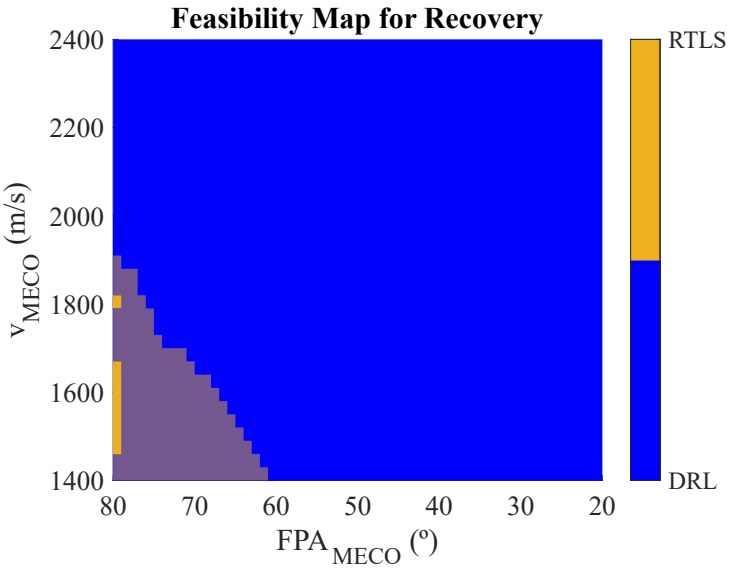

Figure 6.24: *Feasibility region for the recovery of launch vehicle of the analysed case. The intersected area (violet) means that both strategies are feasible, and that DRL is more efficient.*

results can be included in the mission analysis and GNC missionisation process of any reusable space launcher. Moreover, this methodology can be further generalised through the parametric analysis of a launcher characterised by mass ratio and ΔV budget, in contrast to the application to a specific launch vehicle . This approach would broaden the field of applicability over a wide range of vehicles with similar engine efficiency ratio, providing guidance for the sizing and trade-offs of different system options.

Future work foresees the evaluation of a specific mission scenario where a set of requirements must be fulfilled and the integration of the GNC subsystem. This open a possible collaboration within the Ascension consortium with ESR14.

"I don't feel like a hero. I'm just a man who was doing his job."
Chesley "Sully" Sullenberger - Sully

CHAPTER 7

Conclusions and Future Work

The growing need to find more economic, ecological and sustainable solutions for space access has led space agencies and private companies to invest on the development of reusable space vehicles both for space access and in-orbit studies. The capability of a space transportation system to be adapted to specific missions and to be able to perform multiple mission scenario, especially for what concerns the entry phase, prompt the necessity of a Mission Analysis and GNC missionisation process and tool for autonomous re-entry vehicles which reduces the tailoring efforts between each re-flight and mission.

The aim of this thesis is to develop a multidisciplinary, parametric and flexible framework to deal with the Mission Analysis and GNC missionisation for re-entry vehicles. This problem is tackled in an innovative way by embedding a minimum set of disciplines within an unique multidisciplinary environment in order to take into account the interactions and the coupling among the analyses. The tool uses MDO techniques to handle and optimally tune a set of user-defined mission and system parameters. The proposed tool can be used both for preliminary analysis during the first phases of the design, and in the latest phases where the mission and system requirements are well

defined. This vast topic cannot be fully explored within a Ph.D. of a single person. The proposed tool, in fact, includes multiple engineering blocks and modules for which it is possible to improve the level of fidelity. However, the present work tried to contribute to the scope by proposing a modular and flexible tool, that can be used for diverse analyses. The thesis transversely covered various aspects of the development of a multidisciplinary tool for the missionisation of re-entry vehicles missions.

The first part of the thesis presents an overview of the re-entry problem, trying to underline the complexity and the multidisciplinary nature of this problem. The background aims at showing which are the challenges and the analyses needed to obtain a safe re-entry trajectory, as well as introducing some concepts that are treated along the thesis. Moreover, it wants to highlight the variety and diversity of the design of lifting re-entry vehicles in terms of shapes and features, as well as the different recoveries strategies adopted to safely land the re-entry system. This part of the thesis also gives an introduction of the optimal control problem and of the multidisciplinary design optimisation. These two methodologies are, in fact, exploited for the missionisation purposes. The former is crucial to find a flight trajectory in terms of control commands and flight path that fulfils the mission requirements and constraints. The latter is fundamental for the optimal tuning of the considered mission and system parameters while a set of disciplines must be simultaneously satisfied and multiple performance must be taken into account.

The second part of the project concerns with the design and engineering modeling of the tool, as well as the validation of the building blocks. In particular, Chapter 3 describes the high-level architecture of the missionisation tool. Here, the three main modules are detailed. The first module is constituted by the User Interface, which has been designed in order to study a generic re-entry problem in a parametric and standard way thank to a structured organisation of the variables. It allows to set up all the parameters of the problem and the kind of analysis to be performed. The second module is defined by the MDA core. It contains a set of disciplines dealing with geometry and mass estimation, aerodynamic database evaluation, longitudinal trim and static stability analysis, entry corridor assessment, range capabilities estimation, trajectory optimisation and GNC set up. The proposed tool treats all these aspect with a novel approach by combining the analyses in single multidisciplinary software by managing

the input/output relations and the coupling variables. For this reason, the Chapter also presents the DSM of the most general case, which gives a picture of the interactions between the disciplines and variables. Particular attention has been payed for the description of the Missionisation Layer, which can be considered the brain of the tool. It, in fact, rules the kind of analysis to be carried out, from single MDA cycle to multiobjective optimisation problems. The tool is developed in a modular `MATLAB` framework to facilitate the future developments and improvements, as well as the possibility to interface with industry tools. Moreover, the proposed tool is characterised by an inherently flexibility and diverse analyses can be executed, as Chapter 6 presents.

The engineering modeling of the models and the disciplines are described in details in Chapter 4. Here, each discipline is modeled with a mathematical model in order to numerically assess the considered performance. Different existing methodologies in the literature are implemented and combined together. Some of these disciplines have been improved, as for instance the Footprint Evaluation Tool that can deal different atmospheric models. The development takes into accounts a suitable compromise between disciplinary analyses fidelity and required computational and implementation effort. However, due to modular framework higher-fidelity models can be embedded in future developments. Each disciplines went through a validation process in order to assess the implementation with respect to the literature and know results. Moreover, a preliminary sensitivity analysis is performed to identify the most critical parts of the engineering models and where to focus the effort for future improvements. This second part answer the first objective of the research, which is the development of a MA and GNC missionisation tool for re-entry vehicles.

The last part of the thesis addresses the second objective of the research with the selection of representative test cases, ranging from the definition of an end-to-end mission solution, to the preliminary assessment of the mission performance of a family of re-entry vehicles. The first case, which is constituted by an optimal tuning of the mission analysis and the guidance parameters, is used to validate the missionisation tool against a real case scenario and it answers the first definition of missionisation within this research. The solution obtained is, in fact, verified with a high-fidelity simulator with guidance in the loop and through a Montecarlo campaign. The results demonstrates the successful implementation of the tool and the disciplines. This process can be part of the mission design for the latest phases of the

design process. This test case also show the flexibility of the tool in performing coupling analysis and solving different problem, such as the optimal propellant de-orbit manoeuvre. The second and the third application cases are related to the early phase of the design process, and they address the second definition of missionisation within Ascension. The second test case, in fact, shows how the missionisation can be considered during the preliminary studies in order to obtain more robust solution candidates. The process identifies promising solutions within the design space that maximise a set of figures of merit, and it helps the engineers to take decisions whether perform more accurate analyses and local optimisation or not. The third application case assesses the mission performance for different recovery strategy of the first stage of an RLV. It demonstrates how the tool can be used for the definition of an automated design framework that allows to take strategic decisions depending on the mission scenario.

The applications presented in this research effectively demonstrate the successful implementation of the methodology across a broad range of scenarios. The recombination of existing techniques in a novel way has resulted in a multidisciplinary and modular framework that has successfully been employed for both preliminary and more accurate analysis, by handling several aspects and diverse re-entry problem.

As future developments, the aforementioned points, and other improvements may be:

- Improve the implementation of the AEDB tool, if a better estimation of the aerodynamic database of the re-entry vehicle shall be considered. This can be done, by following the same methodology reported in the thesis, but considering more geometrical parameters or creating the datasets with higher-fidelity methods.
- Embed within the FQA tool the evaluation of the lateral and dynamics stability of the vehicle. Moreover, the definition of the AoA trim line may be performed through an optimisation process.
- Embed other disciplines within the MDA core, in order to take into account other aspects and introduce higher level of flexibility during the missionisation process, such as for example the sizing of the TPS or a tool for safety analysis.
- Implement within the Trajectory Optimisation tool other transcription methods that may improve the convergence of the problem in some cases, such as pseudospectral method.

- Consider diverse metamodeling techniques within the Missionisation Layer in order to obtain better performance in terms of accuracy of approximation of the original problem. For instance, either Kriging methods or novel Artificial Neural Network Techniques.
- Consider within the Missionisation Layer an Uncertainty Quantification tool as additional capability in order to increase the basin of analyses to support the mission design process.
- Test the tool with other re-entry problems, as for instance the descent and landing phase with parafoil, in order to further test the flexibility of the tool.

Bibliography

[1] Maurizio Bernard. «Vega Missionization and Post Flight Analyses». PhD thesis. Sapienza Università di Roma, 2009.

[2] Pizzuro Simone, Gabrielli Alessandro, and Cavallini Enrico. «Innovative and fast tool for launchers missionization and trajectory optimization. Applications to the VEGA family launch vehicles with their spin-offs». In: (2021).

[3] Avio. *Vega Family*. 2023. URL: https://www.avio.com/vega.

[4] Gunter D. Krebs. *Chronology of Space Launches, Gunter's Space Page*. 2023. URL: https://space.skyrocket.de/directories/chronology.htm.

[5] JC Harpold and CA Graves Jr. «Shuttle entry guidance». In: *American Astronautical Society* (1978).

[6] Space X. *Space X, Launches*. 2023. URL: https://www.spacex.com/launches/.

[7] Sierra Space. *Sierra Space*. 2023. URL: https://www.sierraspace.com/.

[8] Davide Bonetti et al. «Space Rider Mission Engineering». In: 2019. DOI: 10.13009/EUCASS2019-633.

[9] Antoine Patureau de Mirand, Jean-Marc Bahu, and Olivier Gogdet. «Ariane Next, a vision for the next generation of Ariane Launchers». In: *Acta Astronautica* 170 (2020), pp. 735–749. ISSN: 0094-5765. DOI: https://doi.org/10.1016/j.actaastro.2020.02.003. URL: https://www.sciencedirect.com/science/article/pii/S0094576520300631.

[10] Etienne Dumont et al. «CALLISTO: A Demonstrator for Reusable Launcher Key Technologies». In: *TRANSACTIONS OF THE JAPAN SOCIETY FOR AERONAUTICAL AND SPACE SCIENCES, AEROSPACE TECHNOLOGY JAPAN* 19 (Jan. 2021), pp. 106–115. DOI: 10.2322/tastj.19.106.

[11] James R. Wertz and Wiley J. Larson. *Space Mission Analysis and Design*. Third. Space Technology Library. Microcosm Press and Kluwer Academic Publishers, 1999. ISBN: 1-881883-10-8.

[12] E. Mooij. *Re-entry Systems, Lecture Notes*. 2015.

[13] Ernst Heinrich Hirschel and Claus Weiland. *Selected aerothermodynamic design problems of hypersonic flight vehicles*. Vol. 229. Springer Science & Business Media, 2009.

[14] Dominic Dirkx and Erwin Mooij. *Conceptual shape optimization of entry vehicles*. Springer, 2016.

[15] Claus Weiland. *Aerodynamic data of space vehicles*. Springer Science & Business Media, 2014.

[16] Thomas J Horvath, Scoot A. Berry, and N. Ronald Merski. «X-38 Experimental Aerothermodynamics». In: *AIAA 2000-2685* (2000).

[17] E. Jackson, Christopher Cruz, and W. Ragsdale. «Real-time simulation model of the HL-20 lifting body». In: 92 (Aug. 1992).

[18] Rodrigo Haya Ramos et al. «Validation of the IXV Mission Analysis and Flight Mechanics Design». In: Sept. 2012. ISBN: 978-1-60086-931-0. DOI: 10.2514/6.2012-5966.

[19] *Falcon User's Guide*. 2021.

[20] RRTB Recovery and return to base. *RRTB*. 2023. URL: https://rrtb.eu/.

[21] Jacopo Guadagnini, Gabriele De Zaiacomo, and Leonid Bussler. «Aerodynamic Coefficients Estimation Tool for re-entry Vehicle Missionisation». In: *2nd International Conference on Flight Vehicles Aerothermodynamics and Re-entry Missions and Engineering (FAR)* (2022).

[22] B R A Burns. «HOTOL Space Transport for the Twenty-First Century». In: *Proceedings of the Institution of Mechanical Engineers, Part G: Journal of Aerospace Engineering* 204.2 (1990), pp. 101–110. DOI: 10.1243/PIME_PROC_1990_204_216_02. eprint: https://doi.org/10.1243/PIME_PROC_1990_204_216_02. URL: https://doi.org/10.1243/PIME_PROC_1990_204_216_02.

[23] C. A. Kluever. «Entry Guidance Performance for Mars Precision Landing». In: *Journal of Guidance, Control, and Dynamics* 31.6 (2008), pp. 1537–1544. DOI: 10.2514/1.36950. eprint: https://doi.org/10.2514/1.36950. URL: https://doi.org/10.2514/1.36950.

[24] Ping Lu. «Entry Guidance: A Unified Method». In: *Journal of Guidance, Control, and Dynamics* 37.3 (2014), pp. 713–728. DOI: 10.2514/1.62605. eprint: https://doi.org/10.2514/1.62605. URL: https://doi.org/10.2514/1.62605.

[25] Gabriele De Zaiacomo et al. «Mission engineering for the RETALT VTVL launcher». In: *CEAS Space Journal* 14 (Feb. 2022). DOI: 10.1007/s12567-021-00415-y.

[26] Pedro Simplício, Andrés Marcos, and Samir Bennani. «A Reusable Launcher Benchmark with Advanced Recovery Guidance». In: 2019. URL: https://api.semanticscholar.org/CorpusID:197948184.

[27] Zhengyu Song et al. «Survey of autonomous guidance methods for powered planetary landing». In: *Frontiers of Information Technology and Electronic Engineering* 21 (Mar. 2020). DOI: 10.1631/FITEE.1900458.

[28] Michael Szmuk, Taylor Reynolds, and Behçet Açıkmeşe. *Successive Convexification for Real-Time 6-DoF Powered Descent Guidance with State-Triggered Constraints*. Nov. 2018.

[29] B. Acıkmese and L. Blackmore. «Lossless convexification of a class of optimal control problems with non-convex control constraints». In: *Automatica* 47.2 (2011), pp. 341–347. ISSN: 00051098. DOI: 10.1016/j.automatica.2010.10.037.

[30] John T Betts. «Survey of numerical methods for trajectory optimization». In: *Journal of guidance, control, and dynamics* 21.2 (1998), pp. 193–207.

[31] John T Betts. *Practical methods for optimal control and estimation using nonlinear programming*. SIAM, 2010.

[32] Benoit Chachuat. *Nonlinear and dynamic optimization: From theory to practice*. Tech. rep. 2007.

[33] Paul Boggs and Jon Tolle. «Sequential Quadratic Programming». In: *Acta Numerica* 4 (Jan. 1995), pp. 1–51. DOI: 10.1017/S0962492900002518.

[34] Arkadi Nemirovski and Michael Todd. «Interior-point methods for optimization». In: *Acta Numerica* 17 (May 2008), pp. 191–234. DOI: 10.1017/S0962492-906370018.

[35] Oliver Kramer. *Genetic Algorithm Essentials*. Springer Cham, 2017. DOI: https://doi.org/10.1007/978-3-319-52156-5.

[36] Burcu Adıgüzel Mercangöz. *Applying particle swarm optimization: new solutions and cases for optimized portfolios*. Vol. 306. Springer, 2021.

[37] Mathieu Balesdent et al. «A survey of multidisciplinary design optimization methods in launch vehicle design». In: *Structural and Multidisciplinary Optimization* 45 (May 2012), pp. 619–642. DOI: 10.1007/s00158-011-0701-4.

[38] Renhe Shi et al. «Metamodel-based multidisciplinary design optimization methods for aerospace system». In: *Astrodynamics* 5.3 (2021), pp. 185–215.

[39] Francesco Castellini. «Multidisciplinary Design Optimization for Expendable Launch Vehicles». PhD thesis. Politecnico di Milano, 2012.

[40] Joaquim R. R. A. Martins and Andrew B. Lambe. «Multidisciplinary Design Optimization: A Survey of Architectures». In: *AIAA Journal* 51.9 (2013), pp. 2049–2075. DOI: 10.2514/1.J051895. eprint: https://doi.org/10.2514/1.J051895. URL: https://doi.org/10.2514/1.J051895.

[41] Joaquim RRA Martins and Andrew B Lambe. «Multidisciplinary design optimization: a survey of architectures». In: *AIAA journal* 51.9 (2013), pp. 2049–2075.

[42] Justin S. Gray et al. «OpenMDAO: An open-source framework for multidisciplinary design, analysis, and optimization». In: *Structural and Multidisciplinary Optimization* 59.4 (Apr. 2019), pp. 1075–1104. DOI: 10.1007/s00158-019-02211-z.

[43] Liu Dasheng. «Multi objective particle swarm optimization: Algorithms and applications». In: (2009).

[44] Giovanni Medici et al. «Multi-Disciplinary Optimisation of Re-entry Vehicles from TAEM to Landing». In: *7th European Conference for Aeronautics and Space Science (EUCASS)* (2017). DOI: 10.13009/EUCASS2017-413.

[45] Davide Bonetti et al. «EDL and GNC Optimization of a Network of Small Mars Landers». In: June 2013.

[46] Davide Bonetti et al. «MDO, Wind Tunnel and Flight Tests of UAVs for Titan Exploration». In: *DASIA 2015 - DAta Systems in Aerospace*. Ed. by L. Ouwehand. Vol. 732. ESA Special Publication. Sept. 2015, 70, p. 70.

[47] Ann-Britt Ryberg. «Metamodel-Based Design Optimization: A Multidisciplinary Approach for Automotive Structures». PhD thesis. Linköping University Electronic Press, 2013.

[48] Felipe Viana et al. «Metamodeling in Multidisciplinary Design Optimization: How Far Have We Really Come?» In: *AIAA Journal* 52 (Mar. 2014). DOI: 10.2514/1.J052375.

[49] Gary Wang and S. Shan. «Review of Metamodeling Techniques in Support of Engineering Design Optimization». In: *Journal of Mechanical Design - J MECH DESIGN* 129 (Apr. 2007). DOI: 10.1115/1.2429697.

[50] Andrew B Lambe and Joaquim RRA Martins. «Extensions to the design structure matrix for the description of multidisciplinary design, analysis, and optimization processes». In: *Structural and Multidisciplinary Optimization* 46.2 (2012), pp. 273–284.

[51] E Mooij. «The motion of a vehicle in a planetary atmosphere». In: *Delft University of Technology, Faculty of Aerospace Engineering, Report LR-768* (1994).

[52] Marco Sagliano. «Development of a Novel Algorithm for high Performance Reentry Guidance». PhD thesis. Universitat Bremen, 2016.

[53] N. Vinh. *Optimal Trajectories in Atmospheric Flight*. Studies in Astronautics. Elsevier Science, 2012. ISBN: 9780444601452.

[54] Amitabh Saraf et al. «Landing footprint computation for entry vehicles». In: *AIAA Guidance, Navigation, and Control Conference and Exhibit*. 2004, p. 4774.

[55] Amitabh Saraf et al. «Design and evaluation of an acceleration guidance algorithm for entry». In: *Journal of Spacecraft and Rockets* 41.6 (2004), pp. 986–996.

[56] Elliot Brendel, Bruno Hérissé, and Eric Bourgeois. «Optimal guidance for toss back concepts of reusable launch vehicles». In: *EUCASS 2019*. 2019.

[57] Federico Toso. «Preliminary design of reusable future space access vehicles». PhD thesis. University of Strathclyde, 2023.

[58] P. Gallais. *Atmospheric Re-Entry Vehicle Mechanics*. Springer Berlin Heidelberg, 2007. ISBN: 9783540736479.

[59] National Oceanic and Atmospheric Administration. «U.S. Standard Atmosphere, 1976». In: Rockville, MD, 1976.

[60] J. M. Picone et al. «NRLMSISE-00 empirical model of the atmosphere: Statistical comparisons and scientific issues». In: *Journal of Geophysical Research: Space Physics* 107.A12 (2002), SIA 15-1-SIA 15–16. DOI: https://doi.org/10.1029/2002JA009430.

[61] nasa.gov. *Rocket Thrust Equation*. URL: https://www.grc.nasa.gov/www/k-12/airplane/rockth.html.

[62] E. Mooij. *The HORUS-2B Reference Vehicle*. 1995.

[63] Gary Harloff and Brian Berkowitz. *HASA: Hypersonic Aerospace Sizing Analysis for the preliminary design of aerospace vehicles*. NASA, 1988.

[64] Antonio Viviani, Luigi Iuspa, and Andrea Aprovitola. «An optimization-based procedure for self-generation of Re-entry Vehicles shape». In: *Aerospace Science and Technology* 68 (2017), pp. 123–134.

[65] J.J. Bertin and R.M. Cummings. *Aerodynamics for Engineers*. Pearson international edition. Pearson/Prentice Hall, 2009. ISBN: 9780132272681. URL: https://books.google.es/books?id=eHmdQgAACAAJ.

[66] Public Domain Aeronautical Software (PDAS). *References for the Digital Datcom Program*. URL: https://www.pdas.com/datcomrefs.html.

[67] Jacopo Guadagnini and Gabriele De Zaiacomo. «Multidisciplinary Modeling for Missionisation of Re-entry Vehicles». In: *AIAA SCITECH 2023 Forum*. DOI: 10.2514/6.2023-1169.

[68] J.D. Anderson and J.D. Anderson. *Hypersonic and High-temperature Gas Dynamics*. AIAA education series. American Institute of Aeronautics and Astronautics, Incorporated, 2019. ISBN: 9781624105142.

[69] Rodrigo Haya Ramos et al. «Flying Qualities Analysis for Re-entry Vehicles: Methodology and Application». In: Aug. 2011. ISBN: 978-1-60086-952-5. DOI: 10.2514/6.2011-6344.

[70] United States. National Aeronautics and Space Administration. *Analysis of Corridor and Guidance Requirements for Supercircular Entry Into Planetary Atmospheres*. Technical report R (series), 1960. 1961.

[71] Marco Sagliano and Erwin Mooij. «Optimal drag-energy entry guidance via pseudospectral convex optimization». In: *Aerospace Science and Technology* 117 (2021), p. 106946.

[72] Xinfu Liu, Zuojun Shen, and Ping Lu. «Solving the Maximum-Crossrange Problem via Successive Second-Order Cone Programming with a Line Search». In: *Aerospace Science and Technology* 47 (Sept. 2015). DOI: 10.1016/j.ast.2015.09.008.

[73] Francesco Topputo and Chen Zhang. «Survey of Direct Transcription for Low-Thrust Space Trajectory Optimization with Applications». In: *Abstract and Applied Analysis* 2014 (June 2014), pp. 1–15. DOI: 10.1155/2014/851720.

[74] Walter Murray. «Sequential quadratic programming methods for large-scale problems». In: *Computational Optimization and Applications* 7.1 (1997), pp. 127–142.

[75] MathWorks.com. *fmincon*. URL: https://it.mathworks.com/help/optim/ug/fmincon.html.

[76] Michael Szmuk, Taylor P. Reynolds, and Behçet Açıkmeşe. «Successive Convexification for Real-Time Six-Degree-of-Freedom Powered Descent Guidance with State-Triggered Constraints». In: *Journal of Guidance, Control, and Dynamics* 43.8 (Aug. 2020), pp. 1399–1413. DOI: 10.2514/1.g004549.

[77] Pedro Simplício, Andrés Marcos, and Samir Bennani. «Guidance of Reusable Launchers: Improving Descent and Landing Performance». In: *Journal of Guidance, Control, and Dynamics* 42.10 (Oct. 2019), pp. 2206–2219. DOI: 10.2514/1.g004155.

[78] zenodo.org. *RETALT-Retro Propulsion Assisted Landing Technologies*. URL: https://zenodo.org/communities/retalt/?q=&l=list&p=1&s=10&sort=bestmatch.

[79] Claus Weiland. «The aerodynamics of real space vehicles in the light of supersonic and hypersonic approximate theories». In: *CEAS Space Journal* 12 (2020), pp. 85–96. DOI: 10.1007/s12567-019-00264-w.

[80] Davide Bonetti et al. «PETBOX: FLIGHT QUALIFIED TOOLS FOR ATMOSPHERIC FLIGHT». In: Mar. 2016.

[81] J. Vos et al. «Aerodynamic investigations of a Vertical Landing Launcher configuration by means of Computational Fluid Dynamics and Wind Tunnel Tests». In: AIAA Scitech 2022 Forum , San Diego, Jan. 1, 2022. DOI: https://doi.org/10.2514/6.2022-1308. URL: https://zenodo.org/record/5814915. published.

[82] A. Marwege et al. «Aerodynamic Phenomena of Retro Propulsion Descent and Landing Configurations». In: FAR2022 , Heilbronn, June 21, 2022. DOI: 10.5281/zenodo.6783922. URL: https://zenodo.org/record/6783922 (visited on 06/21/2022). published.

[83] M. Laureti et al. «Aerothermal Databases and CFD Based Load Predictions». In: FAR2022 , Heilbronn, 2022. DOI: 10.5281/zenodo.6759561. URL: https://zenodo.org/record/6759561. published.

[84] *RETALT: Development of Key Flight Dynamics and GNC Technologies for Reusable Launchers*. Zenodo, Sept. 2022.

[85] Federico Toso and Christie Maddock. «Return and abort trajectory optimisation for reusable launch vehicles». In: *21st AIAA International Space Planes and Hypersonics Technologies Conference*. DOI: 10.2514/6.2017-2250. eprint: https://arc.aiaa.org/doi/pdf/10.2514/6.2017-2250. URL: https://arc.aiaa.org/doi/abs/10.2514/6.2017-2250.

[86] Ansgar Marwege et al. «Retro Propulsion Assisted Landing Technologies (RETALT): Current Status and Outlook of the EU Funded Project on Reusable Launch Vehicles». In: Oct. 2019.

[87] A. Gülhan et al. *RETALT - RETro propulsion Assisted Landing Technologies*. Dec. 2021.

[88] Stefano Gallucci et al. «The AVUM Orbital Module for the Space Rider System». In: 2019. DOI: 10.13009/EUCASS2019-860.

[89] Victor Marco et al. «The IXV guidance, navigation and control subsystem: Development, verification and performances». In: *Acta Astronautica* 124 (Apr. 2016). DOI: 10.1016/j.actaastro.2016.04.010.

[90] N. Pavlis et al. «The Development and Evaluation of the Earth Gravitational Model 2008 (EGM2008) (vol 117, B04406, 2012)». In: *Journal of Geophysical Research* 118 (Apr. 2012). DOI: 10.1029/2011JB008916.

[91] Daniele Gherardi et al. «IXV GNC Subsystem Design and Performances». In: June 2011.

[92] Bonetti Davide et al. «IXV Mission Analysis Post Flight». In: July 2019. DOI: 10.13009/EUCASS2019-630.

[93] Gabriele De Zaiacomo Jacopo Guadagnini and Federico Toso. «Multidisciplinary Design Optimization for missionisation of re-entry vehicles: preliminary mission design and mission capabilities evaluation of winged re-entry vehicle case study». In: *ESA GNC-ICATT*. 2023.

[94] Reddit.com. *Falcon 9 stage 1 landing analysis*. URL: https://www.reddit.com/r/spacex/comments/7ajf09/falcon_9_stage_1_landing_analysis/.

[95] rocketlabusa.com. *Electron*. URL: https://www.rocketlabusa.com/launch/electron/.

[96] Ansgar Marwege et al. «RETALT: review of technologies and overview of design changes». In: *CEAS Space Journal* 14 (2022), pp. 433–445. DOI: 10.1007/s12567-022-00458-9.

[97] Xinfu Liu, Zuojun Shen, and Ping Lu. «Solving the maximum-crossrange problem via successive second-order cone programming with a line search». In: *Aerospace Science and Technology* 47 (2015), pp. 10–20. ISSN: 1270-9638. DOI: https://doi.org/10.1016/j.ast.2015.09.008.

Colophon

This thesis was typeset with LATEX and BibTEX, using a typographical look-and-feel created by Jacopo Guadagnini. The style was inspired by S.Silvestrini, A. Colagrossi, D.A. Dei Tos `PhD_Dis` and by J. Stevens, L. Fossati `phdthesis` styles.